

**Permeability of Lipid Bilayers
Containing Cholesterol**

by

Eugenia Corvera Poiré

Department of Physics, McGill University

Montréal, Québec

Canada

A Thesis submitted to the

Faculty of Graduate Studies and Research

in partial fulfillment of the requirements for the degree of

Master in Science

© Eugenia Corvera Poiré, 1990

*To my parents,
for 27 years of love.*

Abstract

Lipid-cholesterol bilayers are studied by means of a microscopic multi-state lattice model and Monte Carlo computer simulations. The model used is a direct extension of the Pink model for the main transition of pure lipid bilayers. Cholesterol is introduced as a bulky, rigid molecule with no internal degrees of freedom. The model is able to account for the chain melting of lipid molecules, and is expected to be valid at low cholesterol concentrations.

A minimal model for the transport of ions across membranes is used to predict the changes in the passive permeability of lipid-cholesterol bilayers for different cholesterol concentrations and different lipid chain lengths. The model assigns different probabilities of transfer to bulk, clusters and interfaces. The main assumption is that, defects due to bad packing at interfacial regions, cause the membrane to be leaky and allow the ions to permeate it. Therefore the model assigns a high probability of transfer to the interfacial regions.

A peak in the permeability is observed near the transition temperature, which is in accord with experimental data. The results show an increase in the passive ion permeability for increasing cholesterol concentration for the three systems under consideration. Also, an increase in the membrane permeability is predicted for decreasing chain length for all the cholesterol concentrations studied.

Résumé

L'étude de doubles couches lipide-cholestérol a été étudié à partir d'un modèle de treillis microscopique à plusieurs états énergétiques soumis à des simulations de type Monte Carlo. Le modèle utilisé est en fait une extension directe du modèle de Pink appliqué dans le cadre des principales transitions ayant lieu dans les doubles couches lipidiques pures. Les molécules de cholestérol sont représentées comme une masse rigide, sans aucun degré interne de liberté. Ce modèle est en mesure de représenter la fusion des chaînes lipidiques, ce qui est censé être valide à de faibles concentrations de cholestérol.

Un modèle simple tenant compte du transport ionique membranaire est utilisé afin de prédire tout changement de la perméabilité ionique passive de la double couche lipide-cholestérol et ce, pour différentes concentrations de cholestérol et des longueurs variées de chaînes lipidiques. Des probabilités différentes de transfert vers le substrat, les agrégats ou les interfaces sont assumées. L'hypothèse principale réside en ce qu'un mauvais entassement à l'interface crée des défauts dans la membrane, la rendant ainsi plus perméable aux ions. De cette manière, ce modèle donne une grande probabilité de transfert vers les régions interfaciales.

Un accroissement de la perméabilité est observé près de la température de transition, ce qui concorde avec les observations expérimentales. De plus, nos résultats démontrent une augmentation de la perméabilité ionique passive reliée à une augmentation de la concentration de cholestérol dans les trois systèmes qui ont été étudiés. Finalement, un accroissement de la perméabilité membranaire est prévue pour des chaînes lipidiques plus courtes dans tous les cas de concentrations de cholestérol considérés dans cette étude.

Acknowledgements

First I want to thank Martin Zuckermann for many things, academic and non-academic. Most of all for his friendly and open way of relating to people and for his respect for the freedom of his students. It has been a pleasure for me to work with such a nice person during these two years. I also thank Ole Mouritsen for many extremely useful suggestions and encouraging comments. Thanks to John Ipsen for providing the values of some of the parameters; to Frank Jones for some very useful help at the beginning of the project. Special thanks to Betty Pedersen for her invaluable help and her extremely nice manner and to Diane Koziol for her daily smile; to Mr. Antonio de Sausa for making our office a nicer place to work.

Thanks to my beloved Ricardo for the daily life, the daily sharing and much more than I can express here; to my dear friends Karen, Martin and Ahmed for letting me be a part of their lives and for making my stay in Montreal so wonderful; also to Dennis, Linda and Antoine Isabel for the many good times together. Thanks to Bertrand and Linda for their friendship, the good times and the good wines; to Ross for trying again; to him and to Chris my deepest thanks for a warm welcome; to Ian for cheering me up when I need it; to Mohamed for his friendliness, to Jianhua for his good mood and some chinese lessons; to Tony, Bruno, Pascal, Diane, Jacques and Steve for the friendly chats; and to Loki for his community concerns.

Contents

Abstract	iii
Résumé	iv
Acknowledgements	v
List of Figures	viii
List of Tables	x
1 Introduction	1
2 Pure Lipid Bilayers	8
2.1 The Pink Model	8
2.1.1 Van der Waals Interactions between Chains	10
2.1.2 Interactions between Lipid Chains in the Pink Model	15
2.1.3 Relation between Order Parameter and Chain Length	16
2.1.4 Other Interactions	17
2.1.5 The Pink Hamiltonian	18
2.2 Monte Carlo Simulation	19
2.2.1 Effect of Acyl Chain Length	21
2.3 Passive Permeability	24
2.3.1 Number of Particles Striking a Surface	24
2.3.2 Model of Passive Ion Permeability	26
2.3.3 Analysis of Configurations	28
2.3.4 Model Permeability and Monte Carlo Simulations	29
2.3.5 Effect of Acyl Chain Length on the Permeability	34
3 Lipid-Cholesterol Bilayers	37
3.1 Model of Lipid-Cholesterol Bilayers	39
3.1.1 Monte Carlo Simulations	41
3.1.2 Effect of Acyl Chain Length	53
3.2 Passive Permeability of Lipid-Cholesterol Bilayers	61
3.2.1 Analysis of Configurations	61
3.2.2 Model Permeability and Monte Carlo Simulations	62

3.2.3	Effect of Acyl Chain Length on the Permeability	71
3.3	Discussion	79
A	Isothermal-Isobarical Ensemble	81
A.1	A Comment About the Notation	84
B	Monte Carlo Integration	86
B.1	Metropolis Algorithm	87
B.2	Implementation for Lipid Systems	91
	References	95

List of Figures

1.1	Structure of phospholipid and cholesterol molecules.	3
1.2	Structure of a spherical micelle and a bilayer.	3
1.3	Phase diagram of dipalmytoyl phosphatidylcholine in water	5
1.4	Rotational energy of a C-C bond in an alkane chain	6
1.5	Conformations of the three energy minima	6
2.1	Ground and intermediate energy states.	12
2.2	Two long parallel chains	14
2.3	Energy and specific heat of DMPC, DPPC and DSPC bilayers	20
2.4	Area, order parameter and isothermal compressibility of DMPC, DPPC and DSPC bilayers	22
2.5	Particles colliding with an element of area of a wall.	25
2.6	Average cluster size, maximum cluster size and number of clusters for DMPC, DPPC and DSPC	30
2.7	Snapshots of configurations near T_m for DMPC.	33
2.8	Fractional areas of bulk, clusters and interface for DMPC, DPPC and DSPC	33
2.9	Relative permeability of DMPC, DPPC and DSPC bilayers	34
2.10	Snapshots of configurations for different chain lengths	35
3.1	Phase diagram of DPPC-cholesterol bilayers	38
3.2	Total area, lipid area and order parameter of DMPC-cholesterol bilayers	42
3.3	Total area, lipid area and order parameter of DPPC-cholesterol bilayers	43
3.4	Total area, lipid area and Order Parameter of DSPC-cholesterol bilayers	44
3.5	Energy of DMPC-cholesterol bilayers	45
3.6	Energy of DPPC-cholesterol bilayers	46
3.7	Energy of DSPC-cholesterol bilayers	46
3.8	Specific heat of DMPC-cholesterol bilayers	47
3.9	Specific heat of DPPC-cholesterol bilayers	48
3.10	Specific heat of DSPC-cholesterol bilayers	49
3.11	Isothermal compressibility of DMPC-cholesterol bilayers	50
3.12	Isothermal compressibility of DPPC-cholesterol bilayers	51
3.13	Isothermal compressibility of DSPC-cholesterol bilayers	52
3.14	Energy and specific heat of bilayers with $x_C = 0.05$	54
3.15	Energy and specific heat of bilayers with $x_C = 0.10$	55

3.16	Energy and specific heat of bilayers with $x_C = 0.15$	56
3.17	Total area, lipid area and order parameter of bilayers with $x_C = 0.05$	57
3.18	Total area, lipid area and order parameter of bilayers with $x_C = 0.10$	58
3.19	Total area, lipid area and order parameter of bilayers with $x_C = 0.15$	59
3.20	Isothermal compressibility of bilayers containing cholesterol	60
3.21	Fractional areas of bulk, clusters and interface of DMPC-cholesterol bilayers.	63
3.22	Fractional areas of bulk, clusters and interface of DPPC-cholesterol bilayers.	64
3.23	Fractional areas of bulk, clusters and interface of DSPC-cholesterol bilayers.	65
3.24	Snapshots of configurations for several cholesterol concentrations.	68
3.25	Relative permeability of DMPC-cholesterol bilayers	68
3.26	Relative permeability of DPPC-cholesterol bilayers	69
3.27	Relative permeability of DSPC-cholesterol bilayers	70
3.28	Snapshots of configurations for several chain lengths	72
3.29	Fractional areas of bilayers with $x_C = 0.05$	73
3.30	Fractional areas of bilayers with $x_C = 0.10$	74
3.31	Fractional areas of bilayers with $x_C = 0.15$	75
3.32	Relative permeability of bilayers with $x_C = 0.05$	76
3.33	Relative permeability of bilayers with $x_C = 0.10$	77
3.34	Relative permeability of bilayers with $x_C = 0.15$	78
B.1	Periodic boundary conditions.	92

List of Tables

2.1	Energies, lengths and degeneracies of the ground and the intermediate states.	13
2.2	Experimental transition temperatures and interaction constants. . . .	19

Chapter 1

Introduction

Cell membranes are among the main organized structures of living matter. All living structures are enclosed by membranes. Cell membranes are not simply walls to keep the cell components together, but they have important functions in the process of life. Transport is one of the most important functions of cell membranes. It allows the cell to keep some chemical elements and discard others. Selective transport allows the cell membranes to separate two different aqueous solutions and consequently allows the cell to keep a certain internal chemical composition.

Water is essential to the life of a cell. If the amount of water is less than a certain required minimum, the cell dies. In order to understand cell membranes, it is essential to understand the interaction of water with their basic components

In the water molecule two electrons are shared in each bond between hydrogen and oxygen. Nevertheless the oxygen has a larger electronegativity and attracts the electrons more strongly than the hydrogen. This gives a charge distribution that is negative around the oxygen and positive around the hydrogens, making the water molecule polar. Water molecules have a mutual attraction because of their polarity. There are other molecules such as oils and fats that are nonpolar and do not attract each other strongly. When nonpolar substances are in contact with water, they do not mix. This is because the attraction between the water molecules prevents the nonpolar molecules from intercalating between them, and therefore water tends to

expel nonpolar molecules out of its bulk.

The basic structural components of biological membranes are molecules possessing both a polar and a nonpolar part. These substances are called amphiphilic (from the Greek, *amphi*: on both sides, *philos*: love), and are able to interact with polar substances via their hydrophilic part and with nonpolar substances via their hydrophobic part.

Many amphiphilic substances can be found in nature but membranes are basically formed from lipids. There are three major types of lipids in cell membranes: phospholipids (which are the most abundant), cholesterol and glycolipids. Phospholipids are substances with a nonpolar or hydrophobic (from the Greek, *hydro*: water, *phobos*: fear) "tail" and a polar or hydrophilic "head". They are molecules constructed from fatty acids and glycerol. A fatty acid molecule has a long hydrophobic hydrocarbon chain and a carboxylic group which is extremely hydrophilic. The glycerol is attached to two fatty acid chains and to a phosphate group which is in turn connected to another small hydrophilic compound such as choline. A typical phospholipid molecule is shown in figure 1.1. Phospholipids which form lipid bilayers have tails composed of two hydrophobic hydrocarbon chains which vary in length and normally have between 12 to 22 carbon atoms. The structure of the polar head varies considerably from one phospholipid to another. Glycolipids have the same basic structure as the phospholipids but the phosphate and choline groups are replaced by glycosyl groups. The structure of a cholesterol molecule is shown in figure 1.1. Cholesterol has a polar head group, a rigid planar steroid¹ ring structure and a nonpolar hydrocarbon tail.

When lipid molecules are dissolved in water, unfavorable interactions occur between the nonpolar part of the lipids and the water. This causes the formation of aggregates in which the contact between the hydrophobic tails and water is minimized. This unfavorable interaction is known as the *hydrophobic force* and is responsible for the self-organization of lipids in water. Lipid aggregates or *micelles* can have many sizes and shapes. Some form spherical micelles, others form globular or rod-like ag-

¹Steroids are a group of compounds containing four rings and three ring fusions. They play a variety of biological roles.

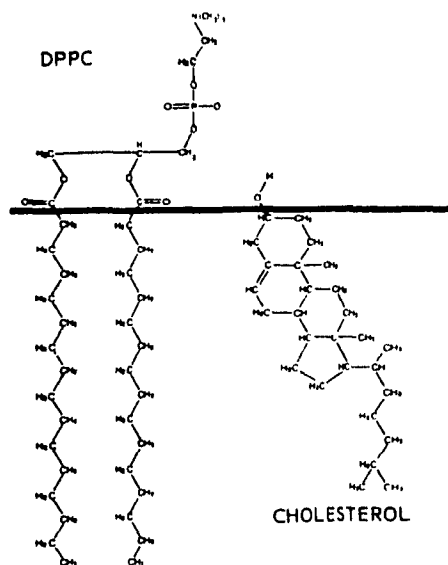


Figure 1.1: Structure of phospholipid and cholesterol molecules.

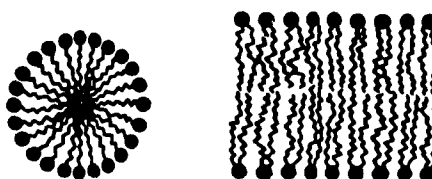


Figure 1.2: Structure of a spherical micelle and a bilayer

gregates and phospholipids form bilayers. A spherical micelle and a bilayer are shown in figure 1.2. The particular micelle geometry adopted by molecules of a particular kind is mainly determined by packing requirements. The most stable geometry is determined by the following three parameters:

- S_0 the optimal surface area occupied by the molecule at the hydrocarbon interface.

- l the maximum length of the chains.

- ν the molecular volume of the hydrocarbon part of the lipid molecule.

Among all the geometries the spherical micelle form has the largest area/volume

ratio and it is favored by lipids with a large value of S_0 . The bilayer has the smallest area/volume ratio and it is favored by lipids with large molecular volume such as phospholipids with tails having two hydrocarbon chains. Other geometries like distorted spheres and cylinders have intermediate values of the area/volume ratio. The parameter $\frac{\nu}{lS_0}$ is known as the *critical packing parameter* and it can be used to predict which micelle geometry will be taken up by molecules of a particular kind.

For a spherical micelle with M molecules the area is $MS_0 = 4\pi R^2$ and the volume is $M\nu = \frac{4}{3}\pi R^3$. The radius is therefore $R = \frac{3\nu}{S_0}$ and it should be less or equal to the maximum chain length. The criterion for lipids to form a spherical micelle is that the critical packing parameter be less or equal $1/3$. For a planar bilayer with M molecules the area is $MS_0 = 2L^2$ and the volume is $M\nu = hL^2$, where h is the height of the bilayer given by $h = \frac{2\nu}{S_0}$. h should be less or equal to twice the maximum chain length. The criterion for lipids to form a planar bilayer is that the critical packing parameter be less or equal 1. The value of the critical packing parameter can be calculated for different geometries. Flat shapes are disfavored due to the contact with water at the edges, so that micellar shapes tend to be smooth. The geometrical prediction for a given critical packing parameter is as follows:

$$\begin{aligned} \frac{\nu}{lS_0} < \frac{1}{3} & \quad \text{spherical micelles} \\ \frac{1}{3} < \frac{\nu}{lS_0} < \frac{1}{2} & \quad \text{globular or cylindrical micelles} \\ \frac{1}{2} < \frac{\nu}{lS_0} < 1 & \quad \text{bilayer} \end{aligned}$$

Most phospholipids spontaneously form bilayers when surrounded by water. There are many forms of phospholipid water systems, and this is why such mixtures are called polymorphic (from the Greek, *poly*: many, *morphe*: form). The major forms are:

- A lamellar² liquid crystalline phase (L_α), characterized by conformationally disordered chains and lateral diffusion of molecules in the plane of the bilayer.

²Lamellar implies a layered structure.

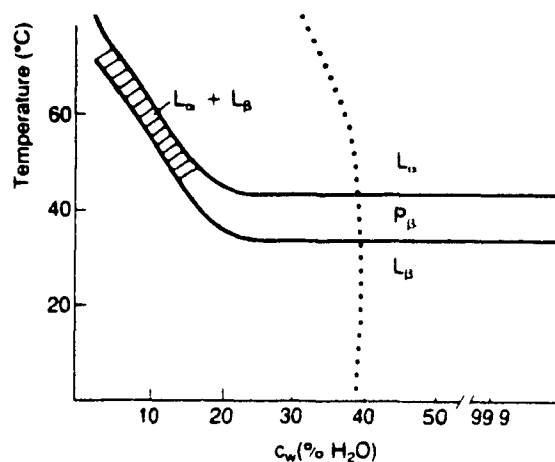


Figure 1.3: Phase diagram of dipalmitoyl phosphatidylcholine in water. Indicated are lamellar gel phase ($L_{\beta'}$), lamellar liquid crystalline phase (L_α) and intermediate ripple phase ($P_{\beta'}$). At high temperatures and low hydration other phases can form. The dotted lines indicate the maximum absorption of water by the homogeneous lipid-water mixture. Adapted from reference [9].

- A lamellar gel phase (L_β), characterized by conformationally ordered chains and a lateral crystalline structure. For lipids with bulky headgroups the acyl³ chains are tilted with respect to the bilayer normal (a prime is added to the nomenclature when the chains are tilted).

- A hexagonal phase (H), in which the lipids are organized into cylinders which form a hexagonal array.

The particular form adopted by the lipid molecules depends on temperature, pressure, and lipid concentration. Figure 1.3 shows the phase diagram of dipalmitoyl phosphatidylcholine which under most temperatures and water concentrations is in a lamellar form. At low water concentrations, there is a single lamellar phase, whereas at high water concentrations phase separation occurs and pure water coexists with the lamellar phase. Between the gel and the liquid crystalline phases a phase called *the ripple phase* ($P_{\beta'}$) sometimes occurs for lipids with bulky polar headgroups. This phase is characterized by layers with a rippled surface. In this phase the chains have high conformational order as in the gel phase.

³The chains are often called acyl chains. Acyl is the univalent group RCO where R is an organic group attached to one bond of the bivalent carbonyl group CO

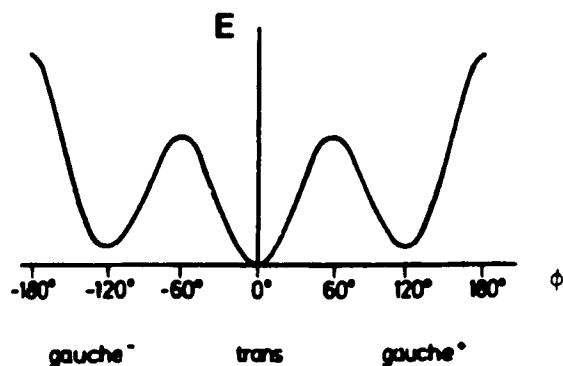


Figure 1.4: Rotational energy of a C-C bond in an alkane chain. The angle ϕ is the rotation angle from the *trans* configuration.

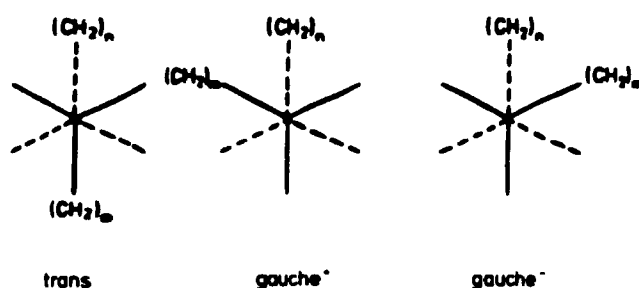


Figure 1.5: Conformations of the three energy minima. The conformations are shown along the C-C bond. The solid lines represent the bonds of the carbon at the front, the dotted lines represent the bonds of the carbon at the back.

The phase transition $P_{\beta'} \rightarrow L_{\alpha}$ is called the main transition and involves what is known as *chain melting*, in which the chains become conformationally disordered. It also involves a melting of the lateral crystalline structure. The transition $L_{\beta'} \rightarrow P_{\beta'}$ is called the pre-transition and involves a deformation of the lateral crystalline structure.

In order to understand the conformational order of the lipid chains it is useful to examine the rotational energy spectrum of a saturated C-C bond in an alkane chain. This spectrum has the form shown in figure 1.4 and exhibits three energy minima which correspond to the conformations shown in figure 1.5. The lowest energy minimum corresponds to the ground state of a C-C bond and is known as the *trans* configuration. The other two minima are degenerate and are known as *gauche* con-

figurations. A bond in a *trans* configuration is known as a *trans* bond and a bond in a *gauche* configuration is known as a *gauche* bond. A chain with only *trans* bonds is said to be in all-*trans* configuration. The all-*trans* configuration allows the chain to be maximally extended whereas a *gauche* bond alters the direction of the chain. In the gel phase the hydrocarbon chains of saturated diacyl phospholipids are predominantly in the all-*trans* configuration. In the liquid crystalline phase the number of *gauche* configurations for individual C-C bonds increases considerably and consequently the cross sectional area of the chains increases whereas the length of the chains decreases.

The most studied lipid phase transition is the main transition in pure lipid membranes. Model membranes are easier to characterize physically and chemically than biological membranes. The phase transition in model membranes can be more easily understood, and although it is much sharper than phase transitions in biological membranes, it can give some insight into the properties of biomembranes. The study of the phase transition that occur in membranes is very important and has biological relevance. The best known example is an organism called *Acholeplasma Laidlawii*. This organism exhibits a broad transition region during which chain melting occurs and its growth temperature lies within this region [19, 28].

In the first part of this thesis, the properties of pure phospholipid bilayers are studied at the main transition. The pre-transition has a very small latent heat associated with it and will not be considered in this thesis. The transition studied is between the lamellar gel and the liquid crystalline phases. The second part of this thesis is concerned with the changes in the physical properties of lipid bilayers when cholesterol is added in small concentrations. Special attention is paid to the variation of the physical properties with chain length for both pure lipid bilayers and lipid bilayers containing cholesterol.

The main references used for the introduction are [1, 9, 15, 22, 24].

Chapter 2

Pure Lipid Bilayers

2.1 The Pink Model

The theoretical model used in this thesis to describe the behavior of pure lipid bilayers is a multi-state lattice model due to Pink [2, 25]. The Pink model was constructed assuming that the two monolayers forming the lipid bilayer do not interact, so that the system is considered as consisting of two independent monolayers. Also, the two chains forming the lipid molecule are considered to be independent of each other. Each monolayer is modeled by a two dimensional triangular lattice, and each site of the lattice represents a saturated lipid chain in one of ten different conformational states. The characteristics of these states are obtained by examining properties of the lipids in three dimensions. Therefore, although the model is two dimensional, it contains information relating to three dimensions.

The conformational states of the Pink model are chosen on the basis of rotational isomerism of alkane chains. The continuous spectrum for each saturated C-C bond (figure 1.4, page 6) can be replaced by the three conformational states corresponding to the three energy minima. This approximation is called *Rotational Isomeric Model*.

The possibility for each C-C bond of being in one of three states gives a finite number of possible configurations for a free lipid chain, 3^{m-1} , where m is the number of carbons in the chain. For free chains with $m = 14, 16, 18$, the number of possible

states will be of the order 10^6 to 10^8 . For lipid chains in a bilayer, the number of possible configurations is much lower than in the case of a free chain because of the steric interactions with neighboring chains.

The Pink model assumes that the chains can have angles of 120° between C-C bonds (instead of 109.5°). Therefore the chain conformations can be mapped into a triangular lattice (note that this is not the lattice of the membrane). The Pink model selects ten different conformational states. The ground state of the chain is the all-*trans* state, for which all the C-C bonds are in *trans* configuration. There are 8 intermediate energy states, which are low energy excitations of the all-*trans* configuration and which were selected according to the following rules:

- The first two chain segments are kept fixed in a *trans* configuration.
- The chains have at most three *gauche* bonds.
- The length of the chains is at most three units shorter than that of the all-*trans* configuration.
- The chains do not fold back upon themselves.

In addition to these rules there are two constraints imposed on the possible configurations which are described below.

The first two *trans* segments define a plane. The first *gauche* bond takes the molecule out of the plane in two possible directions. This is why it has a two-fold degeneracy. The first constraint is the following: if a second *gauche* bond occurs (as in states 5 to 9) it is only allowed to return the molecule to the plane. Therefore a second *gauche* bond is non-degenerate. If a third *gauche* bond occurs (as in states 8 and 9) the molecule again comes out of the plane in two possible directions and the *gauche* bond has a two-fold degeneracy except if the second and third *gauche* bonds are next to each other. In this case only one of the directions is allowed and this is the second constraint imposed in order to minimize steric hindrance. In the latter case the third *gauche* bond is non-degenerate.

All lipid chain conformations with the same energy and the same length are considered to be in the same conformational state. The tenth state is a high energy state

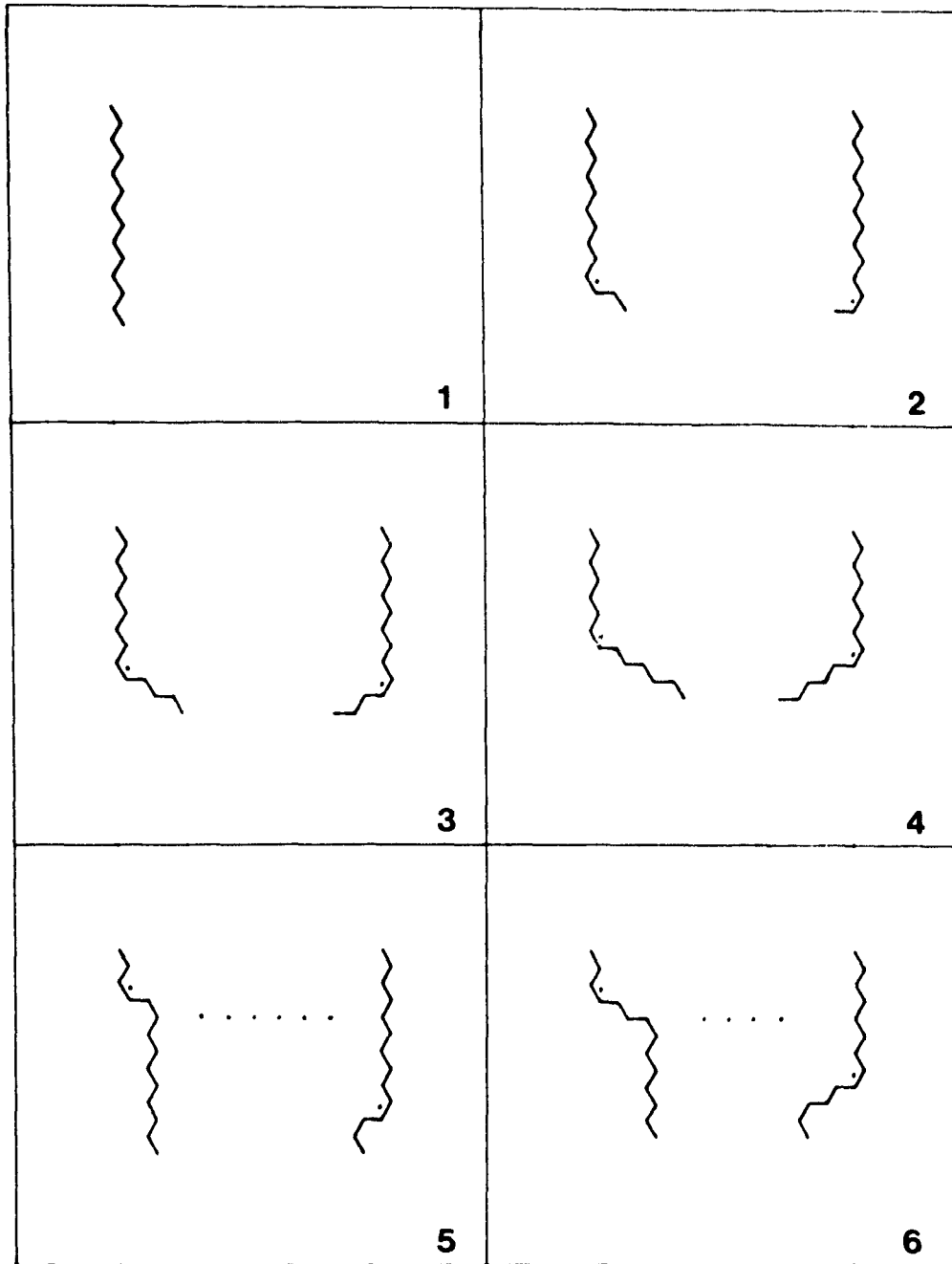
characteristic of the liquid crystalline or fluid phase and it is a combination of many disordered states.

The Pink model requires a knowledge of the internal energy, the cross sectional area and the degeneracy associated with each conformational state. The all-*trans* state is considered to be a state with zero internal energy, its cross sectional area is determined from experimental data [31] as $A_1 = 20.4\text{\AA}^2$, and it is non-degenerate. The internal energy of the intermediate states is determined by the number of *gauche* bonds. The energy required to form a *gauche* bond from a *trans* configuration is $E_g = 0.45 \times 10^{-13} \text{erg}$. The cross sectional areas are obtained from the assumption that the volume of the chain remains constant, i.e. $A_n = A_1 \frac{L_1}{L_n}$ where L_1 is the length of the all *trans* configuration ($L_1 = m - 1$ in units of projected chain segments), and L_n is the length of the intermediate state. This assumption is based on experimental evidence from dilatometry experiments on lipid bilayers [32] and was first used in reference [18]. The degeneracies are obtained by counting the number of possible configurations with the same energy and the same length. Figure 2.1 shows the mapping for the ground state and the 8 intermediate energy states. The figure caption explains how the degeneracies of the intermediate states are obtained. It is important to consider the constraints described on page 9. Table 2.1 shows a summary of the properties of the ground and intermediate conformational states. The parameters of the high-energy or "melted" state are set as follows. The cross sectional area is assumed to be independent of the chain length and is set to $A_{10} = 34\text{\AA}^2$. The degeneracy is assumed to be proportional to 3^m , and is given by $D_{10} = 6 \times 3^{m-6}$. The energy is assumed to be linear in the chain length, and is given by $E_{10} = (0.42m - 3.94) \times 10^{-13} \text{erg}$.

To understand the interaction between the lipid molecules in the Pink model we study the Van der Waals interaction between long parallel chains in the next section.

2.1.1 Van der Waals Interactions between Chains

In this section we follow the analysis of reference [29]. Consider two linear chains of length L each constructed from N identical units of length λ , so that $L = \lambda N$. The



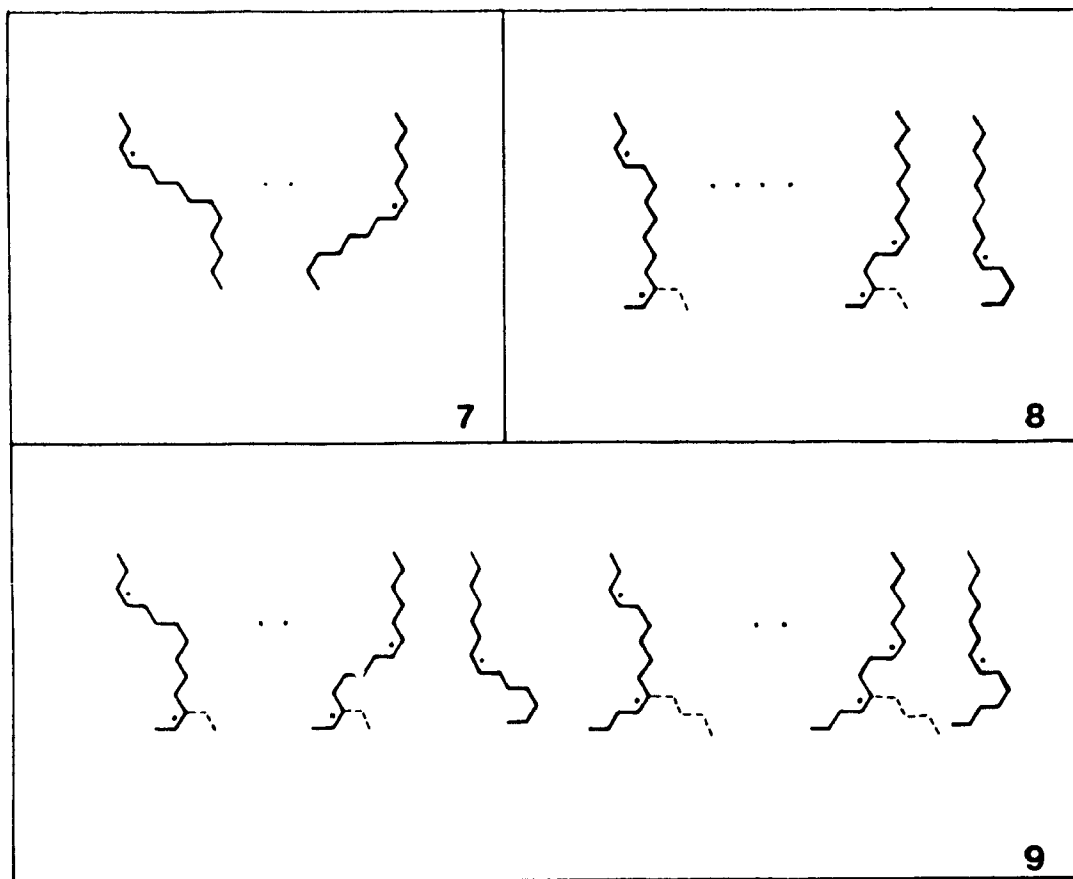


Figure 2.1 *Ground and intermediate energy states.*

1 All-*trans* state for a chain with $m = 14$ carbon atoms.

2-9 Intermediate states for a chain with $m = 14$ carbon atoms. All the possible configurations are drawn for states 2, 3 and 4. The dot beside a gauche bond indicates that the bond has a degeneracy $D = 2$. Therefore the degeneracy of states 2, 3 and 4 is $D = 4$. For states 5, 6 and 7 not all the possible configurations are drawn, but there is a systematic way of drawing all of them. Consider for example state 5. For the configuration drawn at the left there is a sequence gauche-trans-gauche (g-t-g) in the chain segments 3, 4, 5 (counting from the top). For the configuration drawn at the right the g-t-g sequence is in the chain segments $m - 4$, $m - 3$, $m - 2$. The rest of the configurations can be obtained starting from the configuration at the left and moving down the g-t-g sequence until the configuration at the right is obtained. In this case we have $m - 6$ different configurations, each with a degenerate gauche bond. Therefore the degeneracy of state 5 is $D = 2(m - 6)$. The degeneracy of state 6 is obtained moving down the g-t-t-g sequence and its degeneracy is $D = 2(m - 8)$. The degeneracy of state 7 is obtained moving down the g-t-t-t-g sequence and its degeneracy is $D = 2(m - 10)$. For states 8 and 9 the dashed line indicates another possible configuration which is identical to the solid line configuration except for the orientation of the last segments. Note that in the case of the dashed line configuration the last degenerate gauche bond is one segment above than in the solid line configuration. The configurations for the state 8 are obtained moving down the sequence g-t-g and its degeneracy is $D = 8(m - 8)$. The configurations for the state 9 are obtained moving down the sequence g-t-t-g when there is a gauche bond in the segment $m - 2$ ($m - 3$ in the case of the dashed sequence) and moving down the sequence g-t-g when there is a gauche bond in the segment $m - 4$ ($m - 5$ in the case of the dashed sequence). Therefore the degeneracy of state 9 is $D = 16(m - 10)$. The number of dots between configurations is the number of configurations not drawn for a chain with $m = 14$.

State 1	State 2	State 3
$E = 0$	$E = E_g$	$E = E_g$
$L = m - 1$	$L = m - 2$	$L = m - 3$
$D = 1$	$D = 4$	$D = 4$
State 4	State 5	State 6
$E = E_g$	$E = 2E_g$	$E = 2E_g$
$L = m - 4$	$L = m - 2$	$L = m - 3$
$D = 4$	$D = 2(m - 6)$	$D = 2(m - 8)$
State 7	State 8	State 9
$E = 2E_g$	$E = 3E_g$	$E = 3E_g$
$L = m - 4$	$L = m - 3$	$L = m - 4$
$D = 2(m - 10)$	$D = 8(m - 8)$	$D = 16(m - 10)$

Table 2.1: Energies, lengths and degeneracies of the ground and the intermediate states

chains are assumed to be parallel to each other and to be separated by a distance D . D must be large compared to λ . The basic units of a chain are assumed to interact with the basic units of its neighbor via the Van der Waals interaction

$$\omega = \frac{A}{d^6}$$

where A is the strength of the interaction between two basic units and d is the distance between them. From figure 2.2, the distance between these two segments is

$$d = \sqrt{D^2 + \lambda^2(n - n')^2}$$

Therefore the interaction between the chains is given by

$$W = \sum_{n=1}^N \sum_{n'=1}^N \frac{A}{d^6} = A \sum_{n=1}^N \sum_{n'=1}^N \frac{1}{(D^2 + \lambda^2(n - n')^2)^3}$$

Let $x = |n - n'|$. For each value of x there are $2(N - x)$ interactions of equal magnitude except for $x = 0$ where there are only N interactions of equal magnitude. Then W

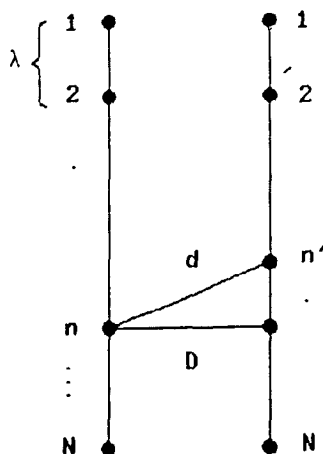


Figure 2.2. Two long parallel chains. The dots represent the central part of each segment.

can be rewritten as follows

$$W = \frac{AN}{D^6} + 2A \sum_{z=1}^{N-1} \frac{1 - \frac{z}{N}}{(\lambda^2 \frac{D^2}{L^2} + \lambda^2 \frac{z^2}{N^2})^3} \frac{1}{N^5}$$

For large N we can replace the sum by an integral

$$W = \frac{2A}{\lambda^6 N^4} \int_0^1 \frac{1-y}{(\rho^{-2} + y^2)^3} dy$$

where $\rho = \frac{L}{D}$, and $y = \frac{z}{N}$. The integrated expression for the interaction energy is

$$W = \frac{A\rho}{4\lambda^2 D^4} \left(3 \arctg \rho + \frac{\rho}{1+\rho^2} \right)$$

When the chain length L is much larger than the distance D between chains $\rho \gg 1$. Therefore $\arctg \rho \simeq \frac{\pi}{2}$ and $\frac{\rho}{1+\rho^2} \ll 1$ and we then find that, for long linear parallel chains,

$$W \simeq \frac{3\pi}{8} \frac{AN}{\lambda D^5} \quad (2.1)$$

This is Salem's result which states that the attraction between the chains is inversely proportional to the fifth power of the intermolecular distance and directly proportional to the length of the interacting molecules. This result is expected to be valid in a region where the molecules are oriented almost parallel to one another.

2.1.2 Interactions between Lipid Chains in the Pink Model

In order to account for the orientational interaction between lipid chains, we need a quantitative way to measure the alignment of the chains. For a single rod making an angle θ with the z axes, the quantity $S = \frac{1}{2}(3 \cos^2 \theta - 1)$ has a value of 1 if $\theta = 0$ and a value of $-\frac{1}{2}$ if $\theta = \frac{\pi}{2}$.¹ For a lipid chain with m carbons in a conformational state α , a measure of the alignment is given by the quantity

$$S_\alpha = \frac{1}{m-1} \sum_{n=1}^{m-1} \frac{(3 \cos^2 \theta_{\alpha n} - 1)}{2}$$

where the summation is over chain segments and $\theta_{\alpha n}$ is the angle between the n^{th} chain segment and the normal to the plain bilayer. For the all-*trans* state of a lipid chain, all the segments form an angle of 30° with the bilayer normal and $S_1 = \frac{5}{8}$.

In the Pink model neighboring acyl chains are assumed to interact via an anisotropic Van der Waals interaction which is a product of the isotropic interaction between two long parallel chains as calculated by Salem and an orientational interaction between individual C-C bonds. The total anisotropic interaction between two neighboring chains in states α and β can therefore be written as follows

$$E_{int} = -J_0 V_{\alpha\beta} S_\alpha S_\beta \quad (2.2)$$

where J_0 is an interaction constant that depends on the chain length. S_α and S_β are referred to as the nematic acyl chain order parameters for the two molecules and are given by

$$S_\alpha = \frac{8}{5} \frac{1}{(m-1)} \sum_{n=1}^{m-1} \frac{(3 \cos^2 \theta_{\alpha n} - 1)}{2} \quad (2.3)$$

The factor $\frac{5}{8}$ is due to normalization with respect to the all-*trans* configuration. $V_{\alpha\beta}$ is given by

$$V_{\alpha\beta} = \frac{(2r_1)^5}{(r_\alpha + r_\beta)^5}$$

¹The reason why this quantity is chosen as a measure of the alignment is that for a system of rods, the average value of S is a measure of the order of the system. If all the rods are aligned parallel to one another as in the case of the ordered phase of a nematic liquid crystal, the average value of S is 1. If the rods have a random orientation, $\langle \cos^2 \theta \rangle = \frac{1}{3}$ and the average value of S is 0. See reference [7].

where r_α is the radius of the lipid chain in state α .

Defining $\delta_{\alpha\beta}$ as the difference of the radius of lipids α and β , $r_\alpha = r_\beta + \delta_{\alpha\beta}$. $V_{\alpha\beta}$ can be approximated as

$$V_{\alpha\beta} \simeq \frac{r_1^5}{r_\alpha^{5/2} r_\beta^{5/2}} \left(1 + \frac{5}{4} \delta_{\alpha\beta} \left(\frac{1}{r_\alpha} - \frac{1}{r_\beta} \right) \right)$$

However $\delta_{\alpha\beta}$ is generally small, and therefore to a good approximation

$$V_{\alpha\beta} \simeq \frac{r_1^5}{r_\alpha^{5/2} r_\beta^{5/2}}$$

This can be written in terms of the areas as

$$V_{\alpha\beta} = V_\alpha V_\beta = \left(\frac{A_1}{A_\alpha} \right)^{5/4} \left(\frac{A_1}{A_\beta} \right)^{5/4} \quad (2.4)$$

where it is assumed that the projections of the lipid chains onto the membrane plane are circles. This form of the interaction is not expected to be valid for the "melted" state because the chains are far from being parallel to each other. A weakening factor is therefore introduced such that $V_{10} = \omega \left(\frac{A_1}{A_{10}} \right)^{5/4}$. ω has been chosen as $\omega = 0.4$ [21].

2.1.3 Relation between Order Parameter and Chain Length

A geometrical relation between the nematic order parameter and the length of a chain can be derived as follows. The assumption that the angles between C-C bonds are 120° implies that the angle between the chain segments and the bilayer normal is either 90° or 30° as can be seen in figure 2.1. The segments making an angle of 90° do not contribute to the chain length. The length of a chain in any conformation is then given by $L = L_1 - n_{90^\circ}$ in units of projected chain segments, where L_1 is the length of the all-*trans* state, and n_{90° denotes the number of segments making an angle of 90° with the bilayer normal. The order parameter of a single chain in a given conformation is therefore

$$S = \frac{8}{5(m-1)} \left(n_{30^\circ} \frac{3\cos^2(30^\circ) - 1}{2} + n_{90^\circ} \frac{3\cos^2(90^\circ) - 1}{2} \right)$$

where n_{30° denotes the number of segments which make an angle of 30° with the bilayer normal. Since the total number of segments is $m - 1$, $n_{30^\circ} + n_{90^\circ} = m - 1$ and the expression for S becomes

$$S = \frac{8}{5(m-1)} \left(\frac{5}{8}(m-1) - \frac{9}{8}n_{90^\circ} \right)$$

This gives the following relation for S in terms of the chain length

$$S = \frac{9}{5} \frac{L}{L_1} - \frac{4}{5} \quad (2.5)$$

From the assumption of constant volume S , can be rewritten in terms of the areas by replacing $\frac{A_1}{A}$ for $\frac{L}{L_1}$. Therefore the nematic order parameter for a lipid chain in a conformational state α is given by

$$S_\alpha = \frac{9}{5} \frac{A_1}{A_\alpha} - \frac{4}{5} \quad (2.6)$$

This relation makes it possible to write the interaction Hamiltonian in terms of the areas of individual lipid chains.

2.1.4 Other Interactions

In addition to the Van der Waals interactions between lipid chains there are several other interactions that must also be considered.

- The hard core interactions are taken into account by allowing the acyl chains to lie on a crystalline lattice.

- The interaction of lipid molecules with water is partially taken into account by the existence of the lattice, because lipid molecules do not form aggregates such as bilayers when they are not in contact with water.

- Repulsive forces due to electrostatic interactions between the polar head-groups and steric interactions from both the polar head groups and the lipid chains. The steric interaction prevent the atoms forming the molecules from occupying the space occupied by other atoms. The origin of this interaction is the repulsion between the electronic clouds of the atoms in the chains. The latter two interactions are taken

into account in an approximate manner by the inclusion in the Hamiltonian of an energy proportional to the total area² [2, 18].

$$E_r = \Pi A \quad (2.7)$$

2.1.5 The Pink Hamiltonian

The contributions to the energy described in previous sections give the following Hamiltonian for the Pink model

$$\mathcal{H} = \sum_i \sum_{\alpha} E_{\alpha} \mathcal{L}_{\alpha,i} - \frac{J_0}{2} \sum_{\langle i,j \rangle} \sum_{\alpha,\beta} I_{\alpha} I_{\beta} \mathcal{L}_{\alpha,i} \mathcal{L}_{\beta,j} + \Pi \sum_i \sum_{\alpha} A_{\alpha} \mathcal{L}_{\alpha,i} \quad (2.8)$$

where the first term is the single chain contribution, the second term is the van der Waals interaction between lipid chains and the third term accounts approximately for steric interactions and interactions between polar heads. The indices i and j refer to lattice sites and the indices α and β refer to conformational states. $\mathcal{L}_{\alpha,i}$ is an occupation variable which is defined as

$$\mathcal{L}_{\alpha,i} = \begin{cases} 1 & \text{if the state of the lipid at site } i \text{ is } \alpha \\ 0 & \text{otherwise} \end{cases} \quad (2.9)$$

The lipid chain at site i can only be in one of the ten conformational states, so that $\sum_{\alpha} \mathcal{L}_{\alpha,i} = 1$. I_{α} is defined as $I_{\alpha} = \omega_{\alpha} V_{\alpha} S_{\alpha}$. Using equations 2.4 and 2.6, I_{α} can be written in terms of the areas as follows

$$I_{\alpha} = \omega_{\alpha} \left(\frac{9 A_1}{5 A_{\alpha}} - \frac{4}{5} \right) \left(\frac{A_1}{A_{\alpha}} \right)^{\frac{1}{2}} \quad (2.10)$$

where $\omega_{\alpha} = 1$ for states 1 to 9 and $\omega_{10} = 0.4$. In the second term of the Hamiltonian the symbol $\langle i, j \rangle$ indicates that the sum is restricted to nearest neighbors. The factor $\frac{1}{2}$ avoids double counting.

²See appendix A for an explanation of two possible interpretations of Π .

	$T_m(K)$	$J_0 \times 10^{-13} \text{erg}$
DMPC	296.9	0.618
DPPC	314.0	0.7099
DSPC	327.9	0.815

Table 2.2: *Experimental transition temperatures and interaction constants for different chain lengths.*

2.2 Monte Carlo Simulation

Statistical Mechanics provides a powerful technique for calculating all the thermodynamic functions of the system from its Hamiltonian. For simple Hamiltonians such as a gas of non interacting particles, it is possible to obtain all the thermodynamic functions of the system analytically. For complicated Hamiltonians approximation methods can be used for solving the problem analytically, or one can solve the problem numerically using a computer. Monte Carlo integration methods (described in appendix B) and in particular the Metropolis algorithm (also described in appendix B) provide a way to calculate numerically the integrals involved in the partition function. The implementation of the Metropolis algorithm for pure lipid systems is described in appendix B. In this section numerical results of a Monte Carlo simulation of the Pink model are presented for systems with three different chain lengths, corresponding to DMPC ($m = 14$), DPPC ($m = 16$) and DSPC ($m = 18$) lipid bilayers. The interaction constant, J_0 , depends on the chain length and is fitted for the three systems in order to reproduce the experimental transition temperatures [14]. Table 2.2 shows the experimental transition temperatures [30] and the values of the interaction constant for the three systems studied. Π was set equal to 30dyn/cm [2].

The temperature dependence of the average internal energy and specific heat are shown in figure 2.3. The specific heat was calculated from the energy fluctuations as

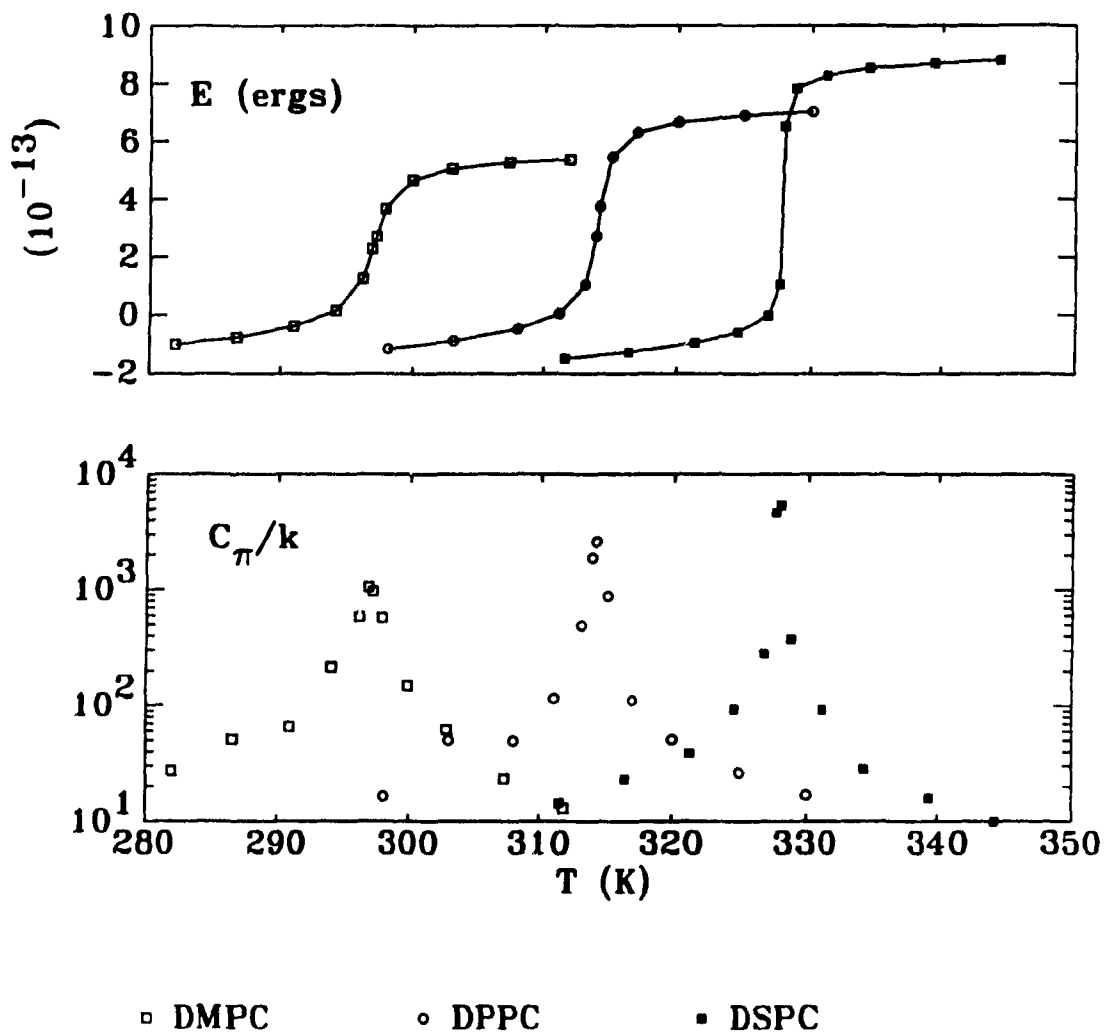


Figure 2.3: Energy per molecule and specific heat per molecule of DMPC, DPPC and DSPC bilayers.

follows

$$C_p = \frac{1}{kT^2} (\langle \mathcal{H}^2 \rangle - \langle \mathcal{H} \rangle^2)$$

In the figure, the specific heat has been divided by the number of lipid molecules.

The temperature dependence of the average area, average nematic order parameter and isothermal compressibility are shown in figure 2.4. The isothermal compressibility \mathcal{K}_T is calculated from the fluctuations in the area

$$\mathcal{K}_T = \frac{1}{kT \langle A \rangle} (\langle A^2 \rangle - \langle A \rangle^2)$$

where A is the total area. In the figure, the isothermal compressibility has not been

divided by the number of lipid molecules. The equations for the specific heat and isothermal compressibility are derived in appendix A.

The results show an abrupt jump in the energy, area and order parameter with a low temperature phase known as *gel* phase characterized by the 9 lowest energy conformational chain states, and a high temperature phase known as *fluid* phase characterized by the 10th conformational state. A mean field solution of the model which does not account for thermal fluctuations predicts a first order phase transition with jump discontinuities for the energy, area and nematic order parameter [2, 25]. The computer simulation which fully accounts for thermal fluctuations predicts an abrupt but continuous jump for these functions [21] as can be seen in figures 2.3 and 2.4. Although strictly speaking there is no phase transition predicted by the simulation³ we will refer to this abrupt jump as a transition and to the temperature at which the jump occurs as the transition temperature. The transition is accompanied by strong fluctuations as can be seen from the results for the specific heat and lateral area compressibility figures. This is an indication that the system is close to a critical point.

2.2.1 Effect of Acyl Chain Length

From figures 2.3 and 2.4 it can be seen that the longer the chain the more abrupt the transition. As the chain length decreases, the transition becomes smoother and more continuous. This is because the thermal fluctuations become larger at the “wings” of the transition temperature with decreasing chain length. As the chain length decreases, the energy differences between the two phases becomes smaller as shown in figure 2.3. At the “wings” of the transition temperature an enhancement of the response functions is observed for decreasing acyl chain length as can be seen from the figures showing the specific heat and lateral compressibility. At the transition temperature, the peak in the response functions decreases as the chain length decreases. This

³We have recently shown that for the set of parameters that we use here, there is no phase transition predicted by the simulation and the system is beyond a critical point [3]

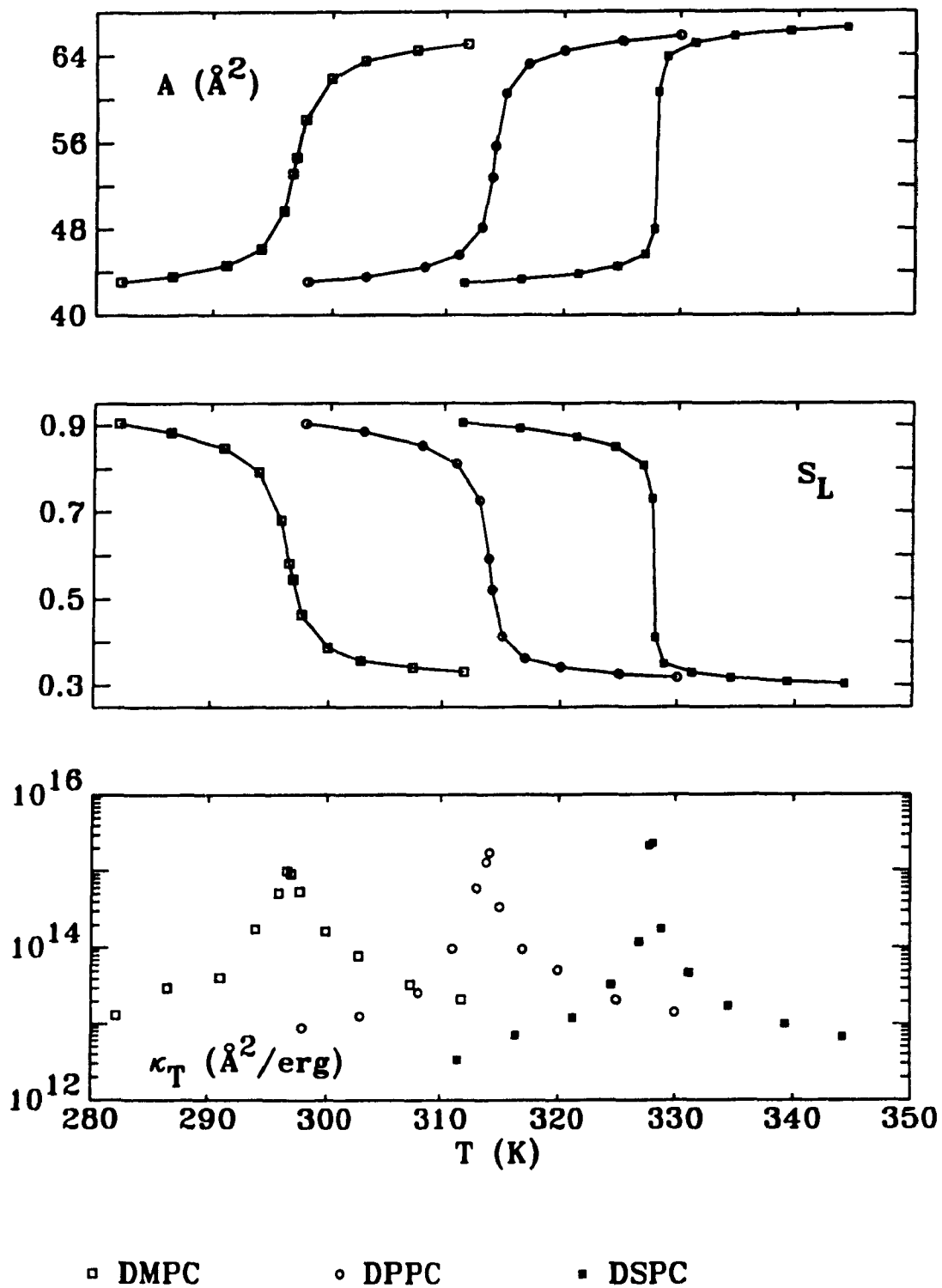


Figure 2.4: Area per molecule, nematic order parameter and isothermal compressibility of DMPC, DPPC and DSPC bilayers.

implies that at the transition temperature the fluctuations increase with increasing chain length.

2.3 Passive Permeability

Ion transport in biological membranes is mediated by channels or pores that are formed by proteins which are able to discriminate between different type of substances and can be open or close to the flux of matter. This is the main form of transport of matter across biological membranes. There is however another type of transport known as passive transport, which is due to diffusion of matter across the membrane.

The pure lipid bilayer is characterized by an extremely low permeability to ions diffusing passively through it. However near the fluid to gel phase transition an enhancement of the passive ion permeability had been experimentally observed at both sides of the transition [23].

At temperatures far away from the transition temperature, domains of lipids in states, which are characteristic of the unstable phase at that temperature, occur rarely and are due to thermal fluctuations. However as the transition temperature is approached, the fluctuations increase and an increase in the number of clusters or domains of the unstable phase appear in the stable phase. There are thus more fluid clusters in the gel phase, and more gel clusters in the fluid phase.

It has been proposed [4, 6, 16, 23] that the enhancement of the passive ion permeability near the gel to fluid transition is related with the amount of interface between gel and fluid domains. At the interfacial region, defects due to bad packing make the membrane leaky and allow the ions to permeate it. A formalism for calculating the passive ion permeability of the membrane is presented in the next few sections.

2.3.1 Number of Particles Striking a Surface

In this section we follow reference [27]. Consider an element of area dA of a wall of a container with a gas. Then consider those particles in the vicinity of the wall, whose velocity lies between v and $v+dv$. Such particles suffer a displacement vdt in the time interval dt . All the particles which lie in the infinitesimal cylinder of cross section dA and length vdt that makes an angle θ with the z axis will strike the wall

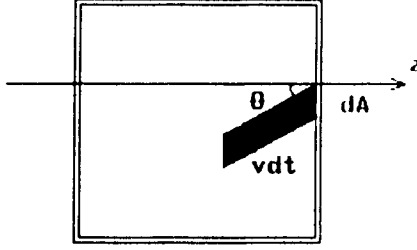


Figure 2.5: Particles colliding with an element of area of a wall. Adapted from reference [27]

in the time interval dt .

If $f(\mathbf{v})$ is the velocity distribution for the gas, $f(\mathbf{v})d^3\mathbf{v}$ is the mean number of particles per unit volume with velocity between \mathbf{v} and $\mathbf{v} + d\mathbf{v}$. The number of particles that strike the area dA in the time interval dt is equal to $(dAvcos\theta dt) \cdot (f(\mathbf{v})d^3\mathbf{v})$ because the volume of the cylinder is $dAvdtcos\theta$.

The total number of particles that strike a unit area of the wall per unit time is given by

$$\Phi = \int_{v_z > 0} v \cos\theta f(\mathbf{v}) d^3\mathbf{v}$$

The integral is over velocities for which the z component is positive, since the molecules with $v_z < 0$ travel away from the wall. If the gas is in thermal equilibrium, $f(\mathbf{v})$ depends only on the magnitude of \mathbf{v} . The volume element is given by $d^3\mathbf{v} = v^2 dv \sin\theta d\theta d\phi$, so that the integral for Φ becomes

$$\Phi = \int_0^\infty v^3 f(v) dv \int_0^{\pi/2} \cos\theta \sin\theta d\theta \int_0^{2\pi} d\phi$$

The integration over θ evaluated between 0 and $\frac{\pi}{2}$ satisfies the condition $v_z > 0$. This gives the equation

$$\Phi = \pi \int_0^\infty v^3 f(v) dv$$

which can be related to the mean velocity of a particle in the gas, as shown below.

The mean velocity of a particle in a gas is given by

$$\langle v \rangle = \frac{1}{n} \int v f(\mathbf{v}) d^3\mathbf{v} = \frac{4\pi}{n} \int v^3 f(v) dv \tag{2.11}$$

where $n = \frac{N}{V}$ is the total number of particles per unit volume. This expression leads to the result

$$\Phi = \frac{n}{4} \langle v \rangle$$

It is important to remember that Φ is the number of molecules which strike a unit area of the wall per unit time. Therefore the number of molecules striking a wall of area A in the time interval dt is given by

$$dN = \frac{n}{4} \langle v \rangle A dt \quad (2.12)$$

Mean Velocity of a Particle in a Gas

The classical velocity distribution for a particle of a dilute gas in thermal equilibrium is the Maxwell distribution given by

$$f(v) = n \left(\frac{m}{2\pi kT} \right)^{3/2} e^{-\frac{mv^2}{2kT}} \quad (2.13)$$

where $n = \frac{N}{V}$ is the total number of particles per unit volume and m is the mass of the particle.

The mean velocity of a particle in a gas is given by equation 2.11. For a gas with a Maxwell velocity distribution the mean velocity is given by the following expression

$$\langle v \rangle = 4\pi \left(\frac{m}{2\pi kT} \right)^{3/2} \int_0^{\infty} v^3 e^{-\frac{mv^2}{2kT}} dv$$

which after integration is

$$\langle v \rangle = \sqrt{\frac{8kT}{\pi m}} \quad (2.14)$$

2.3.2 Model of Passive Ion Permeability

From section 2.3.1, the number of particles striking a wall of area A of a container in a time interval dt is given by

$$dN \propto n \langle v \rangle A dt$$

Consider a liposome⁴ of volume V and internal area A with an internal ion concentration n . In this case, the wall is formed by the lipid bilayer and the particles striking the wall are the ions. The number of ions leaving the liposome in a time interval dt is then given by

$$dN_L \propto n \langle v \rangle APdt$$

where P is the probability of an ion crossing the membrane after it has collided it. $n = \frac{N_R}{V}$ is the number of ions inside the liposome (or *retained* by the liposome) per unit volume at a certain time.

If we assume that the ion concentration is small inside the liposome, we can assume a Maxwell velocity distribution for the ion gas and the mean velocity of a particle is given by equation 2.14. Therefore the number of ions leaving the liposome in a time interval dt is

$$dN_L = cA^{-1/2}T^{1/2}PN_Rdt$$

where c is a constant.

Now, the number of particles retained by the liposome plus the number of particles that leave the liposome is equal to the number of particles in the liposome at time $t = 0$, so $N_L(t) + N_R(t) = N_R(0)$. Therefore, we can write an equation for the number of particles retained in the liposome as follows

$$\frac{dN_R}{N_R} = -cA^{-1/2}T^{1/2}Pdt$$

This expression, after integration, gives an exponential time dependence for the fraction of ions retained in the liposome

$$\frac{N_R(t)}{N_R(0)} = e^{-cA^{-1/2}T^{1/2}Pt}$$

In the model used in this thesis [4, 6], the probability of an ion crossing the membrane is considered as a sum of three terms

$$P(T) = a_b(T)p_b + a_c(T)p_c + a_i(T)p_i$$

⁴Bilayers made in the form of spherical vesicles are called liposomes

where b stands for *bulk*, c for *clusters*, and i for *interface*. p_b , p_c and p_i denote the corresponding probabilities of crossing the membrane, and a_b , a_c and a_i are the fractional areas occupied by the bulk, the clusters and the interface.

This model of passive ion permeability requires the knowledge of the fractional areas occupied by the bulk, the clusters and the interface, as well as the values of the transfer probabilities.

A constraint is imposed on the transfer probabilities assuming that the interfacial area is associated with a very high transfer probability $p_i \gg p_b, p_c$. The principal hypothesis is that at the interfacial regions defects due to bad packing make the membrane leaky and allow the ions to permeate it more readily. The model does not assume a specific mechanism by which the transport is performed.

2.3.3 Analysis of Configurations

The Monte Carlo simulations performed for the Pink Hamiltonian allow us to examine the spatial structure of the membrane and thus permit an analysis of membrane heterogeneity and domain formation in the transition region.

A visual examination of the snapshot of a microscopic configuration allows us to observe clusters of the minority phase in the majority phase. However a systematic study of the configurations requires a formal (although somewhat arbitrary) definition of the concepts cluster, bulk and interface. For simplicity we will refer to fluid clusters in a bulk gel phase, but the same definitions apply for the high temperature phase with the exchange of the words *gel* and *fluid*.

Clusters are defined by means of a nearest neighbor connectivity criterion. Two sites a and b each containing a chain in the fluid state are part of the same cluster if, starting at one of the sites (let say a) one can find a "path" from a to b of sites with chains in the fluid state, with the restriction of moving only to nearest neighbor sites.

The definition of *cluster* also involves a decision about how many fluid chains have to be together, in order to consider that they are forming a cluster. In order to study the cluster distribution as a function of temperature, only clusters formed by three

or more fluid chains are considered in this thesis. The interface is defined as the set of the sites other than clusters connected via a nearest neighbor bond to a cluster. The bulk is defined as the set of the sites that are neither clusters or interface.

The clusters fluctuate in position and size, and although they have an equilibrium distribution function, they are not macroscopic entities. As the transition is approached, both the average cluster size and the maximum cluster size are enhanced as can be seen in figure 2.6. This occurs for all three systems under consideration. It is however interesting to note that the number of clusters does not always increase as the transition temperature is approached. Figure 2.6 show that the number of clusters increases as the transition is approached at temperatures far away from the transition. However close to the transition temperature, the number of clusters actually decreases. This implies that clusters are aggregating to form larger clusters.

2.3.4 Model Permeability and Monte Carlo Simulations

A cluster analysis of the configurations obtained from the Monte Carlo simulation permit the calculation of the fractional areas occupied by the clusters, the bulk and the interfaces.

A cut-off of 14 is chosen implying that clusters occupying less than 14 lattice sites will be considered part of the bulk and *clusters of clusters*, i.e. small domains of the majority phase within a cluster, smaller than 14 lattice sites will be considered part of the cluster.⁵

Snapshots of configurations below and above the transition temperature are presented for DMPC in figure 2.7. In part b) of the figure, the minority phase regions are shown, the fluid regions are shown for $T < T_m$, and the gel regions are shown for $T > T_m$. The interfacial regions consistent with a cut-off of 14 are shown in part a) of the same figure. It is easy to see that the amount of cluster regions as well as the amount of the interfacial regions increase as the transition temperature is approached

⁵The width of the permeability peak depends on the size of the defect required for passage of the ion. In this model, it depends on the cut-off for the cluster size. A larger cut-off leads to a sharper peak.

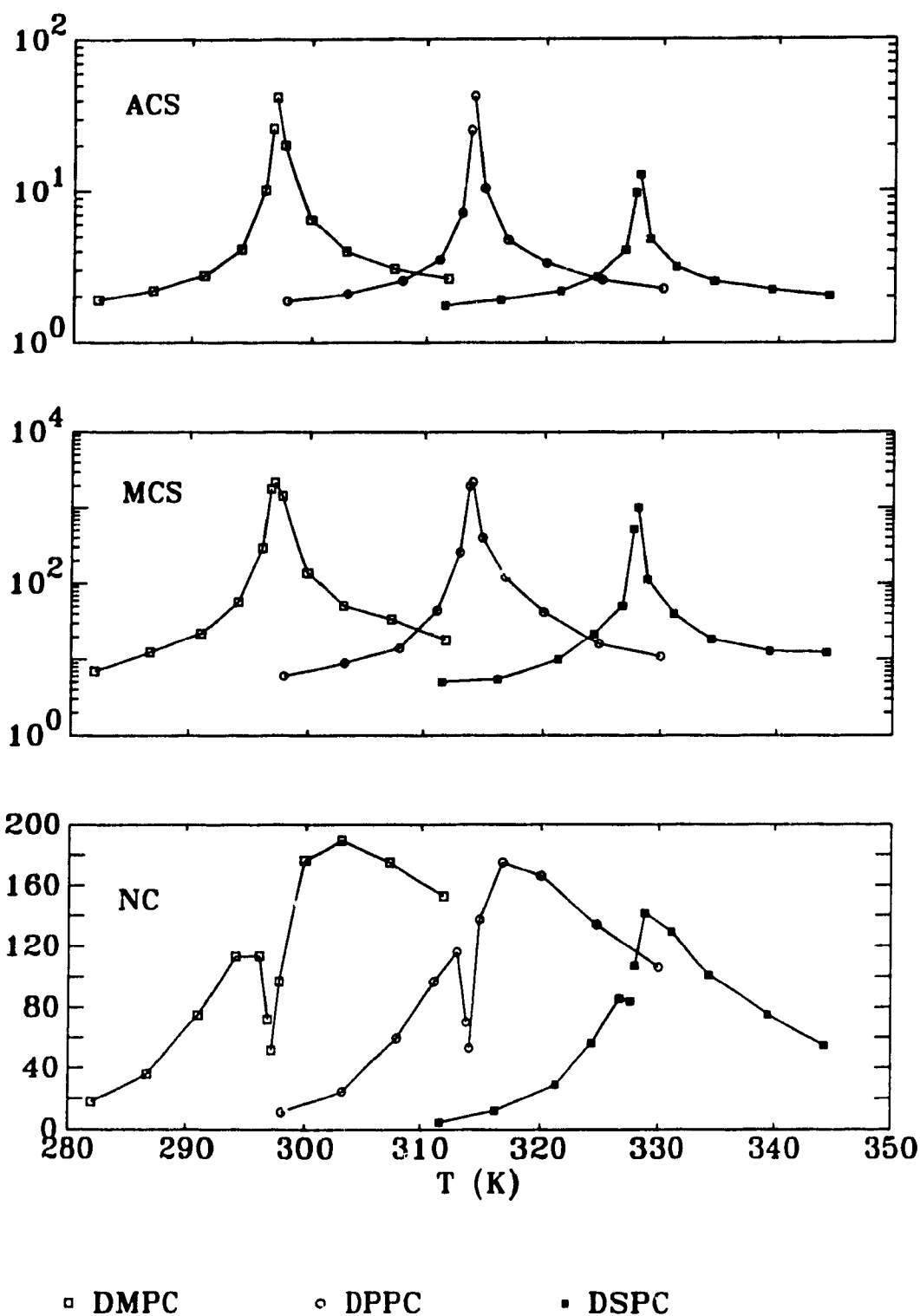


Figure 2.6: Average cluster size, maximum cluster size and number of clusters as a function of temperature for DMPC, DPPC and DSPC. The first two of these are expressed in units of the number of molecules.

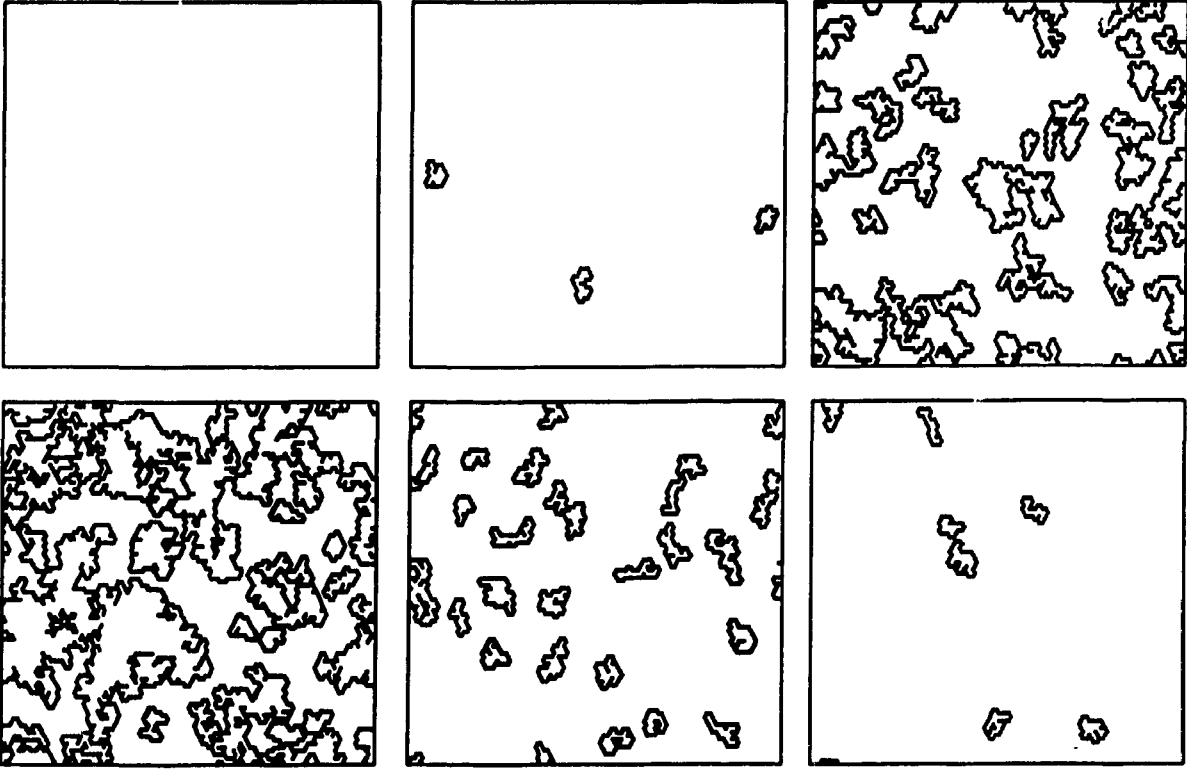
from either side.

The dependence of the fractional areas on temperature is shown in figures 2.8. As the transition temperature is approached from either side, the area occupied by the clusters increases and has a peak at T_m . Consequently the area of the bulk decreases as the transition is approached. The interfacial fractional area also increases as the transition is approached. However very close to the transition temperature, a decrease of the interfacial fractional area occurs for two of the systems under consideration when approaching from the high temperature phase. This is related with the fact that clusters aggregate near T_m . The fractional interfacial area therefore has a peak at a temperature slightly higher than T_m .

The model of section 2.3.2 requires a knowledge of the regional transfer probabilities for the calculation of the permeability. Since the restriction $p_i \gg p_b, p_c$ is part of the basic assumptions of the model, p_i is taken to be equal to 1, and p_b and p_c are fitted in order to reproduce the experimental curve for the permeability of DPPC vesicles to Na^+ ions. The values for p_b and p_c were found to be $p_b = 0.0066, p_c = 0.11$ below T_m , and $p_b = 0.11, p_c = 0.0066$ above T_m [6]. With this choice of values the model assigns a higher probability of transfer to fluid regions than to gel regions. The calculation of these transfer probabilities from first principles requires a knowledge of the specific mechanism of transport across the membrane.

The above information makes it possible to calculate the quantity $R = (\frac{T}{A})^{1/2} P$ which is known as the relative permeability. The relative permeability is proportional to the logarithm of the fraction of ions retained in the liposome. Figure 2.9 shows an enhancement of the relative permeability as the transition temperature is approached. This is in agreement with the experimental observations of Papahadjopoulos [23]. The permeability has a peak at a temperature slightly greater than T_m for two of the systems under consideration. The two points that appear disconnected in the figures are below and above the transition temperature respectively. From the figures it is clear that the model predicts a gap in the passive permeability at the transition temperature. The gap is a consequence of the model and is due to the discontinuity in

a



b

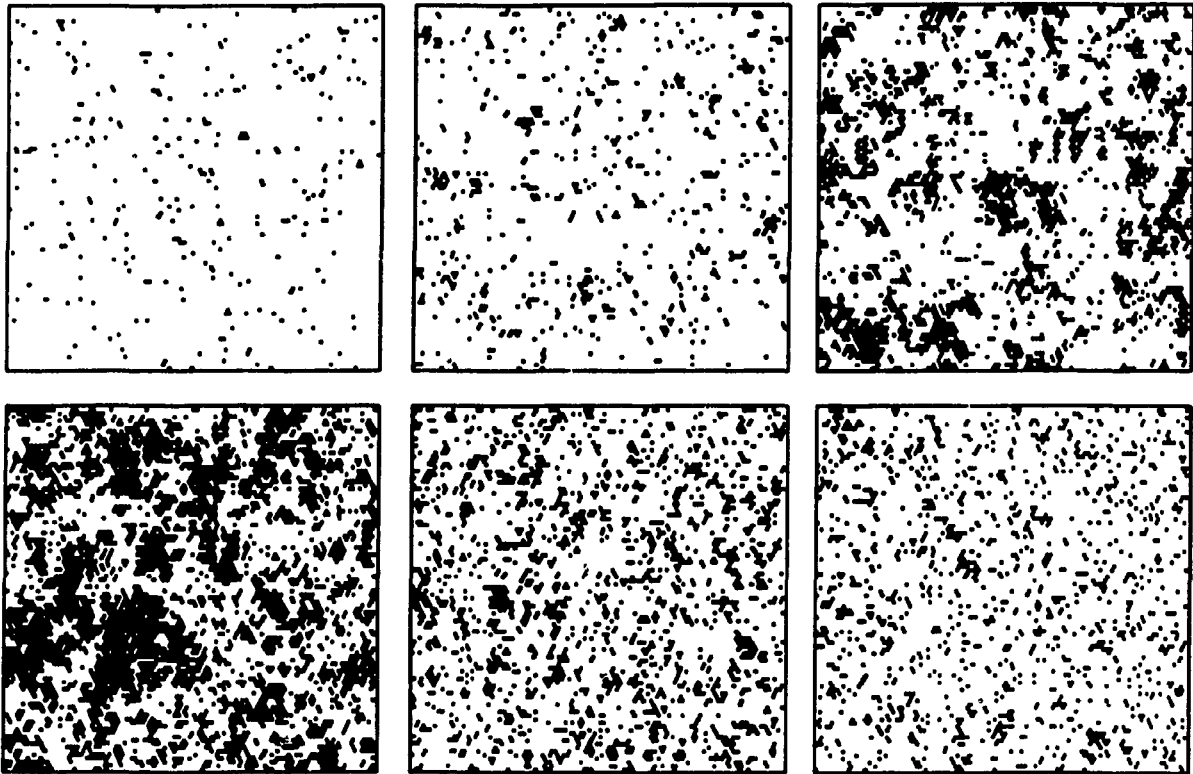


Figure 2.7: Snapshots of configurations near T_m for DMPC are shown on the previous page.

a) Interfacial regions consistent with a cut-off of 14.

b) Regions with the minority phase are shown. The upper row shows regions of fluid for values of T/T_m approaching the transition. From left to right: 0.95, 0.98 and 0.997. The lower row shows regions of gel for values of T/T_m going away from the transition. From left to right: 1.003, 1.02 and 1.05.

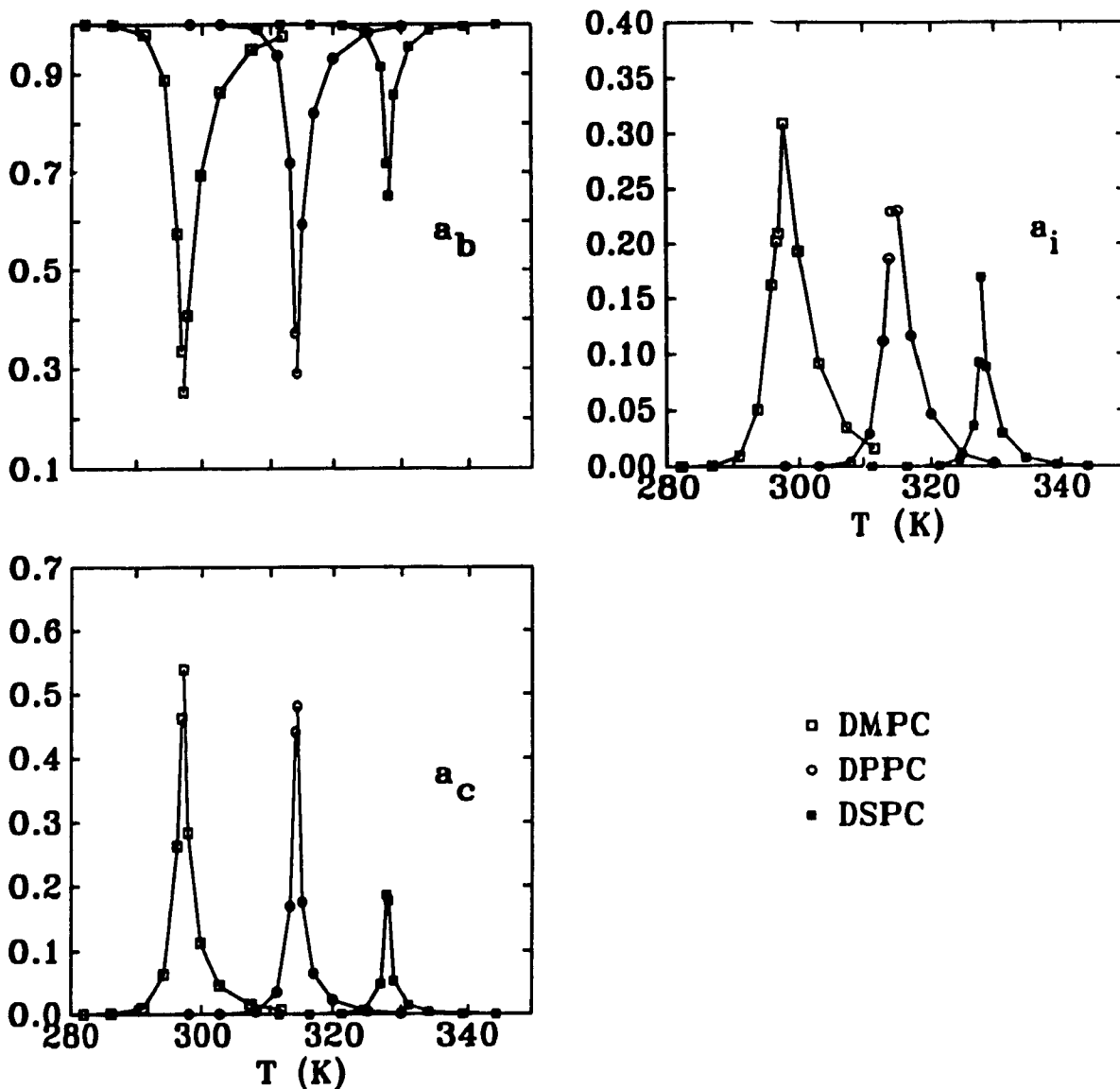


Figure 2.8: Fractional areas of bulk, clusters and interface for DMPC, DPPC and DSPC.

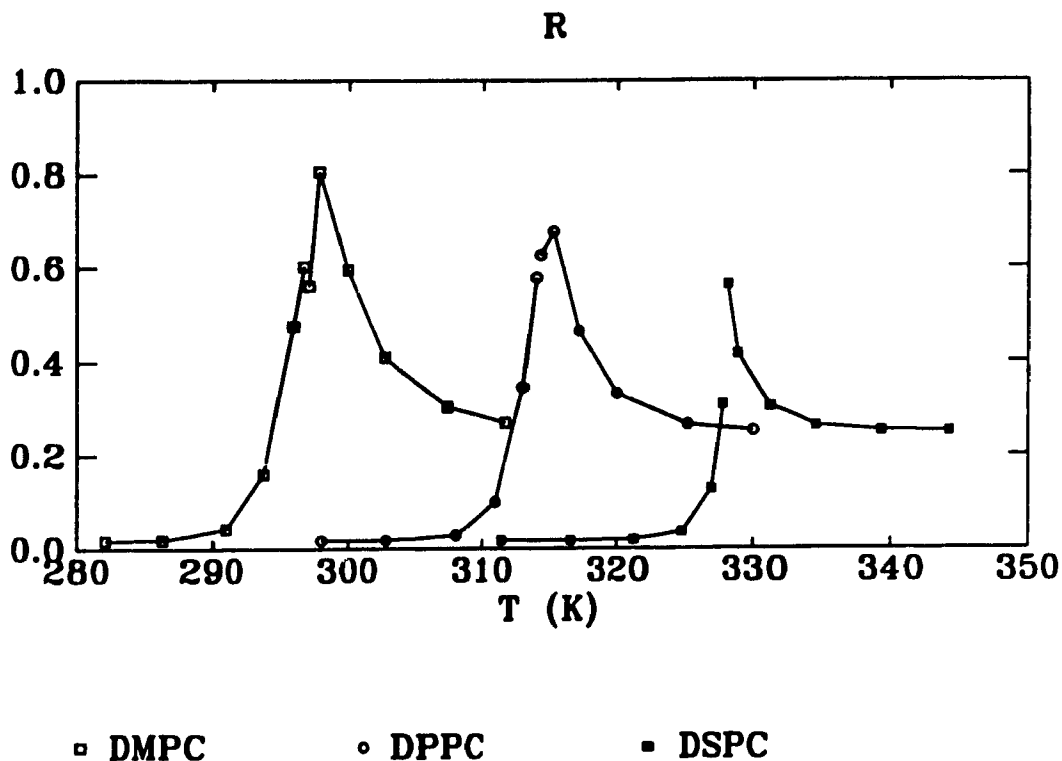


Figure 2.9: Relative permeability of DMPC, DPPC and DSPC bilayers. The units are arbitrary.

the values of p_b and p_c at T_m . The only case in which the model predicts a zero gap is when the fractional areas of bulk and cluster are equal at the transition temperature. This is not the case in general for the model used here since the definition of the interface implies that it has an associated area. We do not expect to see a gap in experimental measurements at the transition region.

2.3.5 Effect of Acyl Chain Length on the Permeability

It was shown in section 2.2.1 that as the length of the chain decreases, an enhancement of the response functions⁶ occur at the “wings” of the transition i.e., at the “wings” of the transition the thermal fluctuations increase as the chain length decreases. This observation implies that the average cluster size, the maximum cluster size and the total number of clusters increase as the chain length decreases. Figure 2.6 shows how

⁶The response functions referred to are the specific heat and the isothermal compressibility.

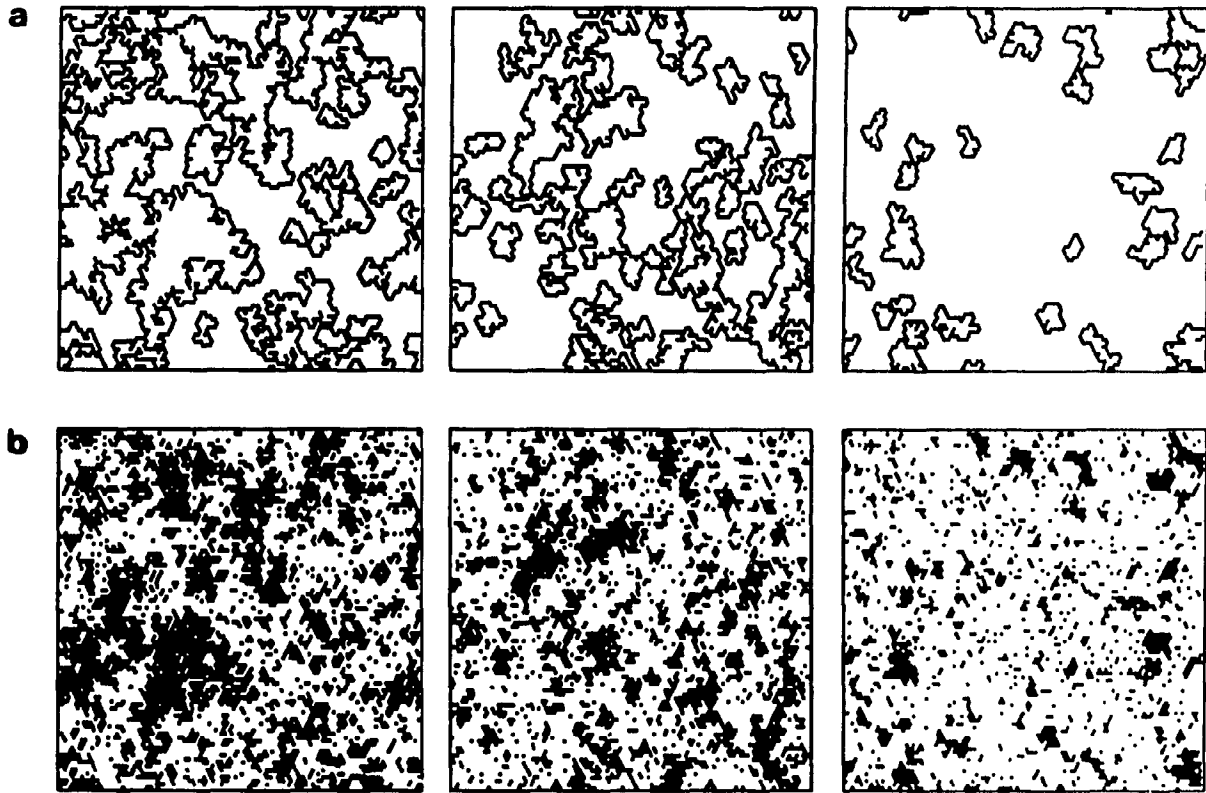


Figure 2.10: Snapshots of configurations for different chain lengths at $T/T_m = 1.003$

a) Interfacial regions consistent with a cut-off of 14.

b) Regions of the gel phase are shown. The left figure corresponds to DMPC ($m = 14$), the middle one corresponds to DPPC ($m = 16$) and the right one corresponds to DSPC ($m = 18$)

the average cluster size, the maximum cluster size and the average number of clusters increase with decreasing chain length. Consequently, an enhancement of the cluster and interface fractional areas is observed on both sides of the transition temperature for decreasing chain length, and a concomitant decrease in the bulk fractional area is observed as shown in figure 2.8.

Snapshots of configurations for three chain lengths are shown in figure 2.10. For this figure, the reduced temperature T/T_m is fixed above the transition temperature. In part b) of the figure the gel phase regions are shown. In part a) of the same figure, the interfacial regions consistent with a cut-off of 14 are shown. It is clear from the snapshots that the number of sites forming the clusters and the number of sites in the interfacial regions, decrease as the chain length increases.

The net result is that in the transition region the relative permeability increases

with decreasing chain length as shown in figure 2.9. This result is very reasonable since the thicker the membrane, the more difficult it is to cross it.

It is clear from the figure that the model predicts that the permeability is independent of chain length at very high temperatures. This is a result of using the same probabilities of transfer for bilayers composed of lipids with different chain length. This assumption is obviously incorrect, but does not affect strongly the permeability in the transition region.

Chapter 3

Lipid-Cholesterol Bilayers

Cholesterol is a determinant for membrane fluidity [1]. Cholesterol molecules orient themselves in a bilayer with their hydroxyl groups close to the polar head groups of the phospholipid bilayer at the level of the glycerol group. The steroid ring structure partially immobilizes the regions of the hydrocarbon chains close to the head group. At high cholesterol concentrations, cholesterol has the effect of preventing the hydrocarbon chains from crystallizing.

The experimentally determined phase diagram¹ of DPPC bilayers containing cholesterol is shown in part *a*) of figure 3.1 [17, 13, 33]. The phase diagram shows three different phases, a solid ordered phase *s_o*, a liquid disordered phase *l_d*, and a liquid ordered phase *l_o* at high cholesterol concentrations. The first letter in this notation refers to the lateral organization. *s* is used when the phase has a lateral crystalline structure and *l* is used when there is no lateral crystalline structure. The second letter refers to the acyl chain conformational order. *o* is used for a phase characterized by chains with a high conformational order and *d* is used for a phase characterized by chains in high energy conformational states. The solid-ordered phase is equivalent to the gel phase of pure lipid bilayers and the liquid-disordered phase is equivalent to the liquid crystalline phase of pure lipid bilayers.

The experimental phase diagram of figure 3.1 and thermodynamic quantities such

¹The phase diagram does not include the phases related to the ripple phase

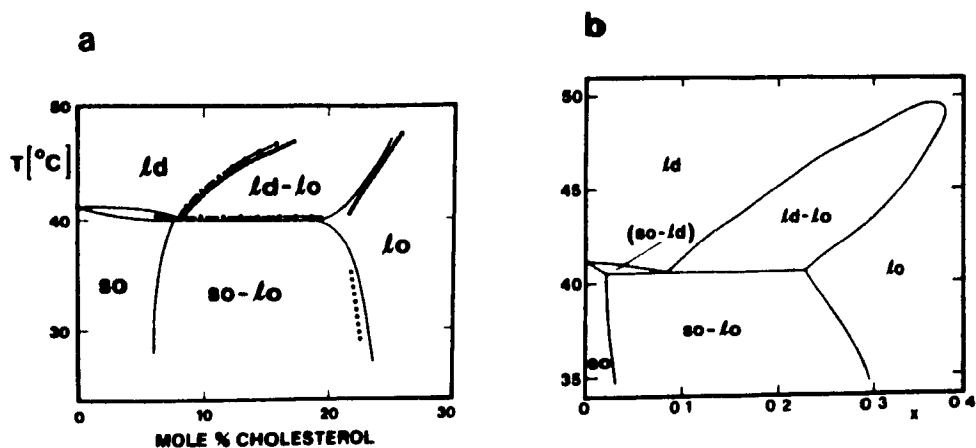


Figure 3.1: a) Experimental phase diagram of DPPC-cholesterol bilayers. The phases are denoted by so (solid-ordered), ld (liquid-disordered) and lo (liquid-ordered). The phase diagram was obtained by a variety of experimental techniques.

b) Theoretical phase diagram obtained from the mean field solution.

as the specific heat of lipid-cholesterol bilayers have been successfully described by a model proposed by Ipsen *et al.* [12]. The model gives a description of lipid monolayers and bilayers in terms of two degrees of freedom, one for the chain conformations and the other for positional order. It is based on the Pink model combined with a modified multi-state Potts model which is used to treat the positional degrees of freedom in an approximate way. The Pink model is described in detail in section 2.1. The modified Potts model assigns a Potts variable to each lattice site. The Potts variables describe the orientation of crystalline domains with which the chain on the lattice site is associated. A domain boundary energy is modeled by allowing acyl chains to interact with a repulsive energy, J_P , if they are in different Potts states and if they are in one of the first nine Pink conformational states. In all other cases the interaction is zero. This is because there are not crystalline domains in the fluid phase characterized by the 10th conformational state. This model was originally proposed for pure lipid bilayers, but it is particularly important for bilayers containing cholesterol. Cholesterol inhibits the formation of a crystalline structure but at the same time makes the acyl chains rigid. Therefore a model with two degrees of freedom, one for the positional order and another for the conformational order is quite appropriate.

The Potts interaction between cholesterol and an acyl chain in one of the nine

conformational states characteristic of the gel state is assumed to be much smaller than the Potts interaction between acyl chains. The model has been solved in a mean field approximation [12]. The parameters for the lipid-cholesterol interactions were chosen to give a qualitative phase diagram as close as possible to the experimental phase diagram. The theoretical phase diagram shown in part b) of figure 3.1 is in good qualitative agreement with the experimental phase diagram. There is a narrow coexistence region between the solid ordered and the liquid disordered phases at low cholesterol concentrations, and a liquid ordered phase at high cholesterol concentrations.

Cholesterol dissolves easily in a phase with no crystalline structure but prefers the neighboring acyl chains to be in a high conformational order. The result is that at low cholesterol concentrations cholesterol prefers both lipid phases equally, but at high cholesterol concentrations, it induces conformational order in the fluid state and inhibition of the crystalline structure in the low temperature phase and a liquid-ordered phase occurs. At this point the conformational and the positional degrees of freedom are decoupled. The problem with the Potts model is that it is difficult to interpret the Potts variables microscopically.

Cruzeiro-Hansson *et al.* therefore proposed a reduced model which is correct for low cholesterol concentrations and which does not involve the Potts variables. The model was then used to predict the permeability of DPPC-cholesterol systems. It is the model used in this thesis to study the chain length dependence of the thermodynamic quantities and the permeability of lipid-cholesterol systems. The model is presented in the next section and is used to study DMPC, DPPC and DSPC lipid bilayers containing small amounts of cholesterol.

3.1 Model of Lipid-Cholesterol Bilayers

Cruzeiro-Hansson *et al.* [5] have studied a simple multi-state lattice model that gives the correct phase behavior at low cholesterol concentrations. The model is an exten-

sion of the Pink model to include the interaction between lipid chains and cholesterol-like molecules. The model therefore can only account for the chain melting transition but not for the change in the lateral crystalline structure. We will continue to use the terms *gel* and *fluid* through the rest of the thesis to refer to the low and high temperature phases respectively. The interaction between lipid molecules and cholesterol is modeled by assuming that cholesterol is a bulky, stiff molecule with no internal degrees of freedom. The cholesterol is assigned an area of 32\AA^2 .

In the Pink model, lipid-lipid interactions are written as the product of two terms. Each term depends only on the state of the lipid at one of the sites, i.e. the interaction between two neighboring lipid chains in states α and β is

$$E_{int} = -J_0 I_\alpha I_\beta$$

where I_α is given by equation 2.10. We assume the same form as for the Hamiltonian of the pure system, and therefore the interaction between a lipid in state α and a neighboring cholesterol is assumed to be

$$E_{int} = -J_0 I_\alpha I_C$$

where I_C is a constant related to the Van der Waals interaction between the hydrophobic part of the cholesterol molecule and the lipid chain. In an analogous way the cholesterol-cholesterol interaction is assumed to have the form

$$E_{int} = -J_0 I_C I_C$$

The lipid-cholesterol system has therefore the following Hamiltonian

$$\begin{aligned} \mathcal{H} = & \sum_i \sum_\alpha E_\alpha \mathcal{L}_{\alpha,i} + \Pi \sum_i \sum_\alpha A_\alpha \mathcal{L}_{\alpha,i} + \Pi \sum_i A_C \mathcal{L}_{C,i} - \\ & - \frac{J_0}{2} \sum_{\langle ij \rangle} \sum_{\alpha\beta} I_\alpha I_\beta \mathcal{L}_{\alpha,i} \mathcal{L}_{\beta,j} - \frac{J_0}{2} \sum_{\langle ij \rangle} I_C^2 \mathcal{L}_{C,i} \mathcal{L}_{C,j} \\ & - \frac{J_0}{2} \sum_{\langle ij \rangle} \sum_\alpha I_\alpha I_C (\mathcal{L}_{\alpha,i} \mathcal{L}_{C,j} + \mathcal{L}_{\alpha,j} \mathcal{L}_{C,i}) \end{aligned} \quad (3.1)$$

where $\mathcal{L}_{C,i}$ is an occupation variable which is defined as

$$\mathcal{L}_{C,i} = \begin{cases} 1 & \text{if there is a cholesterol molecule at site } i \\ 0 & \text{otherwise} \end{cases} \quad (3.2)$$

The Hamiltonian in equation 3.1 contains two new parameters A_C and I_C relative to the Hamiltonian for the pure lipid bilayer (equation 2.8). I_C was determined by the requirement that the phase diagram resemble that of phosphatidylcholine-cholesterol mixtures for cholesterol concentrations up to 10% i.e. with an extremely narrow coexistence region and a very small decrease in the melting temperature. The mean field calculation done by Cruzeiro-Hansson *et al.* [5] and J. Ipsen [14] indicate that $I_C = 0.45$ is a good choice for the three systems considered in this thesis: DMPC, DPPC, DSPC.

The Hamiltonian in equation 3.1 is not specific for cholesterol. It can also represent any other bulky, stiff, amphiphilic molecule.

3.1.1 Monte Carlo Simulations

As in the case of pure lipid bilayers, Monte Carlo simulations are used to determine the thermodynamic properties of the system. The implementation of the Metropolis algorithm for lipid-cholesterol systems is described in appendix B. Systems with low cholesterol concentrations, $x_C = 0.05, 0.10, 0.15$, are studied.

Figures 3.2, 3.3 and 3.4 show the average area per molecule A of the membrane as a function of temperature for several cholesterol concentrations. From the figures it is clear that the transition becomes smoother and the difference in the areas of the two phases is smaller than for the pure system. Nevertheless, the relation between the area and the cholesterol concentration below the transition is quite complicated. In order to observe the effect of cholesterol on the lipid chains, we calculate the lipid area per lipid molecule A_L given by

$$A_L = \frac{A - x_C A_C}{1 - x_C}$$

where A_C is the area of a single cholesterol molecule, A is the total area per molecule and x_C is the cholesterol concentration of the system. Figures 3.2, 3.3 and 3.4 show that cholesterol has an expansion effect in the gel phase and a contraction effect in the fluid phase. This is also indicated by the average nematic order parameter of the lipid

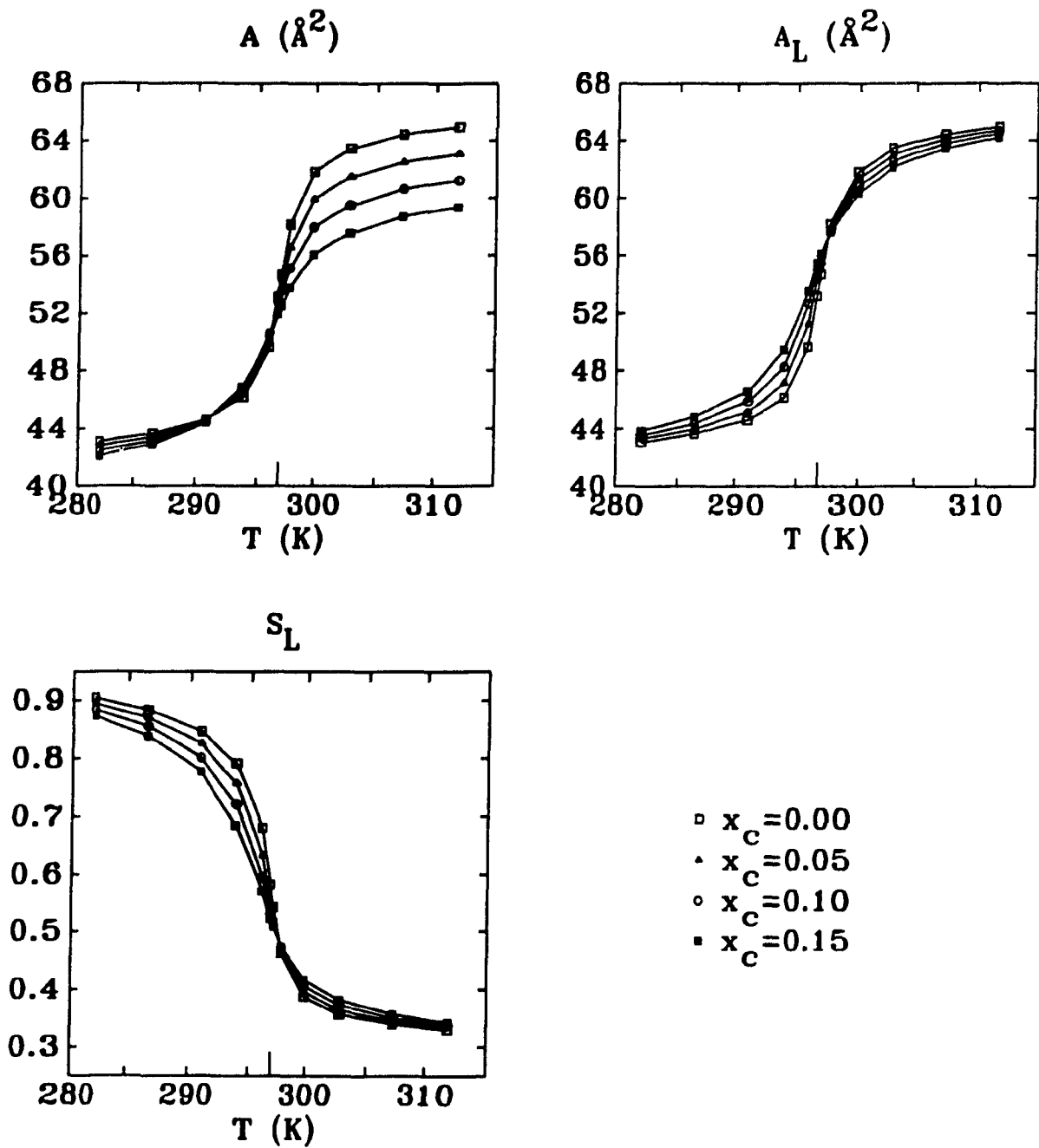


Figure 3.2: Total area per molecule, lipid area per lipid molecule and lipid order parameter of DMPC-cholesterol bilayers.

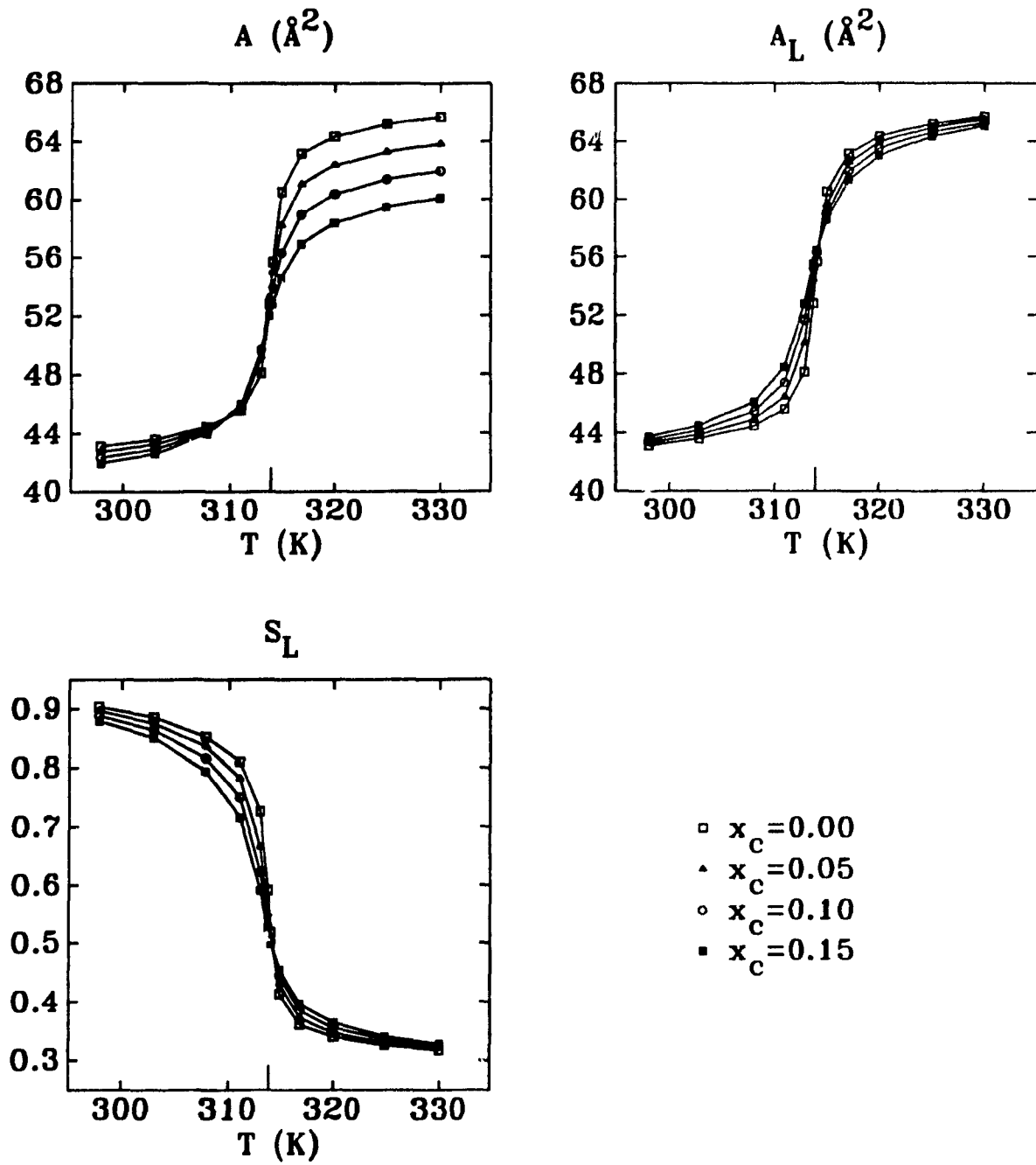


Figure 3.3: Total area per molecule, lipid area per lipid molecule and lipid order parameter of DPPC-cholesterol bilayers.

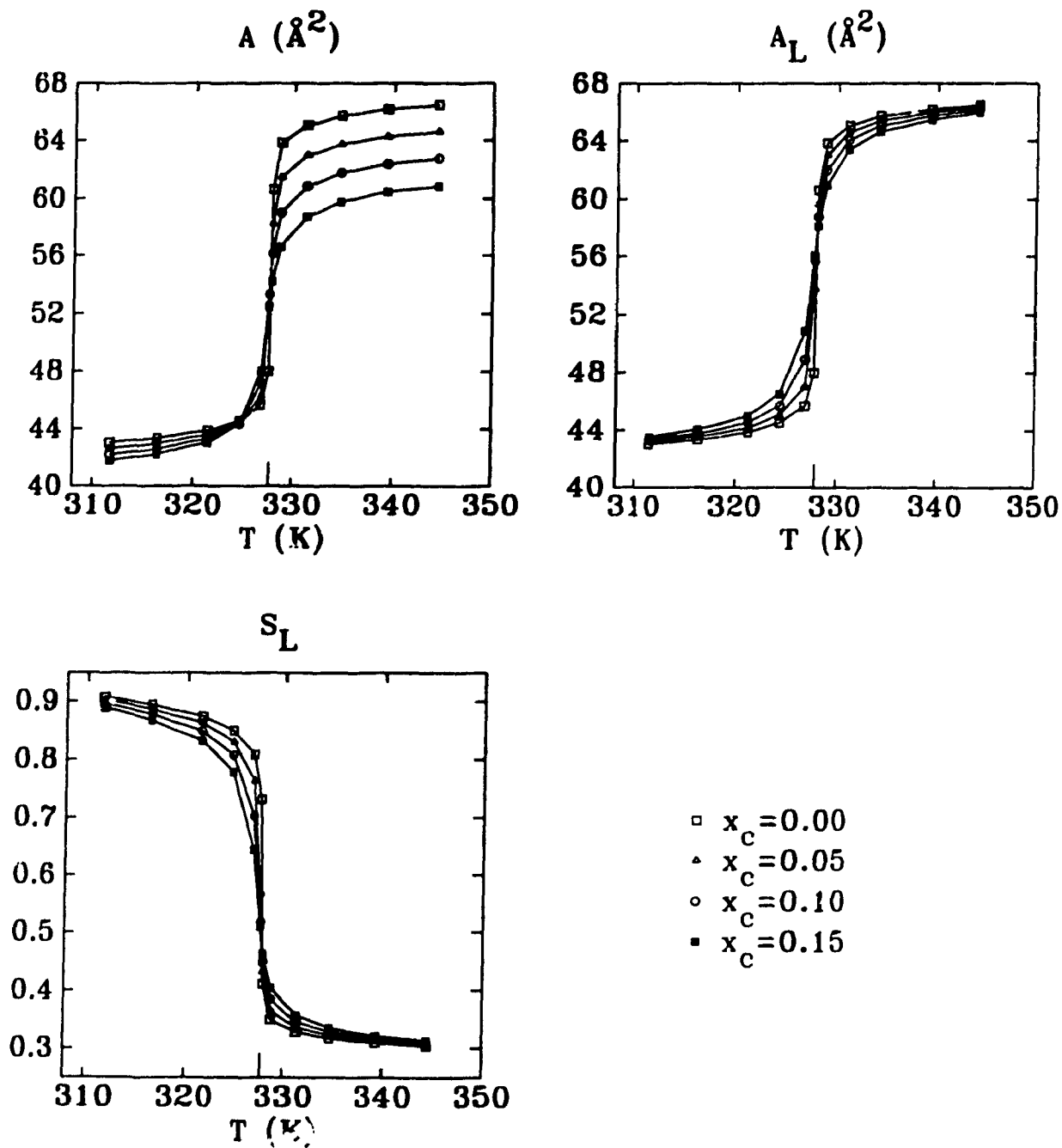


Figure 3.4: Total area per molecule, lipid area per lipid molecule and lipid order parameter of DSPC-cholesterol bilayers.

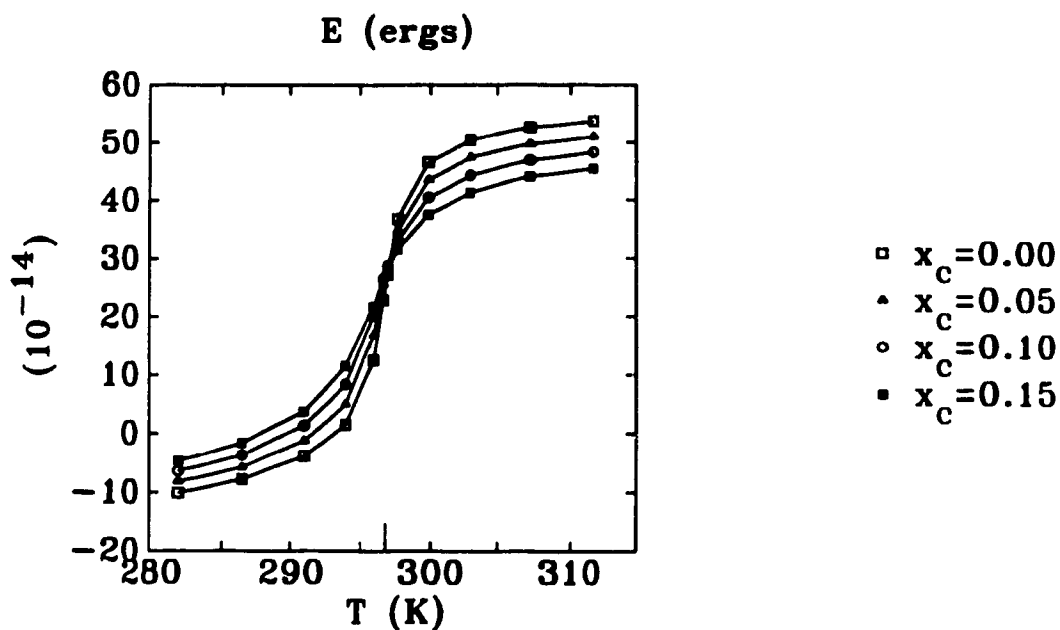


Figure 3.5: Energy per molecule of DMPC-cholesterol bilayers

chains shown in the same figures. Cholesterol induces lipid chains with conformational disorder below the transition temperature and with high conformational order above the transition temperature. This is why the lipid area per lipid molecule increases below the transition temperature and decreases above it.

Figures 3.5, 3.6 and 3.7 show the average energy as a function of temperature for three different cholesterol concentrations. Again, the broadening effect of the cholesterol is observed. The low temperature phase has a higher energy than the pure system and the high temperature phase has a lower energy than the pure system. The model therefore predicts that cholesterol makes the membrane more disordered in the low temperature phase and more rigid in the high temperature phase.

Figures 3.11, 3.12 and 3.13 for the isothermal lateral compressibility and figures 3.8, 3.9 and 3.10 for the specific heat show that the peak in these response functions decreases with the addition of cholesterol, but the addition of cholesterol increases the thermal fluctuations at the “wings” of the transition.

As in the case of the pure lipid bilayer, the response functions were calculated from fluctuations in the area and the energy using the equations derived in appendix A.

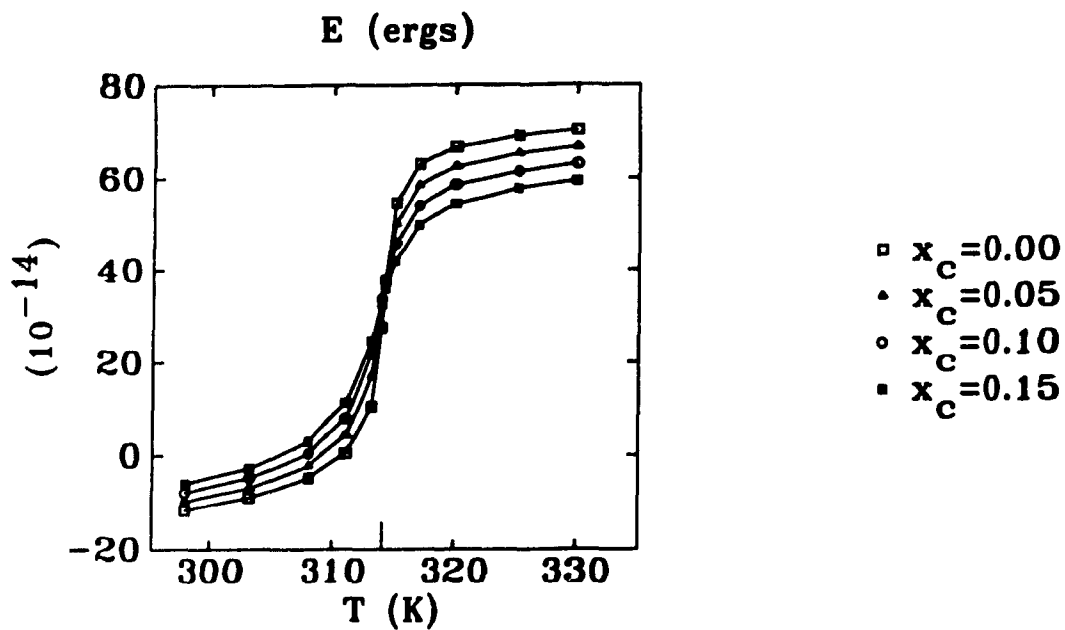


Figure 3.6: Energy per molecule of DPPC-cholesterol bilayers.

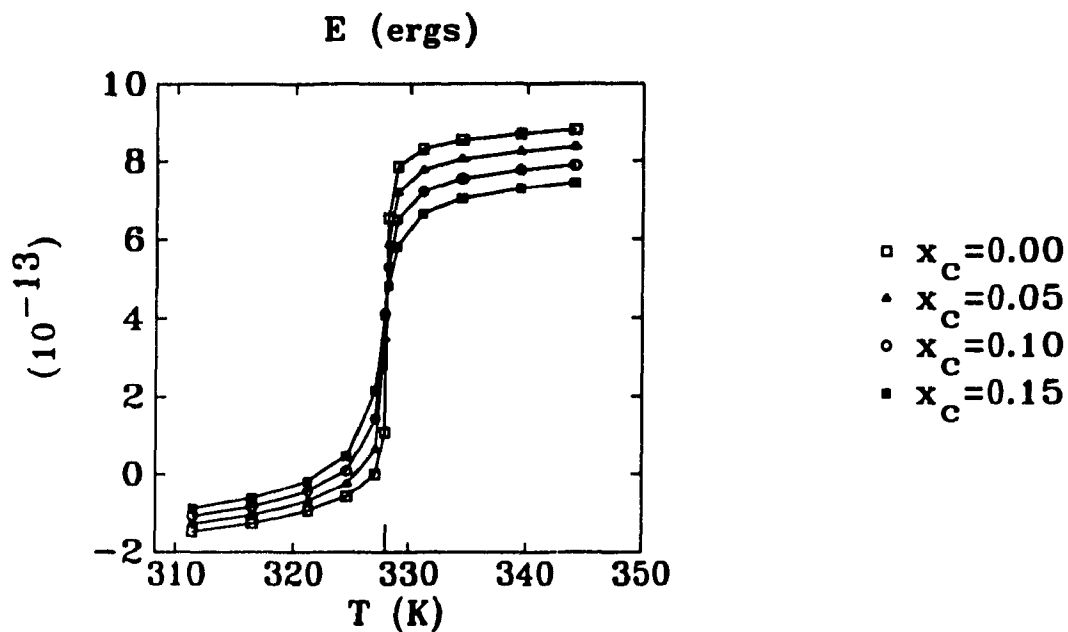


Figure 3.7: Energy per molecule of DSPC-cholesterol bilayers.

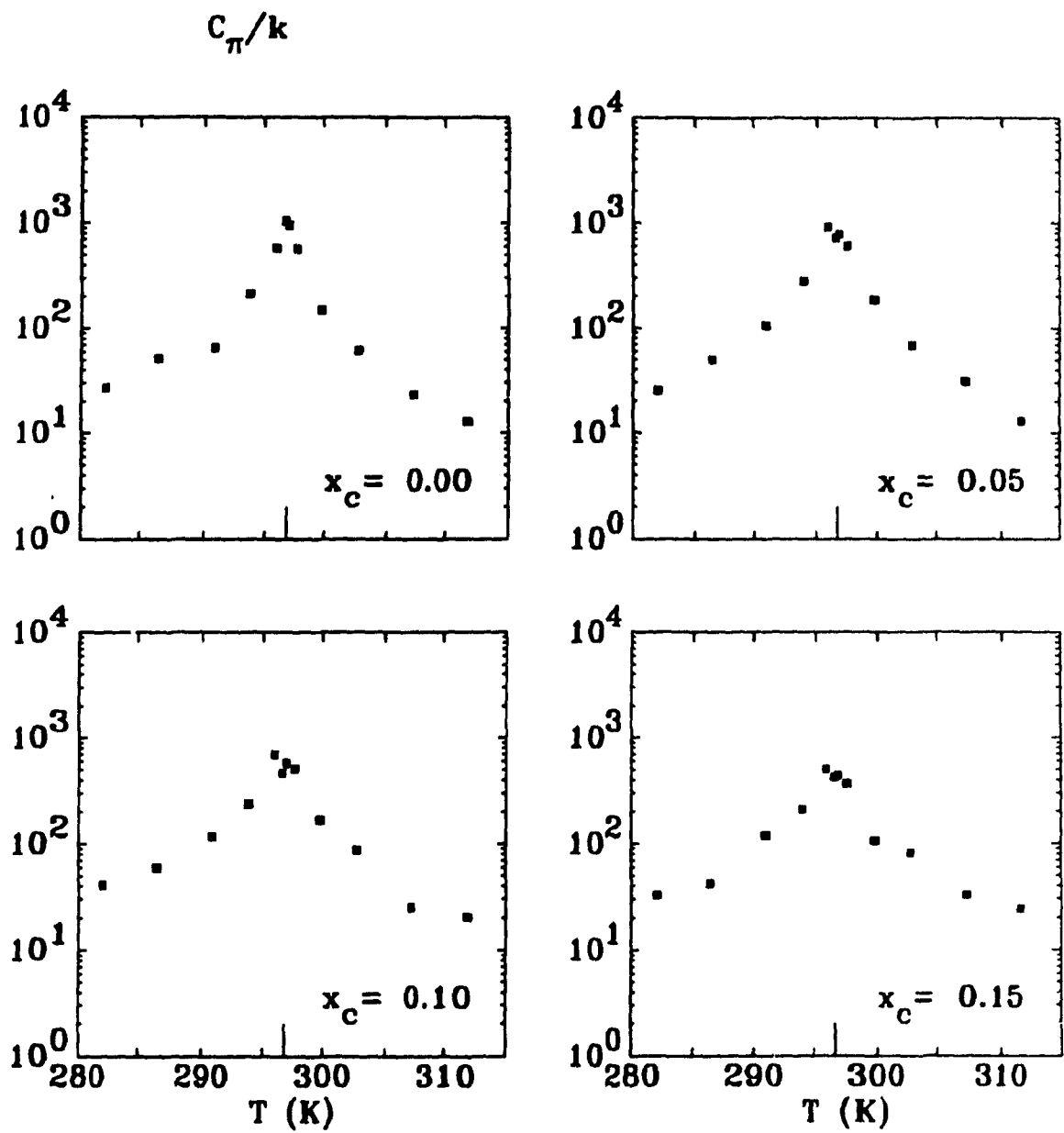


Figure 3.8: Specific heat per molecule of DMPC-cholesterol bilayers.

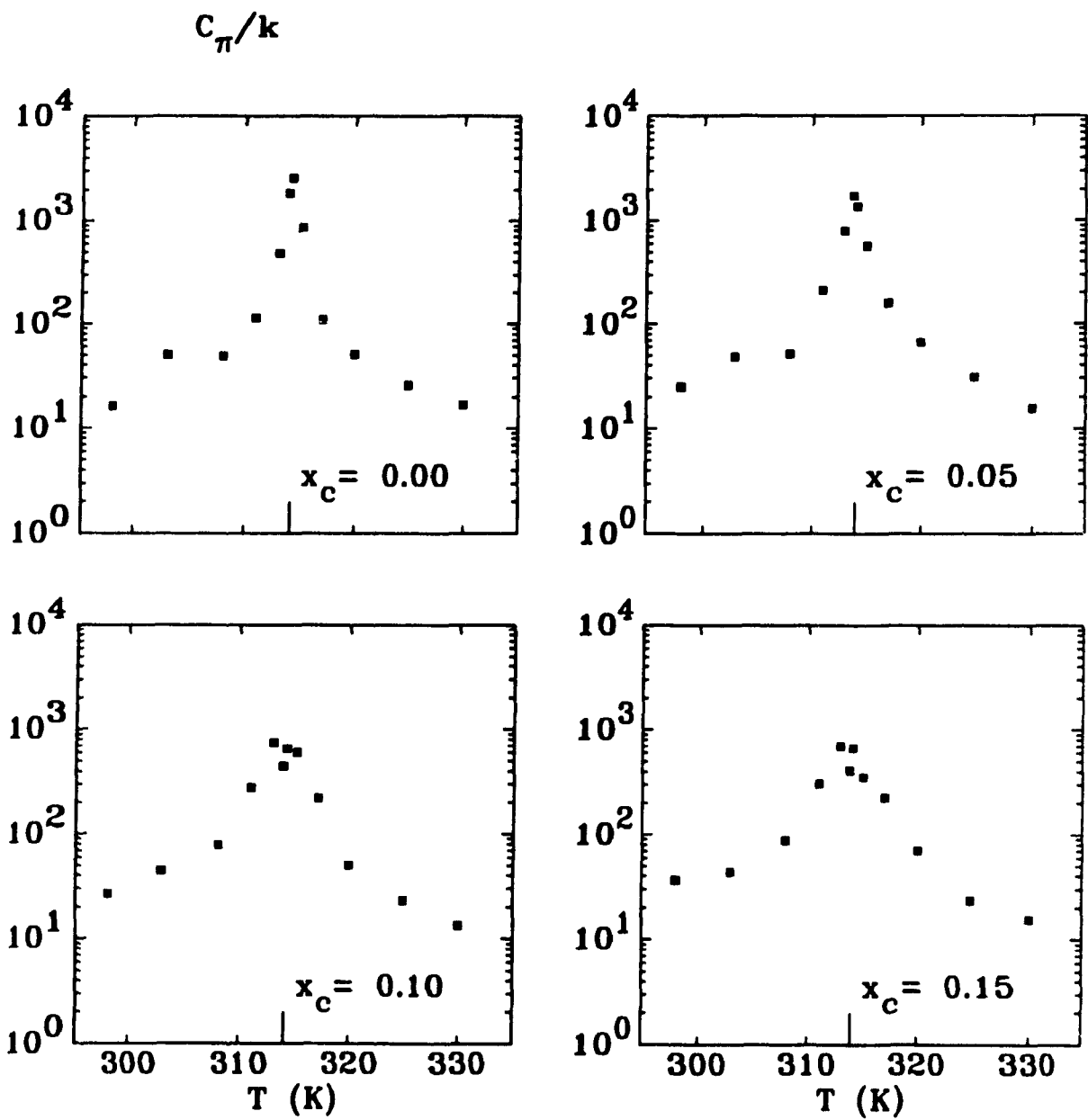


Figure 3.9: Specific heat per molecule of DPPC-cholesterol bilayers.

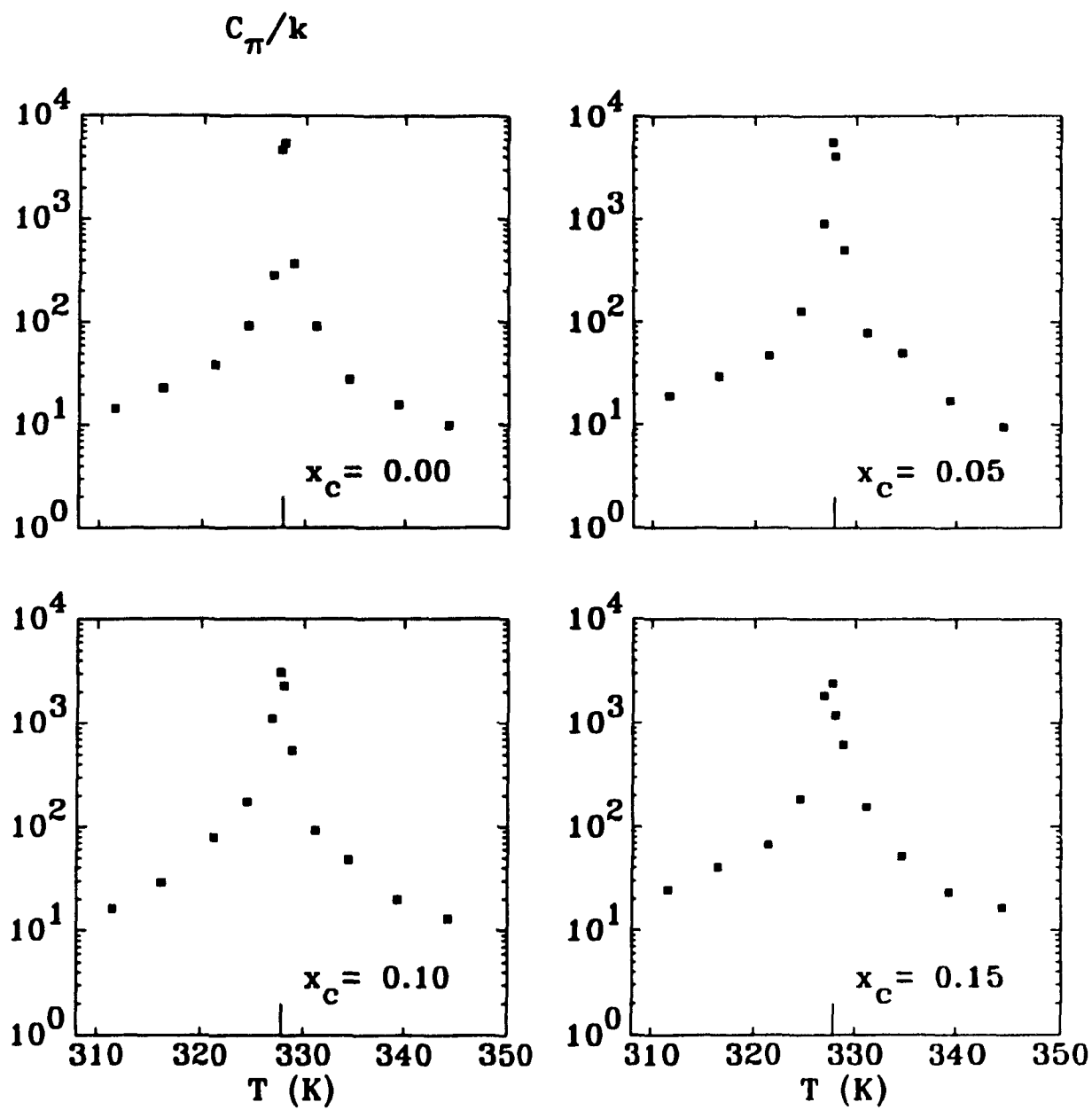


Figure 3.10: Specific heat per molecule of DSPC-cholesterol bilayers

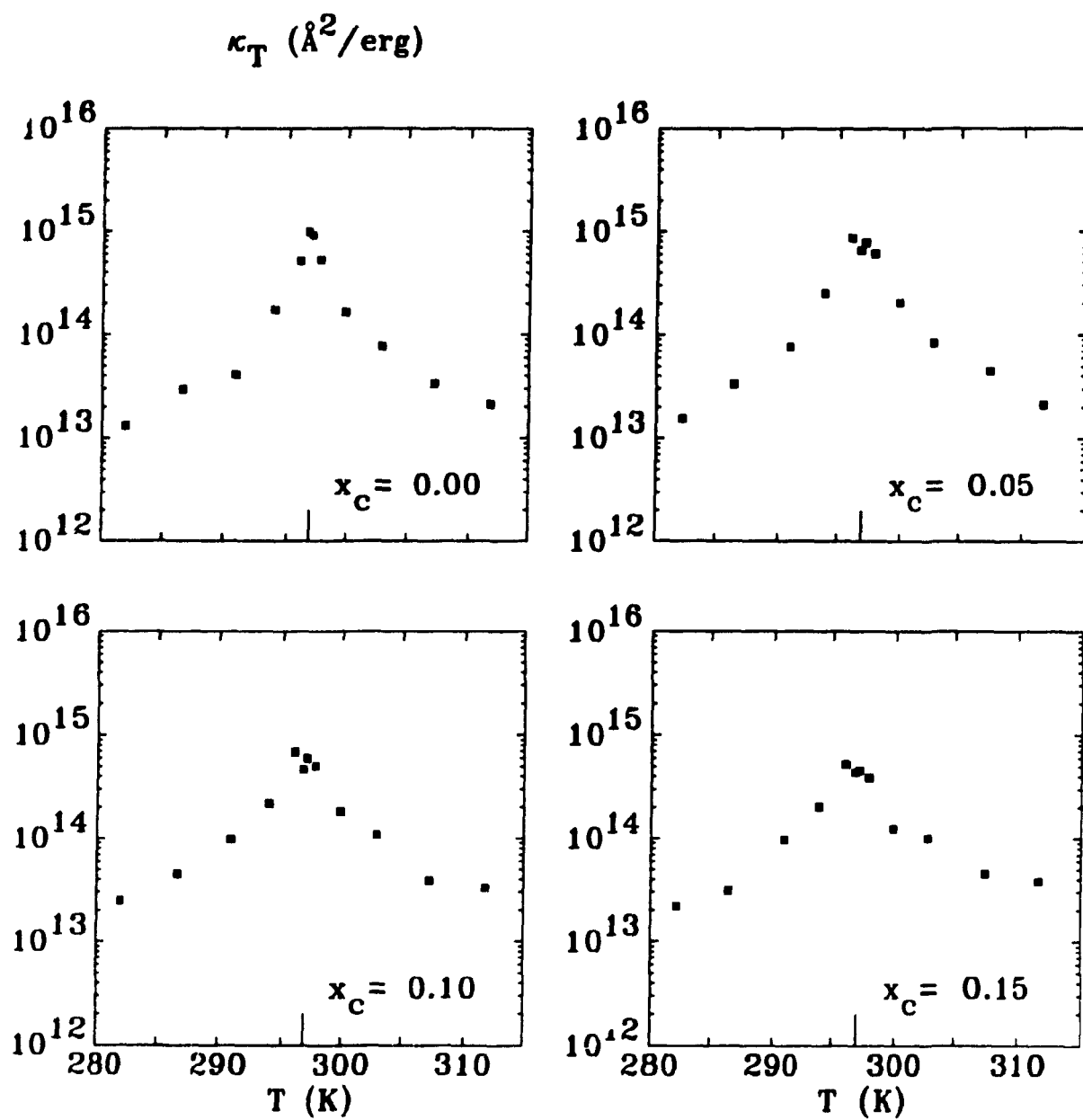


Figure 3.11: Isothermal lateral compressibility of DMPC-cholesterol bilayers.

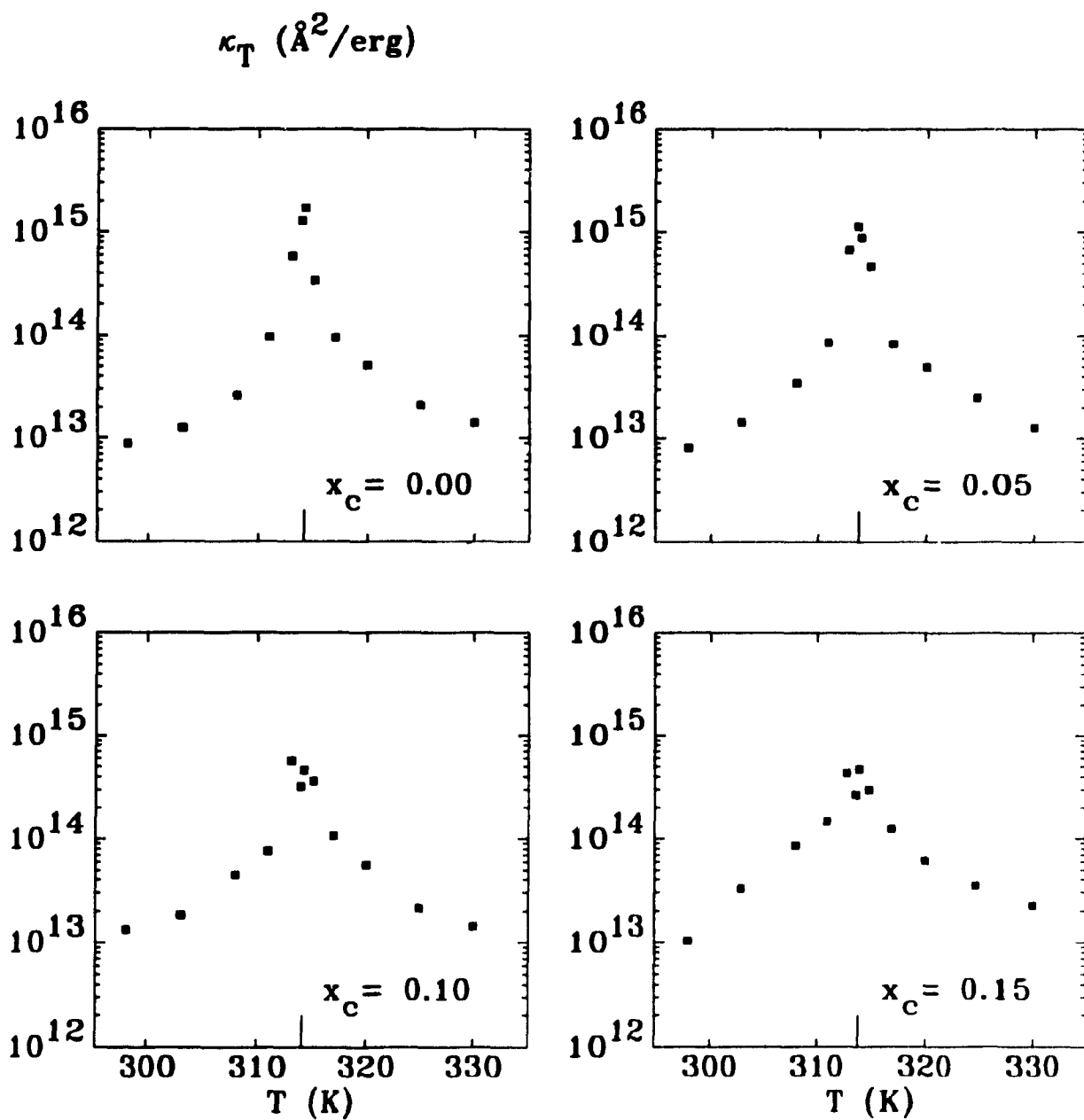


Figure 3 12: Isothermal lateral compressibility of DPPC-cholesterol bilayers

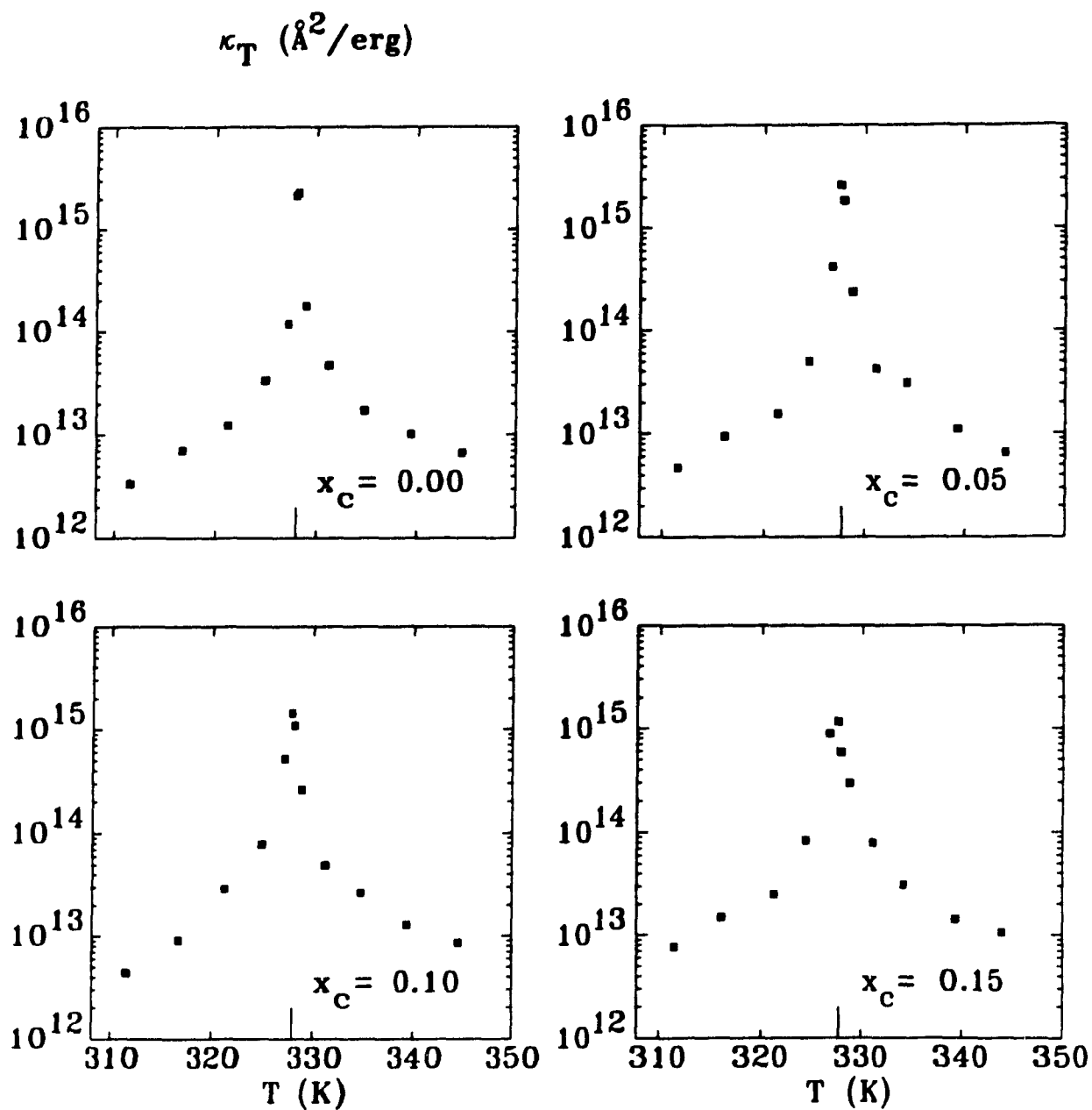


Figure 3 13: Isothermal lateral compressibility of DSPC-cholesterol bilayers.

3.1.2 Effect of Acyl Chain Length

The results for the effect of the chain length in pure lipid bilayers in section 2.2.1 are basically the same as those in this section.

For all the cholesterol concentrations studied, the shorter the chain length the smoother the transition. As can be seen from the figures 3.17, 3.18 and 3.19 for the total area, lipid area and lipid chain order parameter. Also, the energy differences between the two phases is smaller for shorter chain lengths as can be seen in figures 3.14, 3.15 and 3.16.

For all the cholesterol concentrations studied, the peak in the specific heat decreases for decreasing chain length. But an enhancement is observed at the "wings" of the transition for decreasing chain length as is shown in figures 3.14, 3.15 and 3.16. This indicates that the larger the cholesterol concentration the larger the fluctuations at the "wings" of the transition. An enhancement in the isothermal lateral compressibility at the "wings" of the transition is observed for decreasing chain length as is shown in figure 3.20 for all cholesterol concentrations studied.

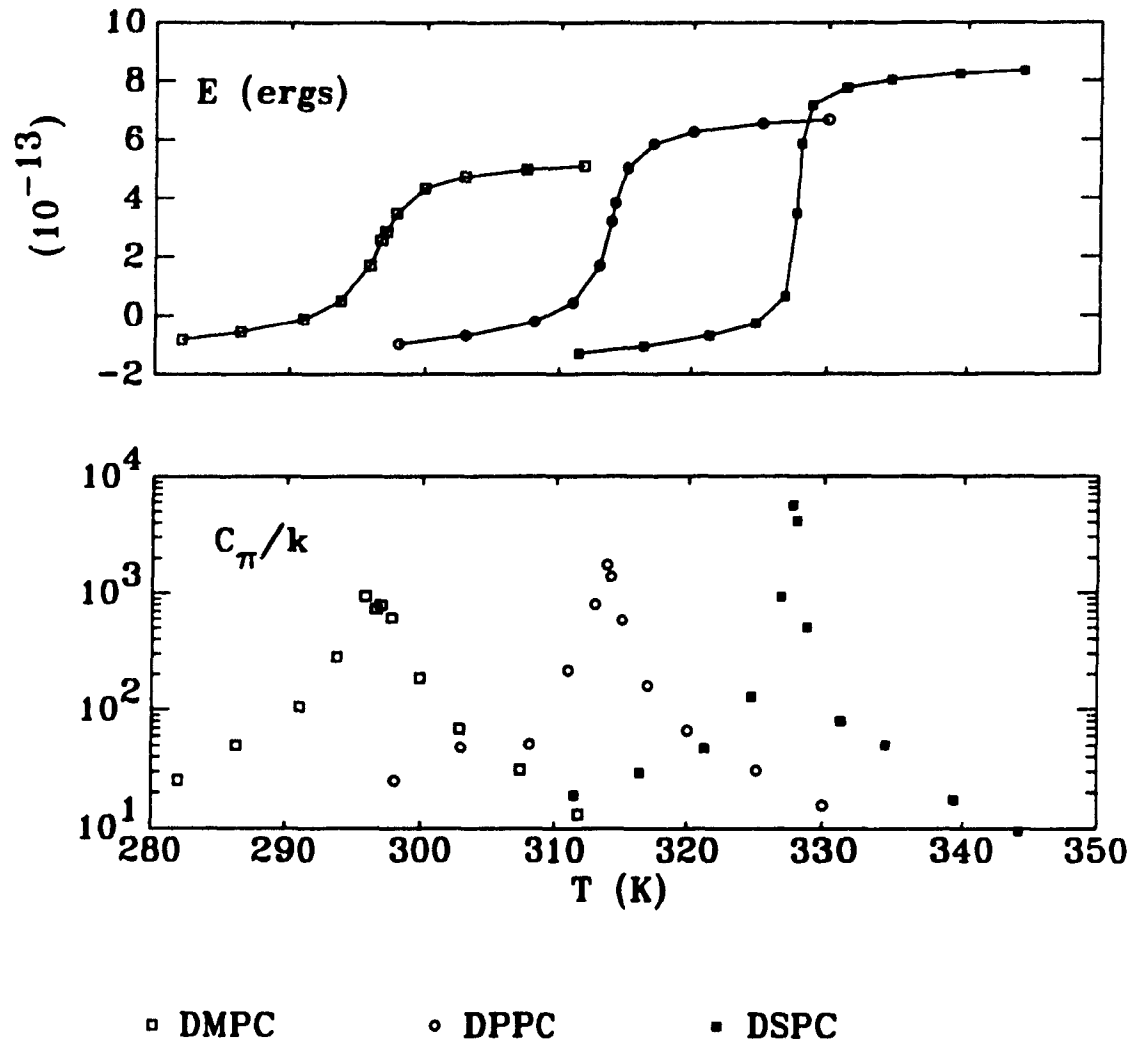


Figure 3.14: Energy and specific heat per molecule of bilayers with $x_C = 0.05$.

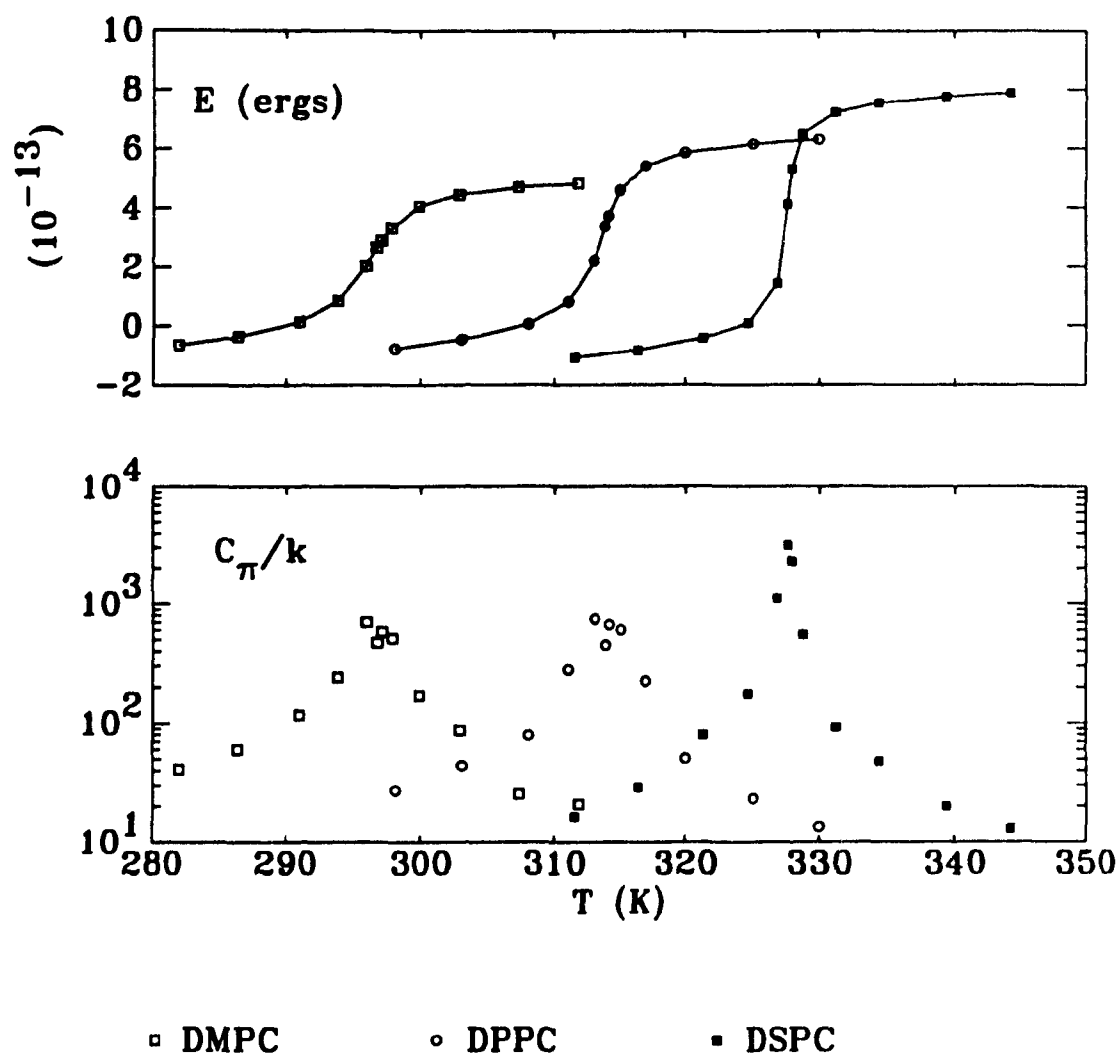


Figure 3.15: Energy and specific heat per molecule of bilayers with $x_C = 0.10$.

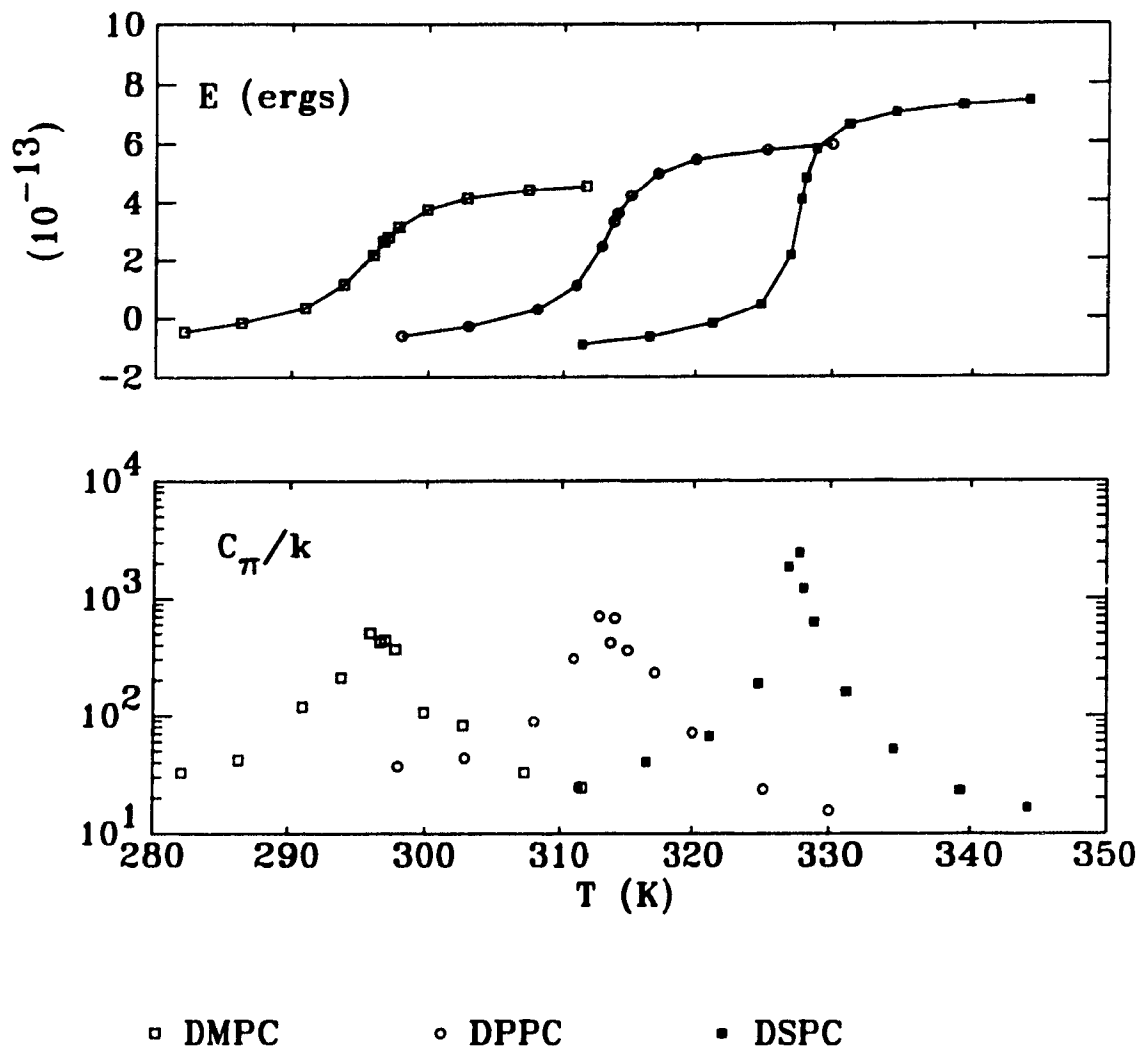


Figure 3.16: Energy and specific heat per molecule of bilayers with $x_C = 0.15$

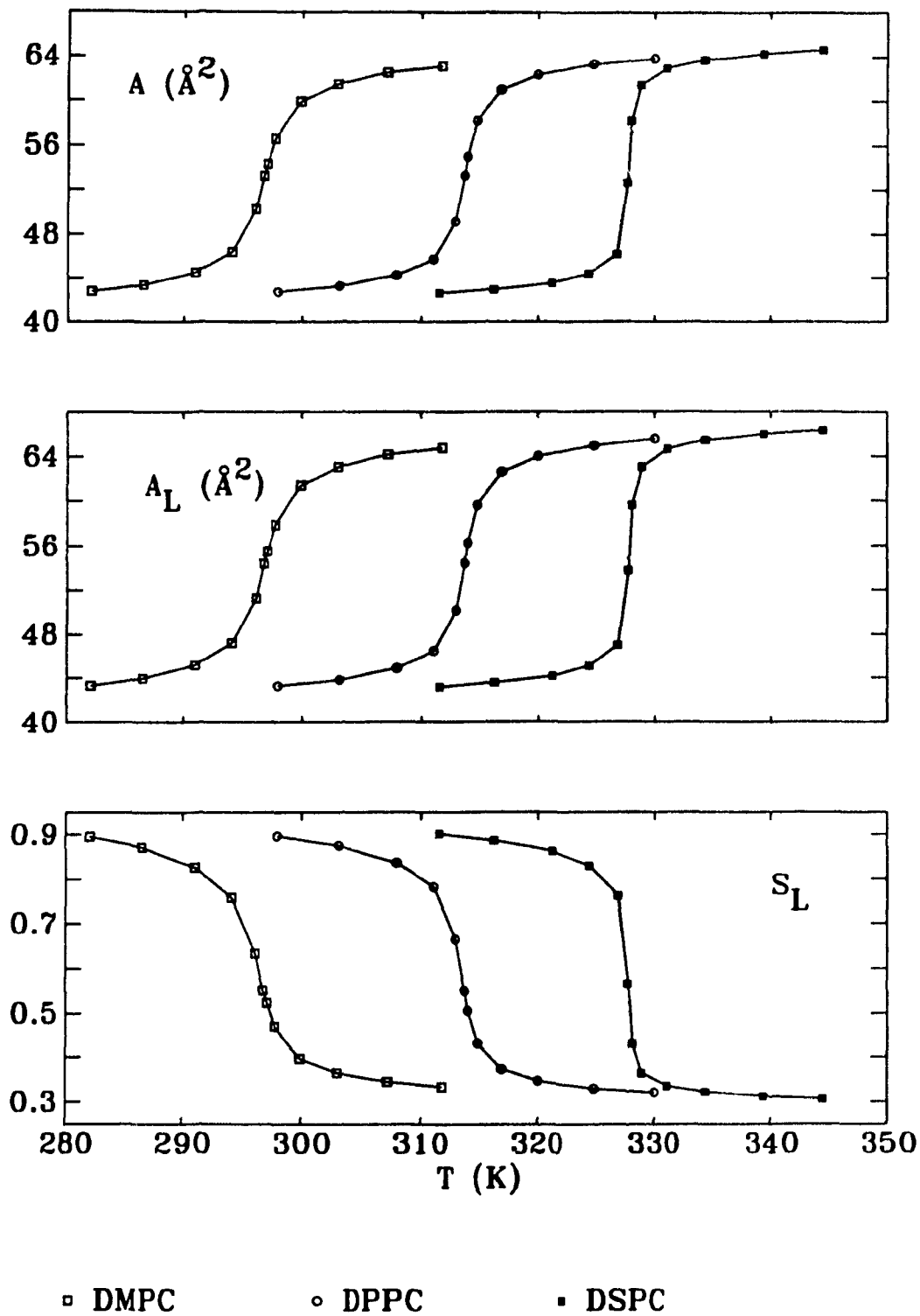


Figure 3.17: Total area per molecule, lipid area per lipid molecule and lipid order parameter of bilayers with $x_C = 0.05$.

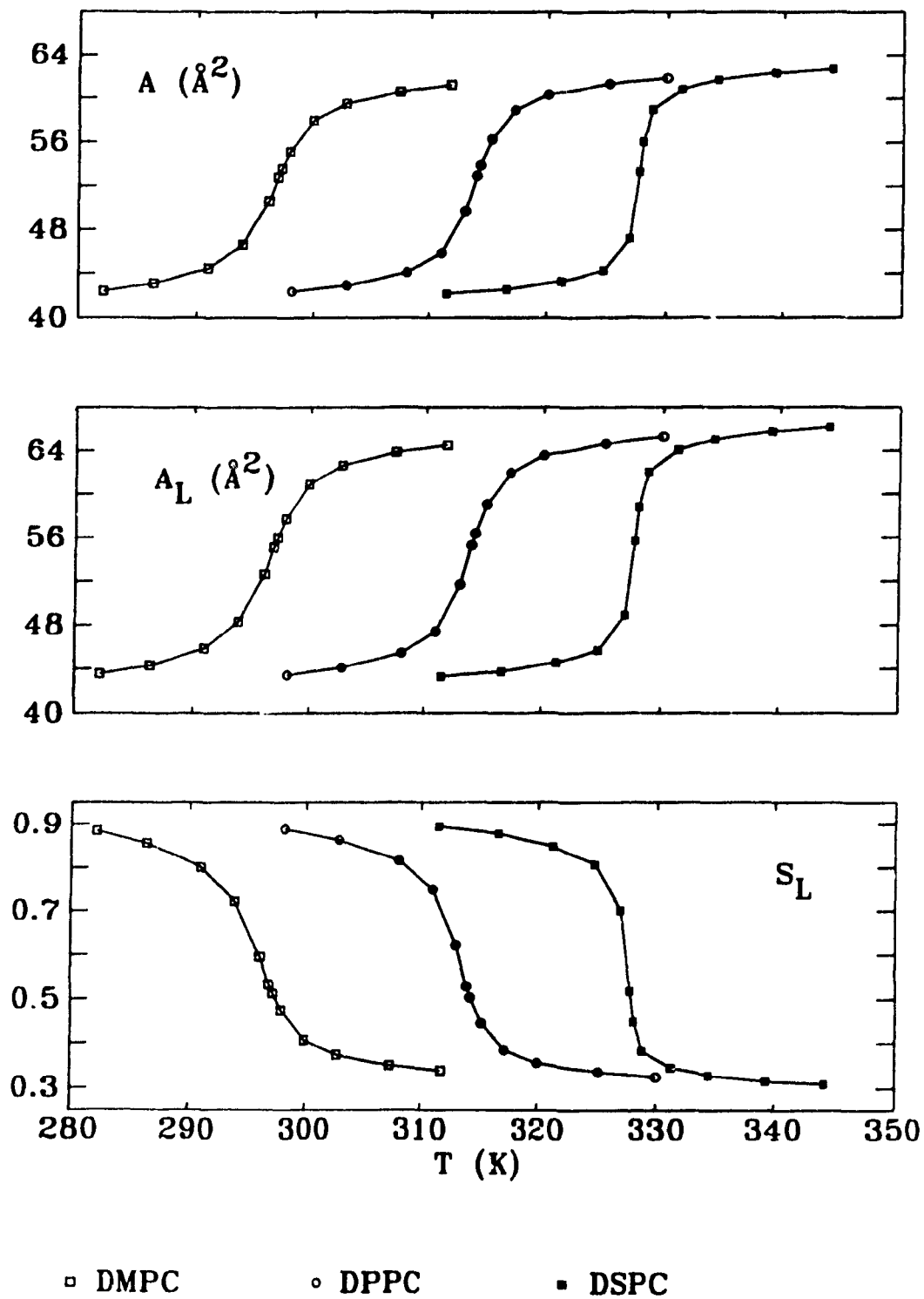


Figure 3.18: Total area per molecule, lipid area per lipid molecule and lipid order parameter of bilayers with $x_C = 0.10$.

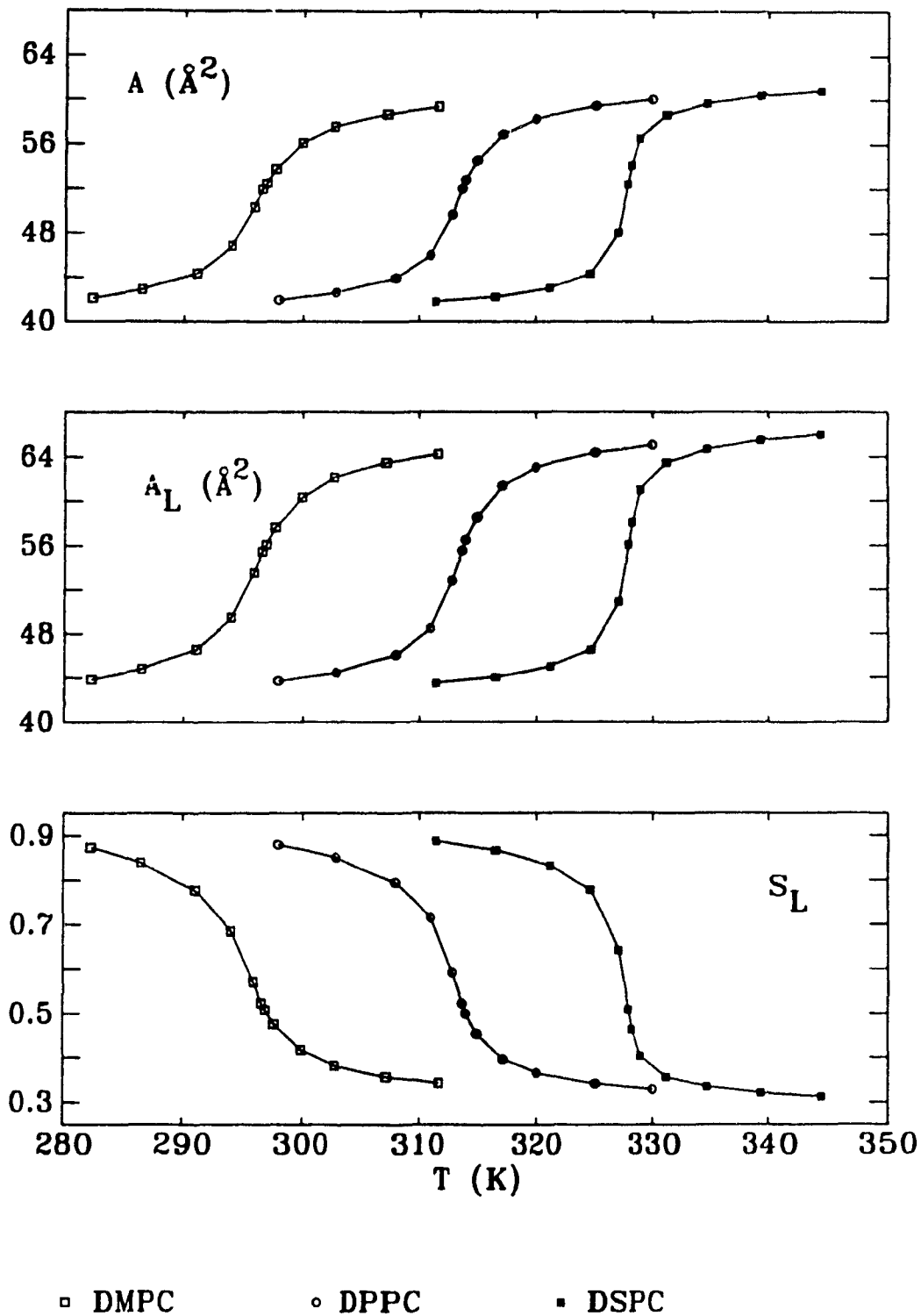


Figure 3.19: Total area per molecule, lipid area per lipid molecule and lipid order parameter of bilayers with $x_C = 0.15$.

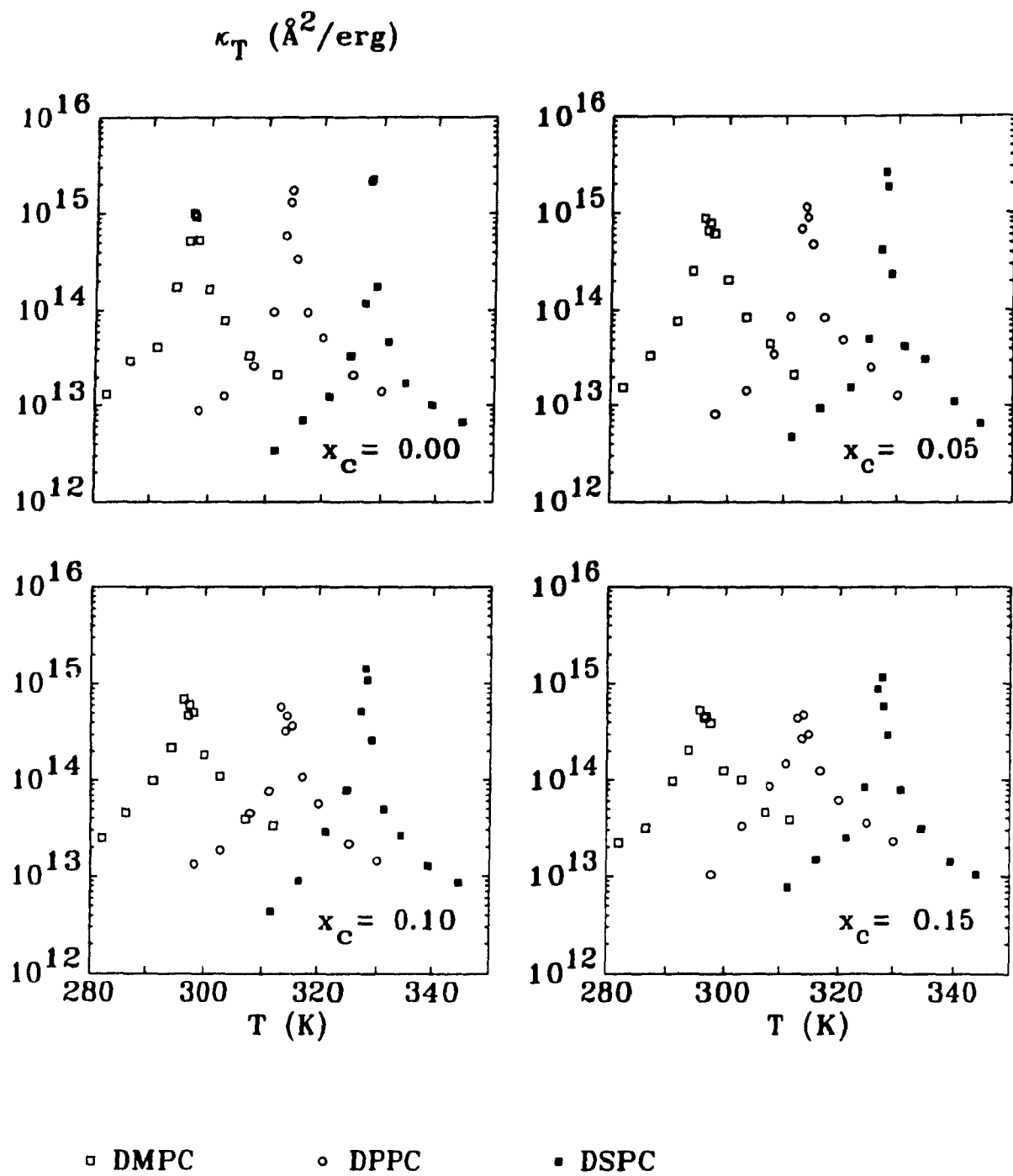


Figure 3 20 Isothermal compressibility of bilayers containing cholesterol

3.2 Passive Permeability of Lipid-Cholesterol Bilayers

The model for the passive permeability of lipid-cholesterol bilayers [5] is a direct extension of the model of pure lipid bilayers [6] studied in section 2.3.2.

The probability of an ion crossing a membrane is now given by

$$P(T) = a_b(T)p_b + a_c(T)p_c + a_{iL}(T)p_i + a_{iC}(T)p_{iC} \quad (3.3)$$

where the interfacial contribution had been separated in two parts, the part of the interface formed by lipids and the part formed by cholesterol. The interfacial regions formed by the lipids are considered to have high probability of transfer because of the same arguments of section 2.3.2. However the interfacial regions formed by cholesterol are not assumed to have a high probability of transfer since, at low cholesterol concentration the cholesterol molecule prefers both lipid phases equally and therefore will not behave like an interfacial defect.

3.2.1 Analysis of Configurations

In the case of the pure lipid bilayer where there are only chains in *gel* or in *fluid* conformational states, a cluster was defined as a set of chains in the minority phase connected by nearest neighbor bonds. In the case of lipid-cholesterol bilayers there is no unique way to define the clusters. We must therefore make a decision as to how the cholesterol molecules are classified. It is explained in the next paragraph how this is treated in this thesis. Again for simplicity we will refer to fluid clusters in a *gel* phase bulk, but the same definitions apply for the high temperature phase with the exchange of the words *gel* and *fluid*.

Consistent with the pure lipid case, only three or more fluid chains are considered to form a cluster. If a cholesterol molecule is a nearest neighbor of a lipid chain forming a cluster, it is considered as part of the cluster.² If a cholesterol molecule is

²This is different from the work of Cruzeiro-Hansson. In her case if a cholesterol molecule is a

a nearest neighbor of a site forming a cluster that is occupied by another cholesterol molecule, it is not considered as part of the cluster. The definitions for interface and bulk are the same of section 2.3.3 for the pure lipid bilayer.

3.2.2 Model Permeability and Monte Carlo Simulations

As in the case of a pure lipid bilayer, the cluster analysis of the configurations obtained from the Monte Carlo simulations permits the calculation of the fractional areas occupied by the clusters, the bulk and the interface.

A cut-off of 14 is chosen implying that clusters occupying less than 14 lattice sites were considered as part of the bulk and *clusters of clusters* (defined on page 29) smaller than 14 lattice sites were considered as part of the cluster.

The dependence of the fractional areas on temperature is shown in figures 3.21, 3.22 and 3.23. As in the case of the pure lipid bilayer, as the transition temperature is approached from either side, the area occupied by the clusters increases and has a peak at T_m . The area of the bulk decreases and the lipid interfacial fractional area increases as the transition is approached. However a decrease of the lipid interfacial fractional area occurs for DMPC and DPPC very close to the transition temperature for the cholesterol concentrations studied, when approaching from the high temperature phase. This is again related with the fact that clusters are aggregating to form larger clusters. The fractional lipid interfacial area has a peak at a temperature higher than T_m . For all the systems and all the cholesterol concentrations studied the cholesterol interfacial fractional area is extremely small but increases as the transition temperature is approached from both sides and in most of the cases it decreases at temperatures very close to the transition.

As can be seen in the same figures, the higher the cholesterol concentration the higher the cluster and interfacial fractional areas and the smaller the bulk fractional area. This indicates that cholesterol induces the formation of clusters above and

nearest neighbor of a lipid chain forming a cluster, it is not considered as part of the cluster but as part of the interface.

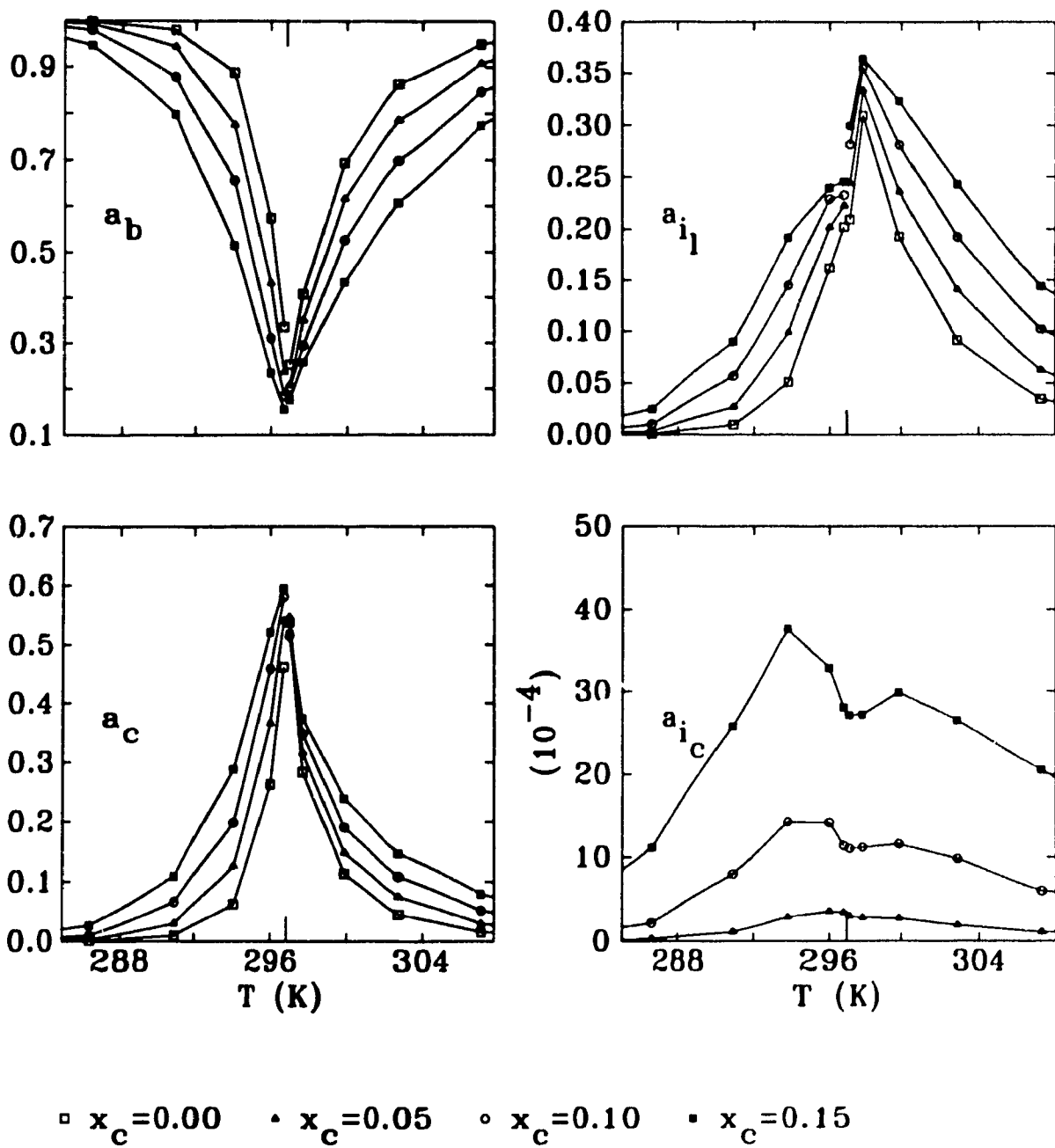


Figure 3.21: Fractional areas of bulk, clusters and interface of DMPC-cholesterol bilayers

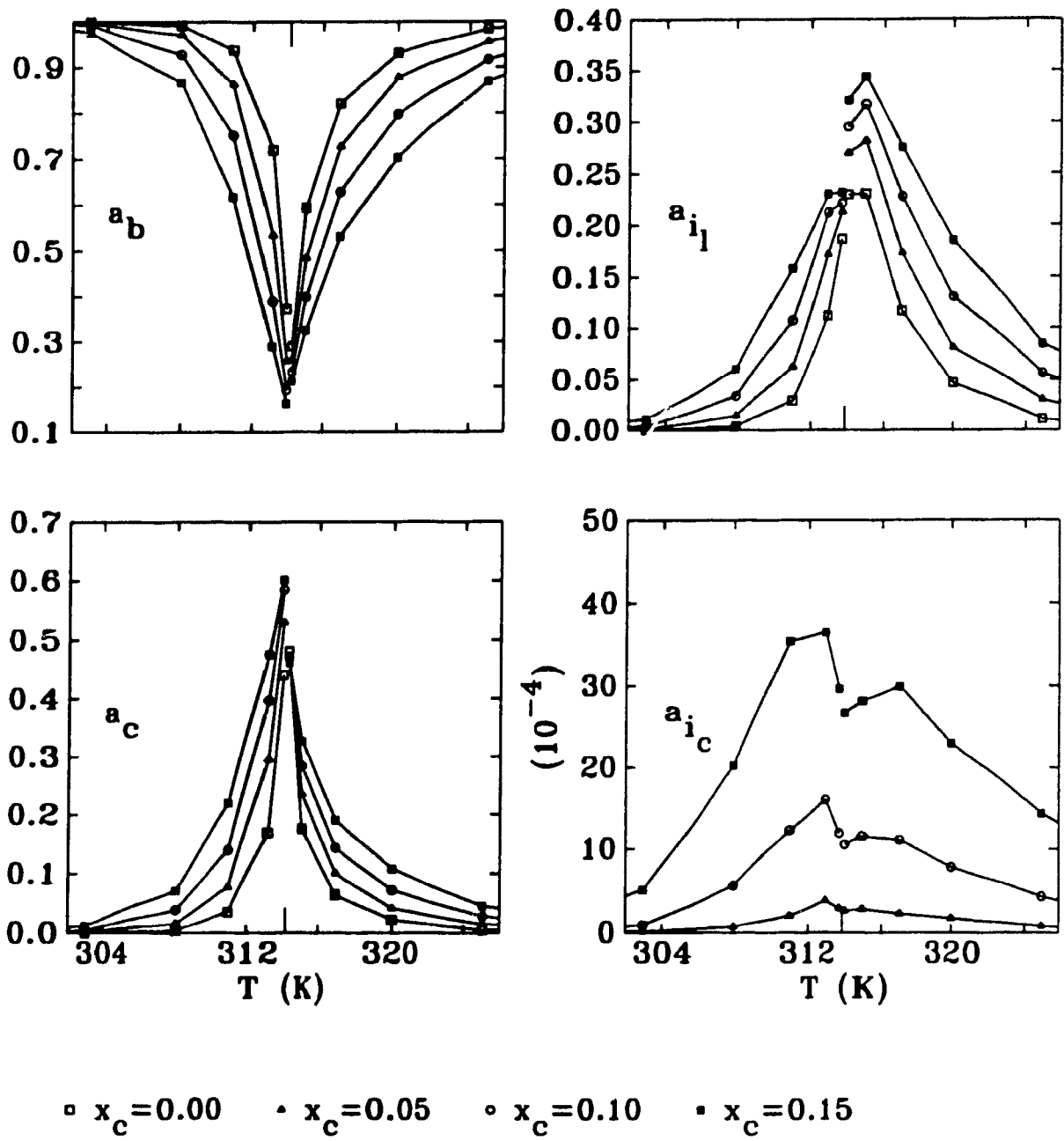


Figure 3.22: Fractional areas of bulk, clusters and interface of DPPC-cholesterol bilayers.

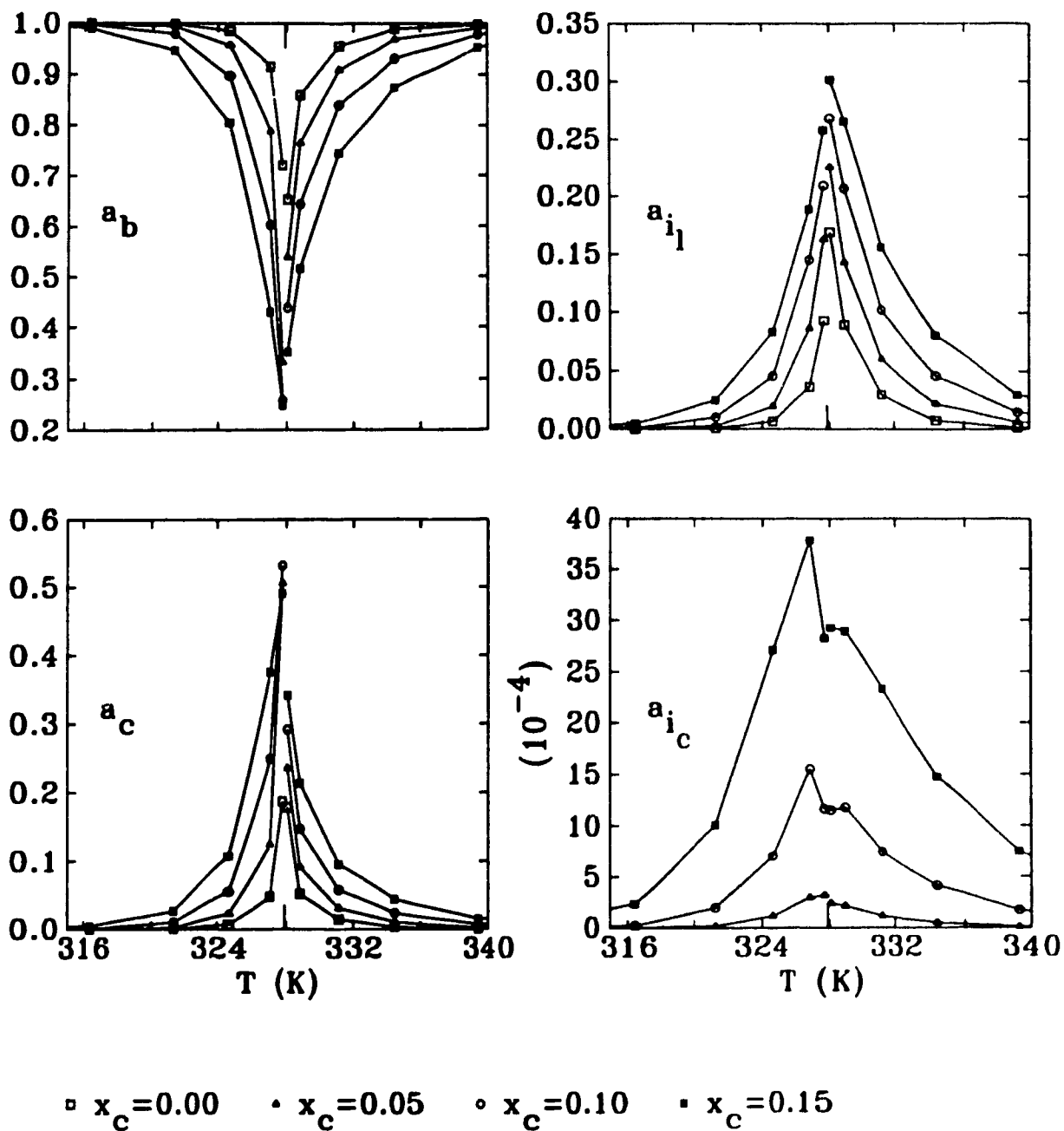


Figure 3.23: Fractional areas of bulk, clusters and interface of DSPC-cholesterol bilayers.

below the transition temperature and consequently causes the amount of interface to increase. Snapshots of configurations of DSPC are shown in figure 3.24 for several cholesterol concentrations. For the figure the temperature is fixed at a value above the transition temperature. The gel phase regions and the cholesterol sites are shown in part *b*) of the figure. In part *a*) of the same figure, the interfacial regions consistent with a cut-off of 14 and the cholesterol sites are shown. Note that the number of sites forming clusters and the number of sites in the interfacial regions increase with increasing cholesterol concentration.

The model of section 3.2 for the permeability of lipid-cholesterol bilayers requires the knowledge of the transfer probability of the interfacial region containing cholesterol. In order to avoid the introduction of new parameters, the interfacial probability of transfer at sites occupied by cholesterol molecules is assumed to be equal to the bulk probability of transfer below the transition [5], i.e. the smallest value for a probability of transfer used in the model for pure lipid bilayers.

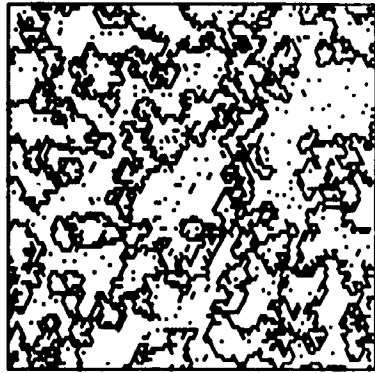
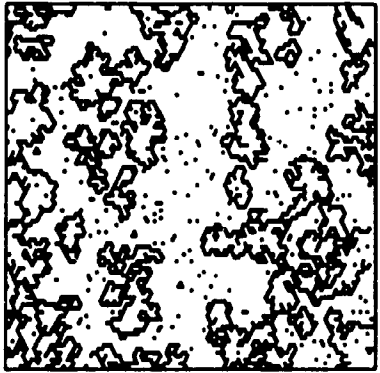
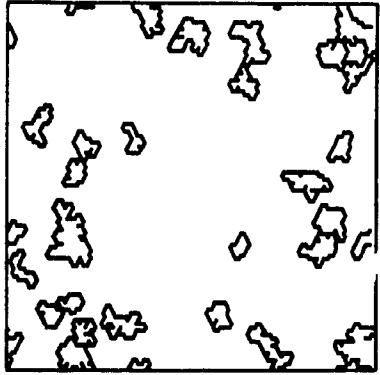
Figures 3.25, 3.26 and 3.27 show the relative permeability as a function of temperature for the cholesterol concentrations studied.

An enhancement of the relative permeability as the transition temperature is approached from both sides is obtained for all the cholesterol concentrations studied. A peak in the relative permeability is obtained at a temperature above the transition temperature. This is a direct consequence of the behavior of the interfacial fractional area as a function of temperature.

As a consequence of both the assumption of a high probability of transfer to the lipid interfacial regions and the increase in the amount of interface for increasing cholesterol concentration, the model predicts an increase in the membrane permeability for increasing cholesterol concentration for all temperatures in the transition region, the effect being more pronounced at the "wings" of the transition.³ This is one of the main predictions of the model. The validity of the model is subject to

³With the choice made by Cruzeiro-Hansson for the classification of cholesterol molecules (see footnote on page 61) the same qualitative behavior is obtained, except that the increase in the permeability is enhanced with the choice made in this work

a



b

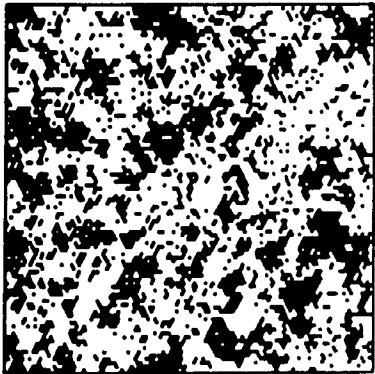
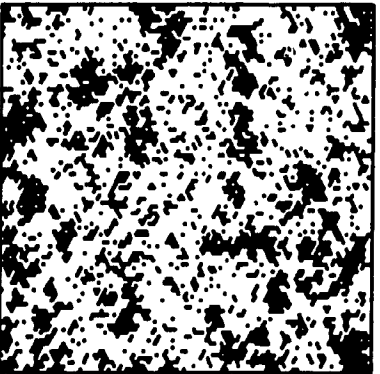
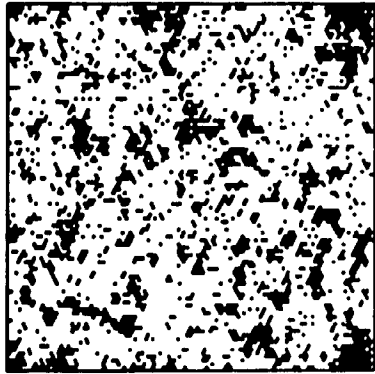
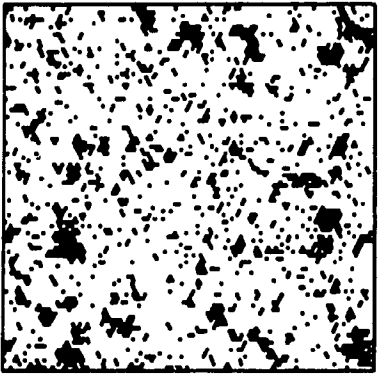


Figure 3.24 Snapshots of configurations for several cholesterol concentrations of DSPC at $T = 228.88K$ are shown on the previous page.

a) Interfacial regions consistent with a cut-off of 14 and cholesterol sites are shown
 b) Regions with the gel phase and cholesterol sites are shown for several cholesterol concentrations. The upper left figure corresponds to $x_C = 0.00$, the upper right corresponds to $x_C = 0.05$, the lower left corresponds to $x_C = 0.10$ and the lower right corresponds to $x_C = 0.15$

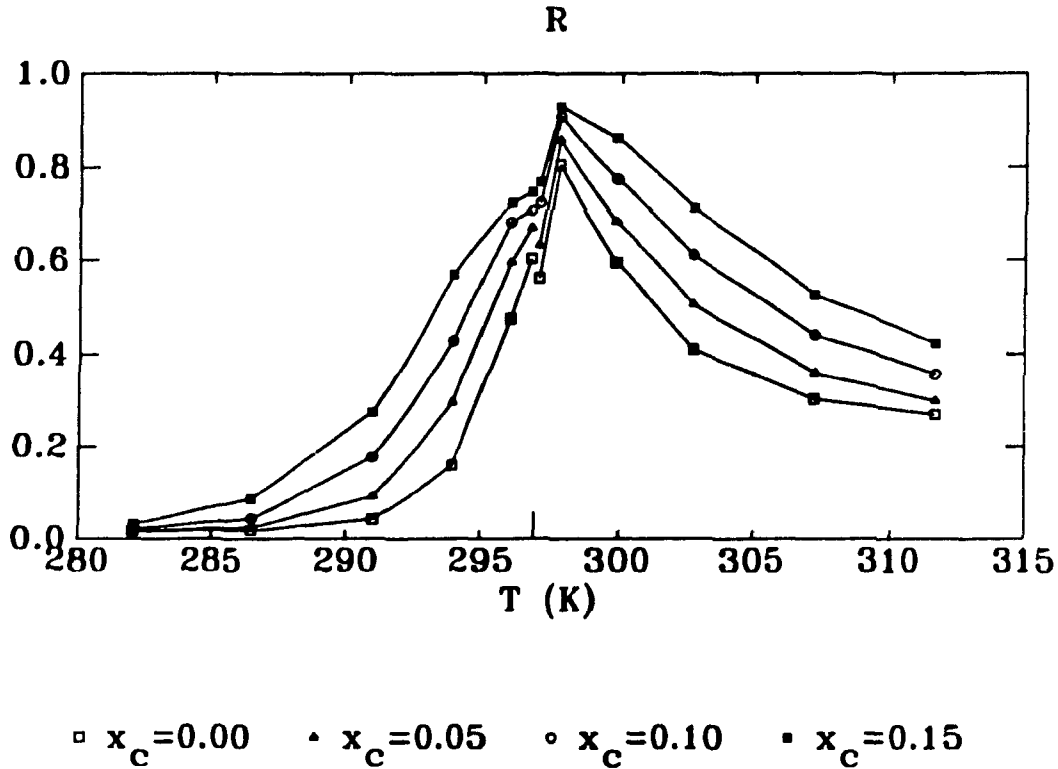


Figure 3.25: Relative permeability of DMPC-cholesterol bilayers. The units are arbitrary.

experimental confirmation. The model for the permeability of lipid-cholesterol bilayers should be valid if an enhancement of the passive ion permeability is observed for lipid-bilayers containing small cholesterol concentrations when increasing cholesterol concentration.

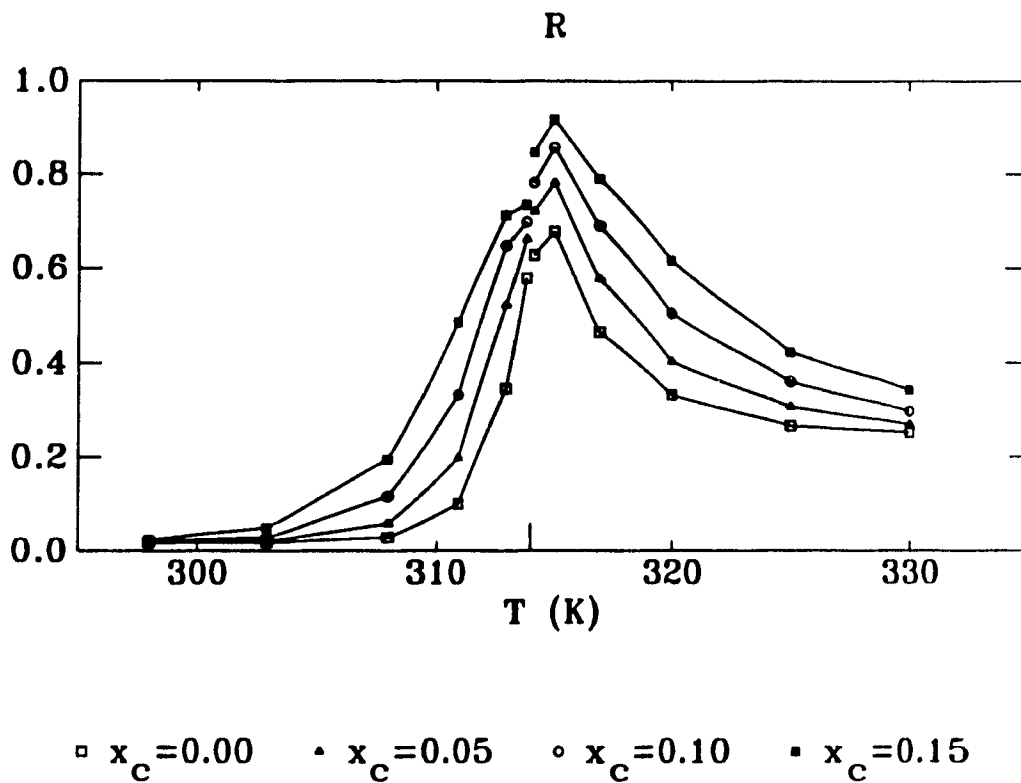


Figure 3.26: *Relative permeability of DPPC-cholesterol bilayers* The units are arbitrary

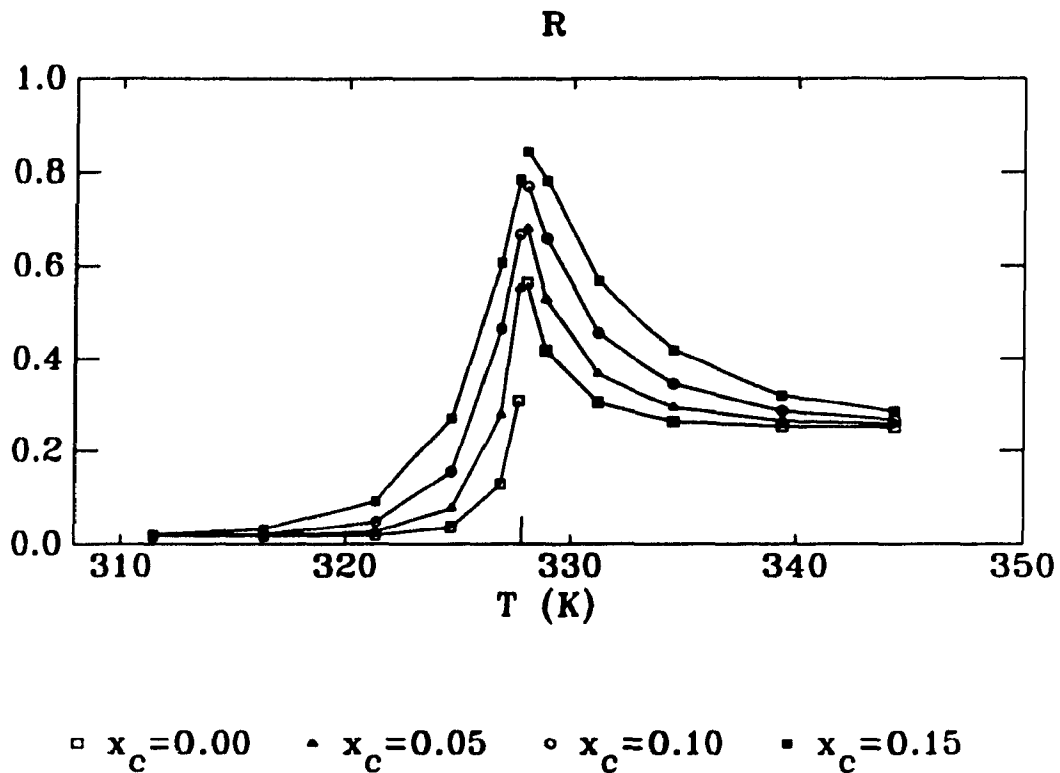


Figure 3.27: Relative permeability of DSPC-cholesterol bilayers. The units are arbitrary.

3.2.3 Effect of Acyl Chain Length on the Permeability

As was seen in section 3.1.1, the thermal fluctuations increase at the "wings" of the transition as the chain length decreases for all the cholesterol concentrations studied. Consequently there are more clusters and there is more interface at a given value T/T_m for a shorter chain than for a longer one. The cluster and interfacial fractional areas are larger for shorter chain lengths at a given value of T/T_m in the "wings" of the transition. A concomitant decrease in the bulk fractional area is observed for short chains at all the cholesterol concentrations studied, as can be seen in figures 3.29, 3.30 and 3.31. Snapshots of configurations for three chain lengths are shown in figure 3.28. In this figure, the reduced temperature T/T_m is fixed to be above the transition temperature and the cholesterol concentration is also fixed. The gel phase regions and the cholesterol sites are shown in part b) of the figure. The interfacial regions consistent with a cut-off of 14 and the cholesterol sites are shown in part a) of the figure. Note that the number of sites forming the clusters and the interfacial regions decrease for increasing chain length.

The results for the relative permeability are similar to those for pure lipid membranes in that the relative permeability increases with decreasing chain length for a given value of T/T_m . This happens for all cholesterol concentrations studied and can be seen in figures 3.32, 3.33 and 3.34.

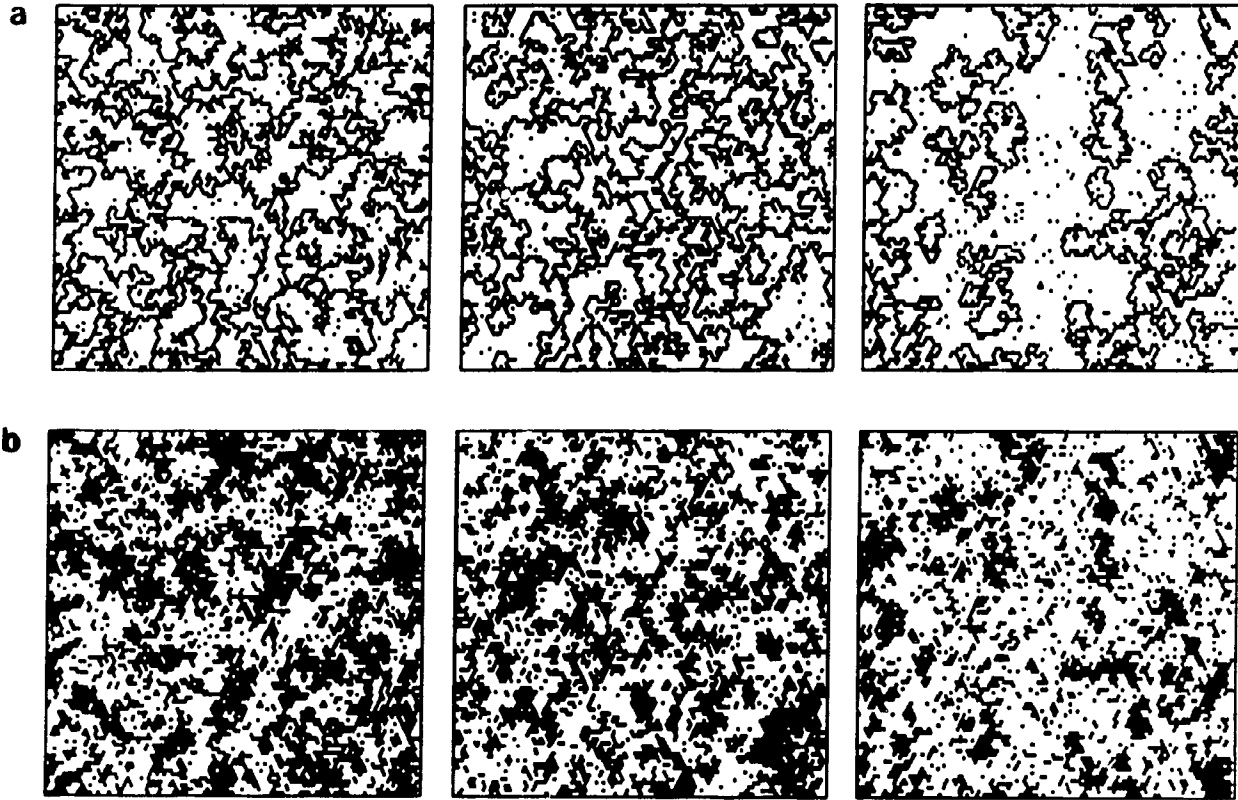


Figure 3.28: *Snapshots of configurations for several chain lengths at $T/T_m = 1.003$ and $x_C = 0.10$.*
 a) Interfacial regions consistent with a cut-off of 14 and cholesterol sites are shown.
 b) Regions with the gel phase and cholesterol sites are shown. The figure on the left corresponds to DMPC ($m = 14$), the central figure corresponds to DPPC ($m = 16$) and the figure at the right corresponds to DSPC ($m = 18$)

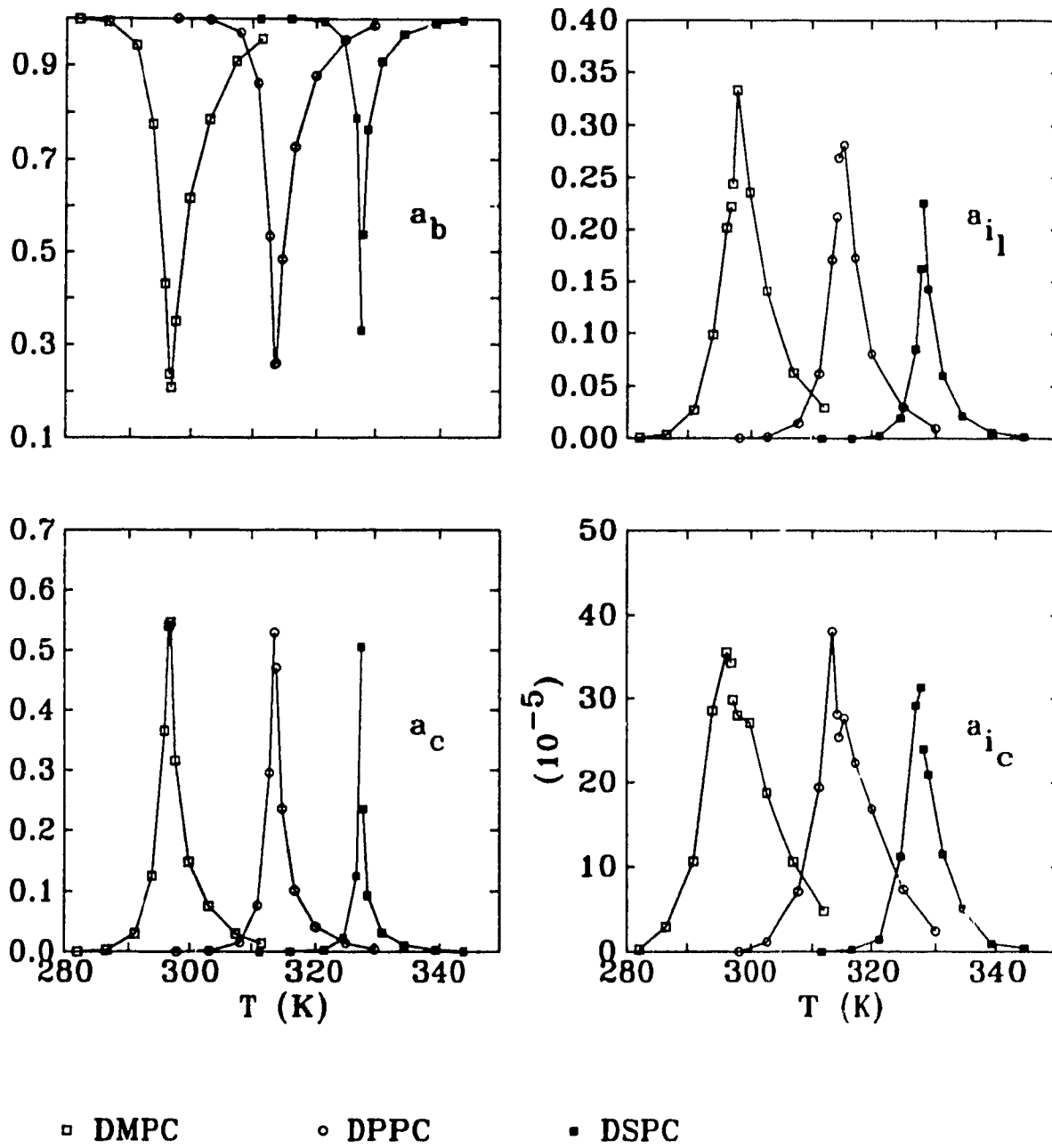


Figure 3.29: Fractional areas of bilayers with $x_c = 0.05$

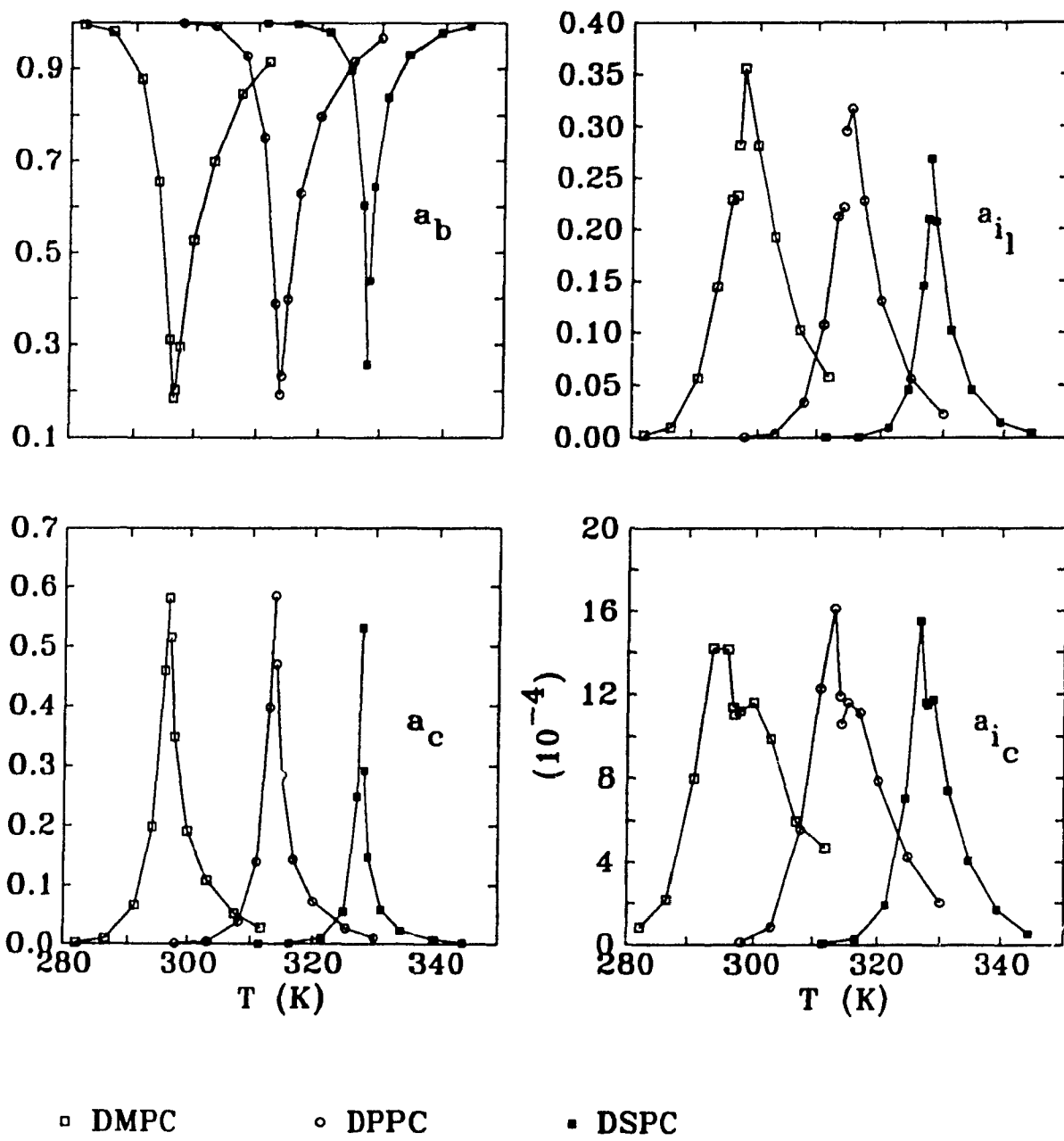


Figure 3.30: Fractional areas of bilayers with $x_C = 0.10$.

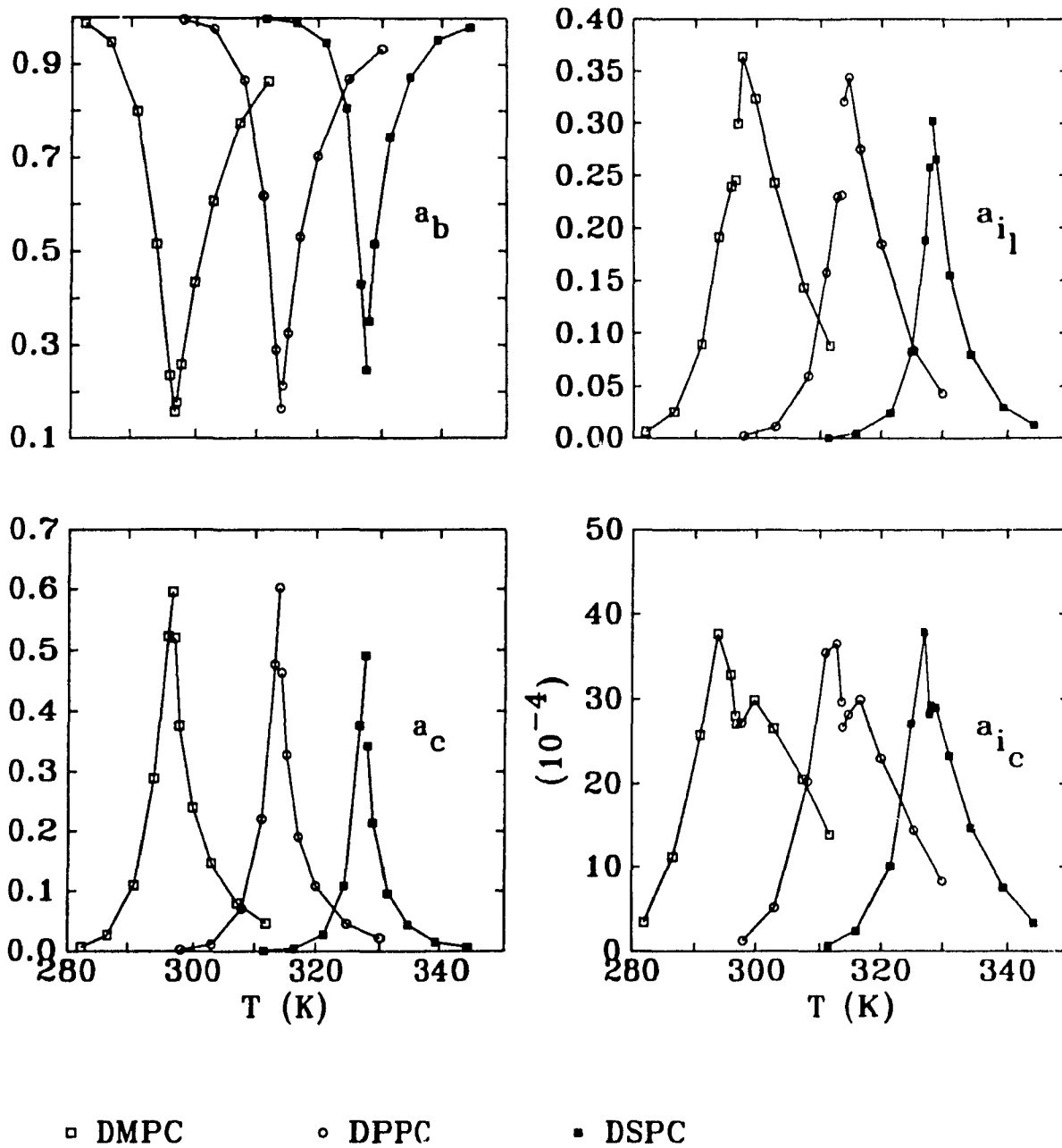


Figure 3 31: Fractional areas of bilayers with $x_c = 0.15$

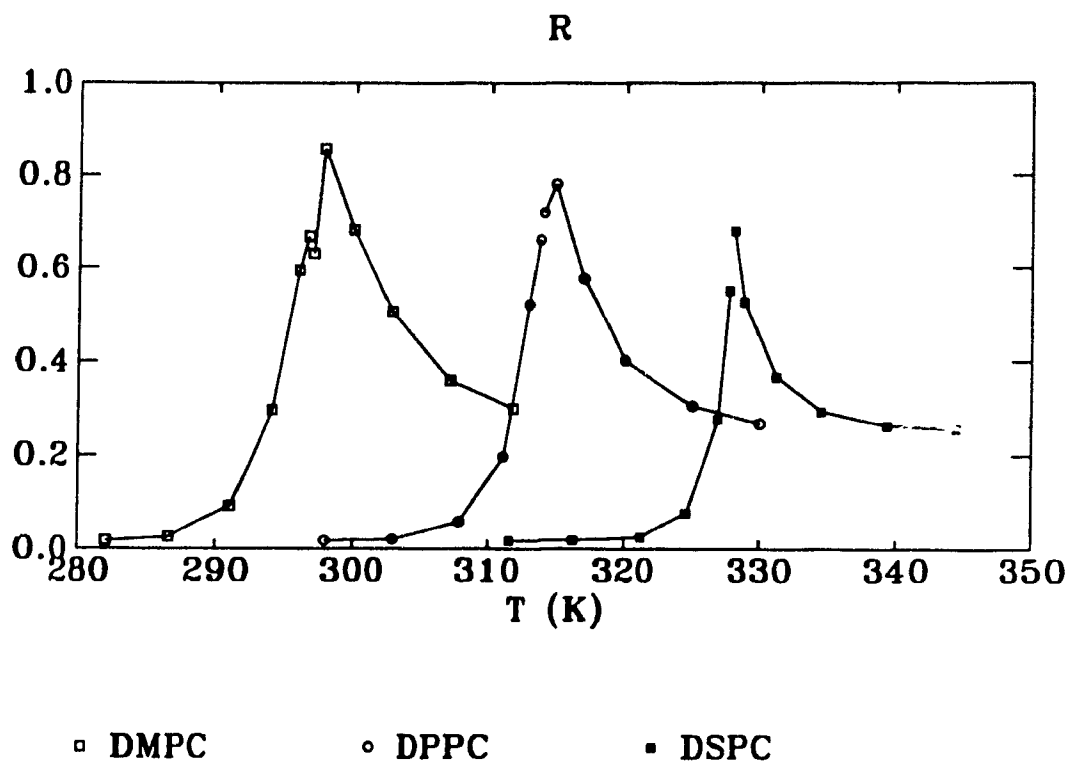


Figure 3.32: Relative permeability of bilayers with $x_C = 0.05$ The units are arbitrary

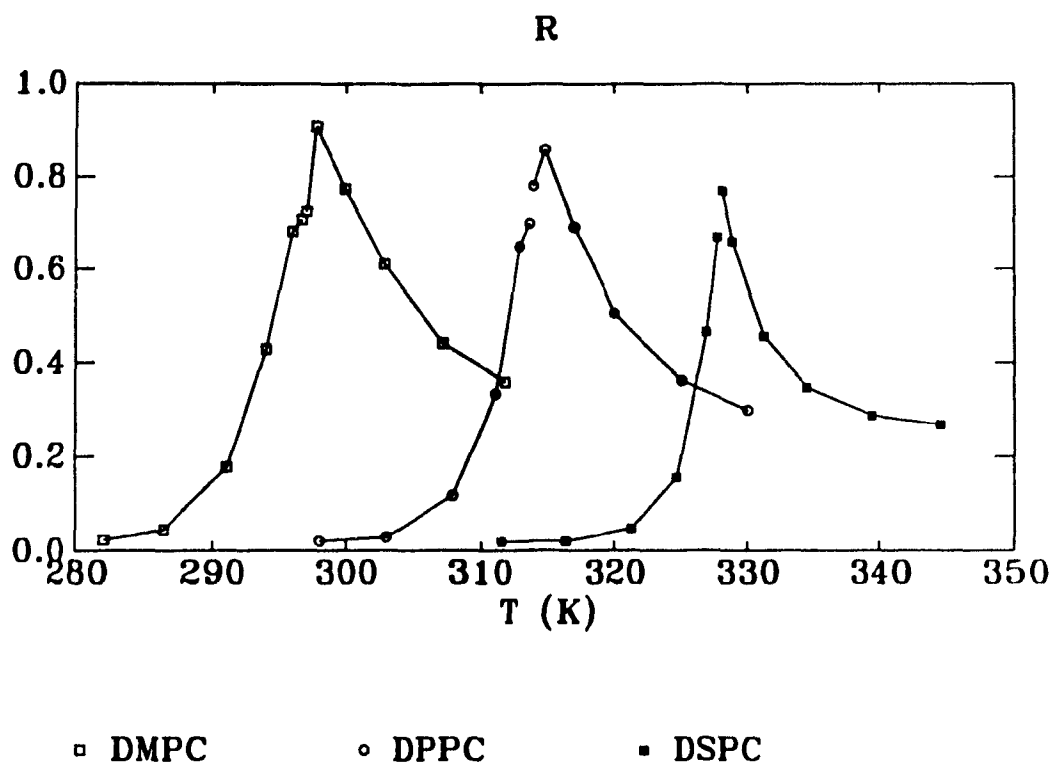


Figure 3.33: Relative permeability of bilayers with $x_C = 0.10$. The units are arbitrary.

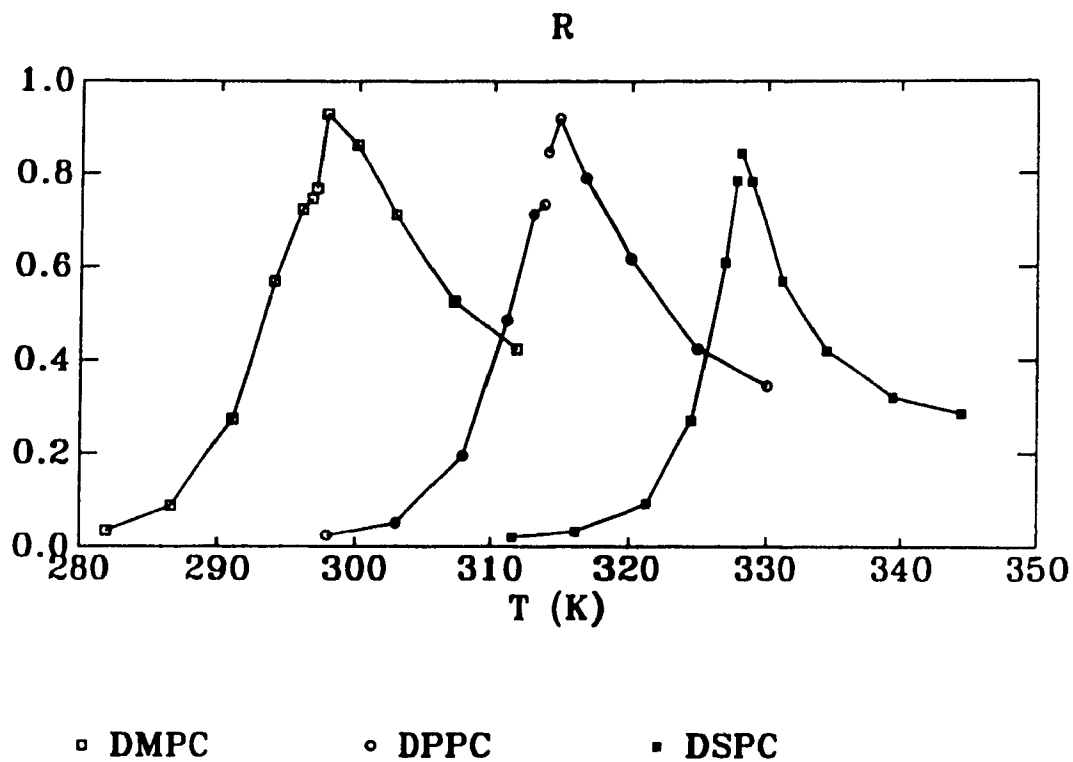


Figure 3.34: Relative permeability of bilayers with $x_C = 0.15$. The units are arbitrary.

3.3 Discussion

In the present work a minimal model for the passive ion permeability is applied to lipid bilayers of three different chain lengths and four small cholesterol concentrations. The formation of clusters and interfaces is related to fluctuations. This is the reason why the model predicts larger permeabilities for lipid-cholesterol membranes formed by shorter acyl chains. Our approach is different from that of Georgallas *et al.* which directly relates the permeability to the fluctuations in the area⁴ [10]. In our model it is the local event of the formation of an interface rather than the total fluctuations in the area which induces an enhancement of the passive ion permeability. The different predictions of the two models are evident when small amounts of cholesterol are present. In the model used in this thesis, an enhancement of the relative permeability of low cholesterol content lipid membranes is predicted for increasing cholesterol concentration. The enhancement is observed at the transition temperature region and in the "wings" of the transition, the effect being more pronounced in the "wings". By contrast, when our results for the fluctuations in the area at different cholesterol concentrations are substituted into the model of Georgallas *et al.*, a large decrease in the passive permeability at the transition region for increasing cholesterol concentration is found.

The model used in this thesis predicts that for small cholesterol concentrations the permeability increases with increasing cholesterol concentration due to the presence of gel-fluid interfaces. At high cholesterol concentrations experiments show that cholesterol decreases the passive permeability. This is because at high cholesterol concentrations there is no phase transition. In the context of the model used in this thesis this implies a decrease in the permeability due to the absence of interfaces. Also, at high cholesterol concentrations cholesterol tends to increase the chain conformational order [12] and therefore causes the permeability to decrease.

⁴The permeability model of Georgallas *et al.* is based in part on that of Doniach [8] who pioneered the use of two dimensional interaction models for the description of the lipid bilayer and monolayer phase transitions.

Results predicted in this thesis for small cholesterol concentrations suggest that interesting properties are caused by the presence of small amounts of cholesterol. It would therefore be useful to make an experimental study of the passive ion permeability of lipid membranes at very low cholesterol concentrations, where the liquid-ordered phase is not present. It is also important to study bilayers with lipids of different chain length since there are no systematic permeability experiments.

Appendix A

Isothermal-Isobarical Ensemble

Consider a system in contact with a reservoir with which the system can interchange energy and volume. In equilibrium, the temperature and the pressure of the system and the reservoir are the same and have a constant value T and p respectively. The total energy of system plus reservoir is a constant $E_T = E_S + E_R$, and the total volume is also a constant $V_T = V_S + V_R$. The probability of the reservoir having an energy E_R and a volume V_R ¹ is given by

$$\mathcal{P} \propto e^{\frac{S(E_R, V_R)}{k}} \quad (\text{A.1})$$

where k is the Boltzmann constant and S is the entropy. If the system is small compared to the reservoir $\frac{E_S}{E_T} \ll 1$ and $\frac{V_S}{V_T} \ll 1$ and we can expand $S(E_R, V_R)$ around E_T, V_T in the following way

$$\begin{aligned} S(E_R, V_R) &\simeq S(E_T, V_T) + \left(\frac{\partial S}{\partial E_R} \right) (E_R - E_T) + \left(\frac{\partial S}{\partial V_R} \right) (V_R - V_T) \\ &= S(E_T, V_T) - \frac{1}{T} E_S - \frac{p}{T} V_S \end{aligned} \quad (\text{A.2})$$

according to equations A.1 and A.2, for a system at constant temperature and pressure the probability of the system having energy E_S and volume V_S is given by

$$\mathcal{P} \propto e^{-\frac{E_S + pV_S}{kT}} \quad (\text{A.3})$$

¹The probability of the reservoir having an energy E_R and a volume V_R is the probability of the system having an energy E_S and a volume V_S .

In the rest of the appendix, E and V will refer to the system energy and volume respectively. The partition function of the system is given by

$$Q = \sum_{E,V} N(E,V) e^{-\frac{E+pV}{kT}} = e^{-\frac{G}{kT}} \quad (\text{A.4})$$

where $N(E,V)$ is the degeneracy (the number of configurations in phase space with volume V and energy E) and G is the Gibbs free energy. Let us define the enthalpy of a configuration as $H = E + pV$.² The ensemble average of H is the thermodynamic enthalpy given by

$$\langle H \rangle = \frac{\sum_{E,V} (E + pV) N(E,V) e^{-\frac{E+pV}{kT}}}{\sum_{E,V} N(E,V) e^{-\frac{E+pV}{kT}}} \quad (\text{A.5})$$

This can be written as

$$\langle H \rangle = - \left(\frac{\partial}{\partial \beta} \log Q \right)_p = \beta \left(\frac{\partial G}{\partial \beta} \right)_p + G \quad (\text{A.6})$$

The Gibbs free energy has a total differential given by $dG = Vdp - SdT$, from which it follows that the entropy is given by

$$S = - \left(\frac{dG}{dT} \right)_p \quad (\text{A.7})$$

The specific heat is by definition given by

$$C_p \equiv T \left(\frac{dS}{dT} \right)_p \quad (\text{A.8})$$

It can be rewritten in the following way differentiating equations A.6 and A.7

$$C_p = \left(\frac{\partial \langle H \rangle}{\partial T} \right)_p \quad (\text{A.9})$$

The specific heat can be calculated with the fluctuations in the enthalpy in the following way: first, rewriting equation A.5 as

$$\sum (\langle H \rangle - H) N e^{\beta(G-H)} = 0 \quad (\text{A.10})$$

²The word *enthalpy* is used here in the same sense as in reference [26], page 51.

which is possible because $\sum N e^{\beta[G-H]} = 1$. Differentiating equation A.10 with respect to β at constant pressure we have

$$\left(\frac{\partial \langle H \rangle}{\partial \beta}\right)_p + \sum (\langle H \rangle - H) N e^{\beta[G-H]} \left[\beta \left(\frac{\partial G}{\partial \beta}\right)_p + G - H \right] = 0 \quad (\text{A.11})$$

and using equation A.6 we obtain

$$\left(\frac{\partial \langle H \rangle}{\partial \beta}\right)_p + \langle (\langle H \rangle - H)^2 \rangle = 0 \quad (\text{A.12})$$

which permits to calculate the specific heat with the fluctuations in the enthalpy as

$$C_p = \frac{1}{kT^2} [\langle H^2 \rangle - \langle H \rangle^2] \quad (\text{A.13})$$

The volume of the system is calculated as

$$\langle V \rangle = \sum V N e^{\beta[G-H]} \quad (\text{A.14})$$

which can be rewritten as

$$\langle V \rangle = -\frac{1}{\beta} \left(\frac{\partial \log Q}{\partial p}\right)_T = \left(\frac{\partial G}{\partial p}\right)_T \quad (\text{A.15})$$

The isothermal compressibility is defined by

$$\mathcal{K}_T \equiv -\frac{1}{\langle V \rangle} \left(\frac{\partial \langle V \rangle}{\partial p}\right)_T \quad (\text{A.16})$$

Following the same procedure as for the specific heat, we can write \mathcal{K}_T in terms of the fluctuations in the volume. Differentiating

$$\sum (\langle V \rangle - V) N e^{\beta[G-H]} = 0 \quad (\text{A.17})$$

with respect to the pressure at constant temperature we obtain

$$\left(\frac{\partial \langle V \rangle}{\partial p}\right)_T + \sum (\langle V \rangle - V) N e^{\beta[G-H]} \beta \left[\left(\frac{\partial G}{\partial p}\right)_T - V \right] = 0 \quad (\text{A.18})$$

and using equation A.15 we obtain

$$\left(\frac{\partial \langle V \rangle}{\partial p}\right)_T + \beta \langle (\langle V \rangle - V)^2 \rangle = 0 \quad (\text{A.19})$$

which permits to calculate the isothermal compressibility with the fluctuations in the volume as

$$\kappa_T = \frac{1}{kT \langle V \rangle} [\langle V^2 \rangle - \langle V \rangle^2] \quad (\text{A.20})$$

For two dimensional systems, all the equations derived in this appendix are valid if V is replaced by A where A is the area of the system, and p is a force per unit length or lateral pressure.

A.1 A Comment About the Notation

In this thesis we study systems with two Hamiltonians, the Hamiltonian for the Pink model (equation 2.8, page 18) and the Hamiltonian for lipid-cholesterol bilayers (equation 3.1, page 40). Both Hamiltonians have the form

$$\mathcal{H} = E_1 + \Pi A$$

There are two different but equivalent approaches to this problem. The first is to treat Π as a parameter of the Hamiltonian that, although it has units of pressure, is not the pressure of the system. The system is at constant temperature T and constant pressure $p = 0$. The internal energy of the system is $E = \langle \mathcal{H} \rangle = \langle E_1 + \Pi A \rangle$. The enthalpy of the system is equal to the internal energy of the system $H = E + pA = E$ and the Gibbs free energy is equal to the Helmholtz free energy $G = E + pA - TS = E - TS = F$. The specific heat is given by the fluctuations in the energy as

$$C_p = \frac{1}{kT^2} [\langle \mathcal{H}^2 \rangle - \langle \mathcal{H} \rangle^2]$$

The second approach is to treat Π as an external pressure. The system is now at constant temperature T and constant pressure Π . The internal energy of the system is $E = \langle E_1 \rangle$ and the enthalpy is $H = \langle \mathcal{H} \rangle = \langle E_1 + \Pi A \rangle$. The specific heat is given by the fluctuations in the enthalpy as

$$C_\Pi = \frac{1}{kT^2} [\langle \mathcal{H}^2 \rangle - \langle \mathcal{H} \rangle^2]$$

The latter approach is normally used for monolayer systems where an external lateral pressure is applied. For bilayer systems some authors prefer the former approach because bilayers form vesicles and there is no external pressure applied to the system.

Because we are working with bilayers in this thesis, the notation used in the text corresponds to the first of these approaches.

In both cases the ensemble average of a quantity g is given by

$$\langle g \rangle = \frac{\sum_{E_1, A} g N(E_1, A) e^{-\frac{E_1 + \Pi A}{kT}}}{\sum_{E_1, A} N(E_1, A) e^{-\frac{E_1 + \Pi A}{kT}}} \quad (\text{A.21})$$

Appendix B

Monte Carlo Integration

A Monte Carlo method to evaluate integrals consists of integrating over a random sample of points instead of over a regular array of points. There are many Monte Carlo integration methods, and the *sample mean* method is described here. It is based on the *Mean Value Theorem for Integrals* which states that if f is continuous on the interval $[a, b]$ the integral

$$F = \int_a^b dx f(x) \quad (\text{B.1})$$

is determined by the average value of f in the interval, multiplied by the interval size. In order to determine this average, random numbers x_i are chosen from a uniform distribution in the interval $[a, b]$ and the value of $f(x)$ is sampled. The estimated value of the integral for m trials is

$$F_m = (b - a) \frac{1}{m} \sum_{i=1}^m f(x_i) \quad (\text{B.2})$$

This method is more suitable for the evaluation of multi-dimensional integrals where other numerical methods are difficult to apply. The generalization of the *sample mean* method for the evaluation of the integral

$$F = \int_{a_1}^{b_1} \cdots \int_{a_n}^{b_n} dx_1 \cdots dx_n f(x_1, \dots, x_n) \quad (\text{B.3})$$

is straightforward and the estimate of F for m trials is given by

$$F_n = (b_1 - a_1) \cdots (b_n - a_n) \frac{1}{m} \sum_{i=1}^m f(x_{1i}, \dots, x_{ni}) \quad (\text{B.4})$$

where x_1, \dots, x_n are independent random numbers from uniform distributions in the intervals $[a_1, b_1], \dots, [a_n, b_n]$.

There is another way to evaluate the integral in equation B.1 called *importance sampling* method. We rewrite F as

$$F = \int_a^b dx \frac{f(x)}{p(x)} p(x) \quad (\text{B.5})$$

where $p(x)$ is a positive function such that $\int_a^b dx p(x) = 1$ and we evaluate F by sampling the value of $\frac{f(x)}{p(x)}$ according to the probability distribution $p(x)$ and by constructing the sum

$$F_m = \frac{1}{m} \sum_{i=1}^m \frac{f(x_i)}{p(x_i)} \quad (\text{B.6})$$

Note that, in the case of a uniform distribution, $p(x) = \frac{1}{(b-a)}$ and the importance sampling evaluation of F (equation B.6) reduces to the sample mean evaluation of F (equation B.2). The method is generalized for multi-dimensional integrals in a straightforward way by rewriting F in equation B.3 as

$$F = \int_{a_1}^{b_1} \dots \int_{a_n}^{b_n} dx_1 \dots dx_n \frac{f(x_1, \dots, x_n)}{p(x_1, \dots, x_n)} p(x_1, \dots, x_n) \quad (\text{B.7})$$

where $p(x_1, \dots, x_n)$ is a positive function such that $\int_{a_1}^{b_1} \dots \int_{a_n}^{b_n} p(x_1, \dots, x_n) = 1$. We can now evaluate F in equation B.7 by sampling according to the probability distribution $p(x_1, \dots, x_n)$ and constructing the sum

$$F_n = \frac{1}{m} \sum_{i=1}^m \frac{f(x_{1i}, \dots, x_{ni})}{p(x_{1i}, \dots, x_{ni})} \quad (\text{B.8})$$

The numerical methods described above are taken from reference [11]. In the next section a particular case of an importance sampling method is described.

B.1 Metropolis Algorithm

The Metropolis algorithm [20] was originally proposed for the canonical ensemble to calculate thermodynamic quantities of a system at constant temperature and constant volume. For ensembles other than the canonical ensemble such as the

isothermal-isobarical ensemble or the grand-canonical ensemble, the generalization of the Metropolis algorithm is straightforward. In the case of the isothermal-isobarical ensemble the algorithm is exactly as described below with the substitution of E by $E + pV$ ($E + pA$ for 2-dimensional systems). For simplicity, it is presented here in the canonical ensemble. The equilibrium value of a thermodynamic quantity in the canonical ensemble is given by

$$\langle g \rangle = \frac{\int \cdots \int dq_1 \cdots dq_n g N(E) e^{-\frac{E}{kT}}}{\int \cdots \int dq_1 \cdots dq_n N(E) e^{-\frac{E}{kT}}} \quad (\text{B.9})$$

where k is the Boltzmann constant, T is the temperature of the reservoir in thermal contact with the system, E is the energy of the system, n is the number of degrees of freedom, $N(E)$ is the degeneracy of the system¹ and q_1, \dots, q_n are generalized variables. For a fluid system with N particles, $n = 6N$ and the generalized variables are the positions and momenta of the particles. For a magnetic system with N spins, $n = N$ and the generalized variables are spin variables. In the case of models with discrete values of the spin variables such as the Ising model, the integral is replaced by a sum. For a lipid monolayer with N lipid molecules, $n = N$ and the generalized variables are conformational variables (In the case of the Pink model where each lipid chain can be in one of 10 conformational states the integral is replaced by a sum).

For large systems with for example $N \sim 10^{23}$ molecules it is almost impossible to compute integrals by usual numerical methods, and we use Monte Carlo integration methods. The Metropolis algorithm is a special case of an importance sampling method in which configurations are chosen with a probability distribution $\mathcal{P} \propto N(E) e^{-\frac{E}{kT}}$. The thermodynamic quantities can then be estimated as

$$\langle g \rangle_m = \frac{1}{m} \sum_{i=1}^m g(q_{1i}, \dots, q_{ni}) \quad (\text{B.10})$$

Equation B.10 states that the ensemble average of a thermodynamic quantity g is simply obtained by computing the value of g for each configuration chosen with probability $N(E) e^{-\frac{E}{kT}}$ and calculating the arithmetic mean. The Metropolis algorithm is

¹We are using the notation $N(E)$ for the degeneracy and N for the number of particles, spins or molecules.

outlined in the next paragraph and a proof that the method chooses configurations with probability $N(E)e^{-\frac{E}{kT}}$ is given later.

A microstate or configuration of a system is determined by a set of fixed values of the variables which describe the state of the particles or molecules of the system. Let Ω_i denote the values of the variables associated with the i^{th} particle of the system. The configuration of a system is then completely specified by $\Omega = (\Omega_1, \Omega_2, \dots, \Omega_N)$. The Metropolis algorithm can be stated as follows:

- (1) Choose an arbitrary initial configuration Ω^1
- (2) Choose a trial state Ω^*
- (3) Calculate the change in energy $\Delta E = E(\Omega^*) - E(\Omega^1)$. If $\Delta E \leq 0$ the transition to the trial state is accepted $\Omega^2 = \Omega^*$.
- (4) If $\Delta E > 0$ the move is allowed with a probability $e^{-\frac{\Delta E}{kT}}$ in the following way:
 - Choose a random number ξ from a uniform distribution in the interval $[0, 1]$
 - If $\xi \leq e^{-\frac{\Delta E}{kT}}$ the move to the trial state is accepted and $\Omega^2 = \Omega^*$
 - If $\xi > e^{-\frac{\Delta E}{kT}}$ the move to the trial state is rejected and the old configuration is counted as a new one $\Omega^2 = \Omega^1$
- (5) Choose a new trial state Ω^* and repeat the procedure

Ω^1 is the initial configuration, Ω^2 the configuration after applying the algorithm once, etc....

Let $P_{r,s}$ be the *a priori* probability of going from a given state Ω_r to a trial state Ω_s , i.e. $P_{r,s}$ is the probability of choosing Ω_s as the trial state given that the actual configuration is Ω_r . If $P_{r,s}$ is ergodic, the algorithm will lead to a sequence of configurations that will reach any point in the configuration space. This algorithm does not tell us, however, how fast the system evolves in time.

In order to prove that the configurations are chosen with probability $N(E)e^{-\frac{E}{kT}}$ we will show that if the algorithm is applied to all the systems of an ensemble and microscopic reversibility is assumed, the ensemble has a distribution $N(E)e^{-\frac{E}{kT}}$. Secondly, assuming that the ergodic hypothesis² holds, it follows that the algorithm will

²The ergodic hypothesis says that an ensemble distribution is equivalent to a time distribution providing that the time is long enough.

lead to a sequence of configurations with a distribution $N(E)e^{-\frac{E}{kT}}$.

Consider first an ensemble of systems and then a new trial configuration for each system in the ensemble. Assume that the energy of a certain configuration r is greater than the energy of a configuration s , i.e. $E_r > E_s$. Let ν_n denote the number of systems in state n before the trial change. According to Metropolis algorithm the number of systems going from state r to state s is

$$\nu_r P_{r,s}$$

because according to step (3), the transitions to the trial states are accepted if $E_s - E_r < 0$. The number of systems going from state s to state r is

$$\nu_s P_{s,r} e^{-\frac{E_r - E_s}{kT}}$$

because according to step (4) of the algorithm, the transitions are allowed with probability $e^{-\frac{E_r - E_s}{kT}}$. The net number of systems moving from r to s is therefore

$$\nu_r P_{r,s} - \nu_s P_{s,r} e^{-\frac{E_r - E_s}{kT}}$$

If we assume that $P_{r,s} = P_{s,r}$ (microscopic reversibility) we can write the number of systems in state r after the Metropolis algorithm has been applied once to each system in the ensemble as

$$\nu'_r = \nu_r + \sum_s P_{r,s} (\nu_s e^{-\frac{E_r - E_s}{kT}} - \nu_r)$$

The sum over all the states of the a priori probability $P_{r,s}$ of going from r to s is unity and therefore ν'_r can be rewritten as

$$\nu'_r = \left(\sum_s P_{r,s} \nu_s e^{\frac{E_s - E_r}{kT}} \right) e^{-\frac{E_r}{kT}}$$

The number of systems in the ensemble in state r is therefore proportional to $e^{-\frac{E_r}{kT}}$. This result together with the fact that the probability distribution $P_{r,s}$ is ergodic implies that, after applying the algorithm many times, the system will have a probability distribution

$$\nu_r \propto e^{-\frac{E_r}{kT}}$$

This is the number of systems in a microscopic state r with energy E_r . There are many microscopic configurations with the same energy E . The number of systems with energy E is given by

$$\nu_E \propto N(E)e^{-\frac{E}{kT}}$$

where $N(E)$ is the number of different microscopic configurations with energy E

B.2 Implementation for Lipid Systems

For systems in which a large number of states are regrouped into a small number of states, each with its associated degeneracy, the implementation of the Metropolis algorithm must take this into account if one wishes to sample from the small set of states.

The Pink model and the model for lipid-cholesterol bilayers consider thousands of possible microscopic configurations for a lipid chain, but all of them can be regrouped in 10 conformational states each with an associated degeneracy. If when applying the Metropolis algorithm we replace E by $E - kT \log N(E)$ and sample from the ten conformational states, the result is the same as if we sample from all the configurations grouped in the 10 conformational states. The degeneracy of the system $N(E)$ is equal to the product of the degeneracies of individual sites. $N(E) = \prod_i \sum_{\alpha} D_{\alpha} \mathcal{L}_{\alpha i}$ in the case of pure lipid bilayers and $N(E) = \prod_i [\sum_{\alpha} D_{\alpha} \mathcal{L}_{\alpha i} + \mathcal{L}_{C_i}]$ in the case of lipid-cholesterol systems.³ Therefore if for example we wish to calculate the difference in the quantity $E - kT \log N(E)$ between two configurations that are identical except for the conformational state of one lipid chain at one of the sites, the change is given by

$$E - E' - kT \log \frac{N(E)}{N(E')} = E - E' - kT \log \frac{D}{D'}$$

where $E - E'$ will be calculated from the corresponding Hamiltonian and $\frac{D}{D'}$ is the ratio of the degeneracies of the conformational states of the lipid chain in the two

³For notation see pages 18 and 40.

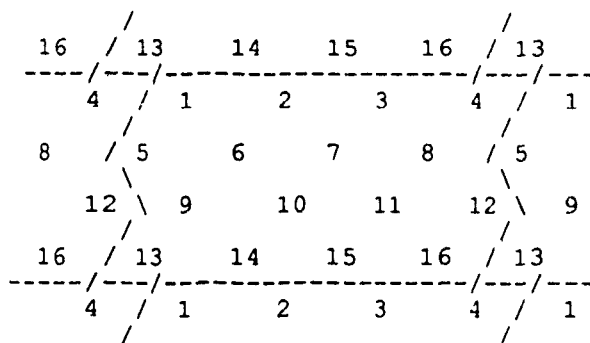


Figure B.1: *Periodic boundary conditions.* In the figure a system of 4×4 is shown.

configurations. The implementation of Metropolis algorithm for lipid systems is described in the following paragraphs. In all the cases, when the algorithm refers to a change of energy, it implies a change in the quantity $E - kT \log N(E)$.

Consider a two dimensional triangular lattice in which each site of the lattice is occupied by a lipid chain in one of ten different conformational states. Periodic boundary conditions are imposed on the system in order to minimize the finite size effects. The boundary conditions used in this work are illustrated for a system of 4×4 lattice sites in figure B.1. In order to implement Metropolis algorithm for the pure lipid membrane, we proceed in the following manner:

1. Choose a lattice site i randomly.
2. Choose a random trial state (from 1 to 10) for the lipid chain at site i and calculate the change in energy involved in the change of state according to the Hamiltonian in equation 2.8, page 18.
3. Follow steps (3) and (4) of Metropolis algorithm (section B.1).

When this algorithm is applied N times where N is the number of sites in the system, the system is said to have evolved one Monte Carlo step. A single Monte Carlo step is our unit of time, but it may not be related to the real time in a physical system because the dynamics of a physical system is very different than that used in Monte Carlo simulations.

For a lipid membrane containing cholesterol, the sites of the triangular lattice can be occupied either by a lipid chain in one of ten conformational states or by a

cholesterol molecule.

To implement Metropolis algorithm for the lipid membrane containing cholesterol, we proceed as follows:

1. Choose a lattice site i randomly.
2. If the site i contains a lipid chain, follow steps 2. and 3. of the procedure for the pure lipid membrane.
3. If the site i contains a cholesterol molecule, select one of its six nearest neighbor sites j randomly. If the site j is occupied by a cholesterol molecule, return to step 1. of this procedure. If the site j contains a lipid molecule, select as a trial state the state with interchanged molecules for sites i and j and compute the change in energy according to the Hamiltonian 3.1. Follow steps (3) and (4) of the Metropolis algorithm described in section B.1. If the trial state is rejected return to step 1. of this procedure, if it is accepted follow steps 2. and 3. of the procedure for the pure membrane for the lipid chain at site i .

When this algorithm has been applied N times the system is said to have evolved one Monte Carlo step.

The results from Monte Carlo simulations presented in this thesis are for a system of $N = 100 \times 100$ lattice sites and in most cases are averages over 50 equilibrium configurations.⁴ In order to average independent configurations, configurations separated by 200 Monte Carlo steps are averaged for temperatures far away from the transition temperature and configurations separated by 1000 or even 2000 Monte Carlo steps are averaged in the transition region. The number of Monte Carlo steps therefore depends on temperature. For temperatures far away from the transition region the total number of Monte Carlo steps is 10000 and for temperatures very close to the transition region the total number of Monte Carlo steps is about 50000.

The dynamics involved in the procedure for the pure lipid membrane consisting only on a change of state (in this case a change of conformational state) at one site is known as Glauber dynamics. This type of dynamics involves a change in the order

⁴The only non averaged quantity presented in the thesis is the maximum cluster size. The maximum cluster size is defined as the largest cluster found within the 50 equilibrium configurations.

parameter of the system. In the case of a lipid system it involves a change in the area.

The dynamics involved in the procedure for the lipid membrane with cholesterol which consists of the interchange between two sites i and j is called Kawasaki dynamics. This type of dynamics conserves the order parameter of the system.

The procedure for the lipid membrane containing cholesterol involves a combination of both types of dynamics, whereas the procedure for the pure lipid system involves only Glauber dynamics.

Bibliography

- [1] Alberts, B., Bray, D., Lewis, J., Raff, M., Roberts, K., and Watson, J.D., *Molecular Biology of the Cell*. Garland Publishing, Inc., 1983.
- [2] Caillé, A., Pink, D., de Verteuil, F., and Zuckermann, M.J., *Can. J. Phys.* **58**, 581 (1980).
- [3] Corvera, E., Laradji, M., and Zuckermann, M.J. , unpublished.
- [4] Cruzeiro-Hansson, L. *Solitons and a Physical Model of Active Transport*. PhD thesis, The Technical University of Denmark, 1988.
- [5] Cruzeiro-Hansson, L., Ipsen, J.H., and Mouritsen, O.G., *Biochim. Biophys. Acta* **979**, 166 (1989).
- [6] Cruzeiro-Hansson, L. and Mouritsen, O.G., *Biochim. Biophys. Acta* **944**, 63 (1988).
- [7] de Gennes, P.G., *The Physics of Liquid Crystals*. The International Series on Monographs on Physics. Oxford, 1975.
- [8] Domach, S., *J. Chem. Phys.* **68**, 4912 (1978).
- [9] Gennis, R. B., *Biomembranes*. Springer-Verlag, 1989.
- [10] Georgallas, A., MacArthur, J.D., Ma, X.P., Nguyen, C.V., Palmer, G.R., Singer, M.A., and Tse, M.Y., *J. Chem. Phys.* **86**, 7218 (1987).
- [11] Gould, H. and Tobochnik, J., *An Introduction to Computer Simulation Methods*. Addison-Wesley, 1988.
- [12] Ipsen, J H., , Mouritsen, O.G., and Zuckermann, M.J., *Biophys. J.* **56**, 661 (1989).
- [13] Ipsen, J.H., Karlström, G., Mouritsen, O.G., Wennerström, H., and Zuckermann, M.J., *Biochim. Biophys. Acta* **905**, 162 (1987).
- [14] Ipsen, J. H. , private communication.

- [15] Ipsen, J. H. *Theoretical Studies of the Lipid Chain-Melting Transition in One- and Two-Component Model Membranes*. PhD thesis, The Technical University of Denmark, 1989.
- [16] Kanehisa, M.I. and Tsong, T.Y., *J. Am. Chem. Soc.* **100**, 424 (1978).
- [17] Maraviglia, B., editor. *Int. School Phys. Enrico Fermi on Physics of NMR Spectroscopy in Biology and Medicine*. North Holland, 1988
- [18] Marčelja, S., *Biochim. Biophys. Acta* **367**, 165 (1974).
- [19] Melchior, D.L. and Steim, J.M., *Biochim. Biophys. Acta* **466**, 148 (1977)
- [20] Metropolis, N., Rosenbluth, A.W., Rosenbluth, M.N., Teller, A.H., and Teller, E., *J. Chem. Phys.* **21**, 1087 (1953).
- [21] Mouritsen, O.G., Boothroyd, A., Harris, R., Jan, N., Lookman, T., MacDonald, L., Pink, D.A., and Zuckermann, M.J., *J. Chem. Phys.* **79**, 2027 (1983).
- [22] Nagle, J.F. and Scott, H.L., *Physics Today* (1978).
- [23] Papahadjopoulos, D., Jacobson, K., Nir, S., and Isac, T., *Biochim. Biophys. Acta* **311**, 330 (1973).
- [24] Peña, A., *Las Membranas de las Células. La Ciencia desde México*. Fondo de Cultura Económica, 1986.
- [25] Pink, D.A., Green, T.J., and Chapman, D., *Biochemistry* **19**, 345 (1980).
- [26] Plischke, M. and Bergersen, B., *Equilibrium Statistical Physics*. Prentice Hall, 1989.
- [27] Reif, F., *Fundamentals of Statistical and Thermal Physics*. McGraw-Hill, Inc., 1987.
- [28] Ruocco, M.J. and Shipley, G.G., *Biochim. Biophys. Acta* **684**, 59 (1982).
- [29] Salem, L., *J. Chem. Phys.* **37**, 2100 (1962).
- [30] Silvius, J.R., *In Lipid-Protein Interactions*, volume 2. Wiley-Interscience, New York, 1982.
- [31] Tardieu, A., Luzatti, V., and Reman, F.C., *J. Mol. Biol.* **75** (1973).
- [32] Trauble, H. and Haynes, D.H., *Chem. Phys. Lipids* **7**, 324 (1971).
- [33] Vist, M. R. Partial Phase Behaviour of Perdeuterated Dipalmitoyl Phosphatidyl Choline-Cholesterol Model Membranes. Master's thesis, University of Guelph, 1984.